Swimming and Flying in Nature—The Route Toward Applications: The Freeman Scholar Lecture

Promode R. Bandyopadhyay
Fellow ASME
Department of Autonomous and Defensive Systems,
Naval Undersea Warfare Center,
Newport, RI 02841
e-mail: promode.bandyopadhya@navy.mil

Evolution is a slow but sure process of perfecting design to give a life-form a natural advantage in a competitive environment. The resulting complexity and performance are so sophisticated that, by and large, they are yet to be matched by man-made devices. They offer a vast array of design inspirations. The lessons from swimming and flying animals that are useful to fluids engineering devices are considered. The science and engineering of this subject—termed "biorobotics" here—are reviewed. The subject, being of dynamic objects, spans fluid dynamics, materials, and control, as well as their integration. The emphasis is on understanding the underlying science and design principles and applying them to transition to human usefulness rather than to conduct any biomimicry. First, the gaps between nature and man-made devices in terms of fluids engineering characteristics are quantitatively defined. To bridge these gaps, we then identify the underlying science principles in the production of unsteady high-lift that nature is boldly using, but that engineers have preferred to refrain from or have not conceived of. This review is primarily concerned with the leading-edge vortex phenomenon that is mainly responsible for unsteady high-lift. Next, design laws are determined. Several applications are discussed and the status of the closure of the gaps between nature and engineering is reviewed. Finally, recommendations for future research in unsteady fluids engineering are given. [DOI: 10.1115/1.3063687]

Keywords: biorobotics, fluids engineering, fluid dynamics

1 Introduction

The goal of this review is to discuss how fluids engineering is benefiting by learning from the march of biology. Fluids engineering has normally taken physics as its fountain of inspiration—and with remarkable successes that dot our life today. Looking at biology for inspiration therefore is a departure. It is thought that the physics discipline is matured, and its return on investment is declining with time. By and large, swimming and flying platforms are visually the same today as they were decades ago, and the efficiency of motors—the most common electromechanical device—remains low, with most of the input energy being wasted and with their operation remaining noisy. Turbulence models, as they are accounting for more and more of flow complexities, are becoming ever so narrowly applicable. There is a need to understand why, while we have more in-depth information about fluid dynamics, the impact on performance is not proportionately as high. Truly predictive capabilities are still scarce. One could list many examples to show that today's engineering—fluids engineering, in our case—has matured to a great extent.

If we look at the march of natural history, one would expect such mature engineering to converge with biology. Therefore, a useful starting point is to quantify the gap between biology and engineering. Understanding the reasons why this gap exists should then be a target of queries and a means to advance. The reason why one should look for convergence of engineering with biology is as follows. Both biology and engineering are designs; they are tradeoffs of many competing mechanisms with sometimes different optimization and cost criteria [1]. If there are gaps between the two, the approach should be to study the underlying mechanisms that are in play and determine whether those in nature should be inducted into engineering. This review examines such approaches and outlines successes.

A relative distinction between science and design, or basic and applied research, can be carried out in the following manner. In an elementary sense, from the point of view of basic and applied research, the broad rationale for biological inspiration in engineering may be viewed as shown schematically in the layered model in Fig. 1 [1]. Physics, which deals with fundamental forces and uncovers the laws of nature, is the core of science. All other layers deal with application in one form or another. The first adjacent layer is chemistry, which can be described as applied molecular physics. The next outer layer is biology, which is nature's application of physics and chemistry into self-contained, autonomous systems. We assign the next outer layer to engineering, which is man's application of physics and chemistry. The disciplines are relatively treated as more basic as we approach the core and more applied as we move to the outer layers. Biology and engineering are then both basically design. The degrees of freedom, number of actuators and sensors, redundancy, and autonomy generally decline in engineering systems compared with biological systems. All this echoes Engineer Fuller, who said that "In nature, technology has already been at work for millions of years" [2]. Biological systems have higher degrees of freedom and, yet, are reliable over many cycles of operation. Cost and reliability, on the other hand, have deterred engineers in the past from building systems based on unsteady principles of aerodynamics or hydrodynamics. Therefore, it is essential that biology-inspired designs have large performance gains, and the induction of new materials, sensors, and power and control technology should help to improve reliability. Appropriate integration of these subsystems is also a key to the technology transition of the principles of swimming and flying

Contributed by the Fluids Engineering Division of ASME for publication in the JOURNAL OF FLUIDS ENGINEERING. Manuscript received October 14, 2008; final manuscript received: October 15, 2008; published online February 9, 2009. Review conducted by Joseph Katz.

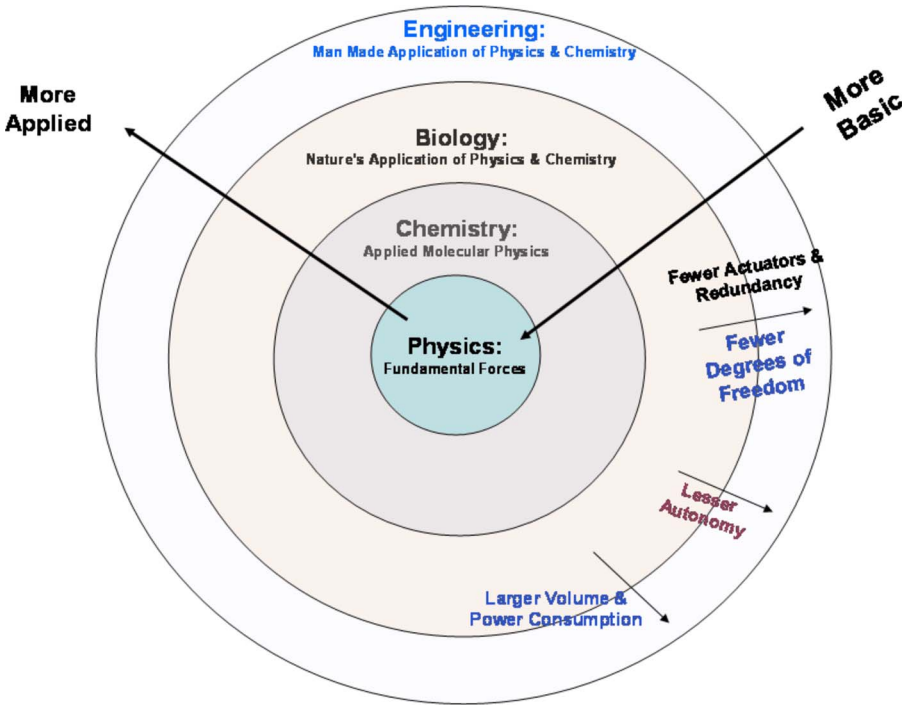

Fig. 1 Schematic of close relationship between biology and engineering [1]

animals. Because both biology and engineering are the subjects of design, the starting questions should be formulated carefully: What basic principles are in play? or, How is it built? The former is rooted in science, while the latter is in biomimicry.

If the goal of new approaches to fluids engineering is to improve performance, the first question that should be asked is as follows: How much improvement should we aim for? For example, if the hydrodynamic efficiency of a lifting surface improves from 50% to 75%, is that a large improvement? We argue below that such an absolute scale is misleading. The answer has to be sought in a systems context, and that is why there is a need to be cognizant of the component sciences that are integrated to build a device with durable advantage. Consider an elementary example. Imagine a person paddling a boat. What would be the impact on the overall efficiency if the hydrodynamic efficiency of the paddle was improved from 50% to 75%? An engineering alternative would have the paddler replaced with motor drives for electromechanical conversion and an engine converting chemical/nuclear fuel to electromotive energy. A well-built electric motor is 30% efficient, and an engine is 20% efficient. So, the result would be a system efficiency improvement of 3–4.5%. This is a sobering finding. We also take this opportunity to note that if the world is faced with a dwindling supply of hydrocarbon-based energy, then clearly addressing the gargantuan energy losses might well be more telling, although less glamorous, than drilling deeper into Earth's crust. One alternative is to bypass the inefficient engine and go directly from fuel to electromotive energy, which is what a fuel cell does. The best practical fuel cell efficiency is below 50–60% due to waste heat, purity and system requirements. Another alternative is to improve the electromechanical efficiency of motors, and for this we need to delve into polymer- and carbon-based artificial muscles. Such muscles are even more efficient when they are in a bath of chemical fuel. So, in principle, biology does provide a design paradigm for impacting not only fluids engineering per se, but also the entire fluids engineering-based system if we are willing to integrate such nature-based hydrodynamic mechanisms with artificial muscles.

There is growing paleontologic evidence for the notion that all living birds of today—from ostriches to hummingbirds to ducks—trace their lineage to those that once lived by the shore. In other words, aquatic birds led to modern birds, and swimming and flying animals have a common ancestry. However, both in nature and in man-made devices, swimming and flying cover a large range of Reynolds numbers and mass, and conflicting requirements of required lift and thrust forces need to be met. Therefore, their design varies considerably. Here, Reynolds number is defined as a ratio of inertia to viscous forces usually in the form $\mathrm{Re}=UL/\upsilon$, where U is the forward speed, L is the length scale, and ν is the kinematic viscosity of the fluid medium.

The interest in high-lift arose among biologists in a bid to explain how flying animals can keep themselves aloft in a low-density medium such as air, which is 840 times lighter than water. Many aquatic animals can control buoyancy, which is not practical in air. Some birds certainly have a very large wing span—the wandering albatross has a wingspan of 3.4 m; an extinct vulture-like bird called the giant teratorn (*Argentavis magnificens*) is estimated to have weighed 75 kg and to have had a wingspan of 8 m. Also, early fossils show insect wing spans of 10–710 mm. Thus, high-lift in animals is certainly an intriguing issue. Since both swimming and flying animals range from the tiniest to very large species, the high-lift mechanism is utilized over a very large Reynolds number range.

At the other end of the spectrum, flying insects weigh from 20 μg to 3 g and span Reynolds numbers from 10 to 10,000. Insects produce far more lift forces than thrust compared with their bodyweights. (For swimming animals, the demand is the opposite, as buoyancy mechanisms are used to support gravity and aquatic animals tend to have a large percentage of saline water in their body making them nearly neutrally buoyant.) Low Reynolds number wings use the fling and clap method of high-lift. But insects of higher Reynolds numbers use a leading-edge vortex for high-lift. In fling and clap, the wings clap above the insect body. While flinging open, they create suction and a high-lift vortex is produced. Although fling and clap produces higher-lift forces than leading-edge dynamic stall vortex, the clap process tends to damage the wings. Not much is known at the lowest Reynolds number of 10, where thrips fly. Thrips have bristled wings. Measurements

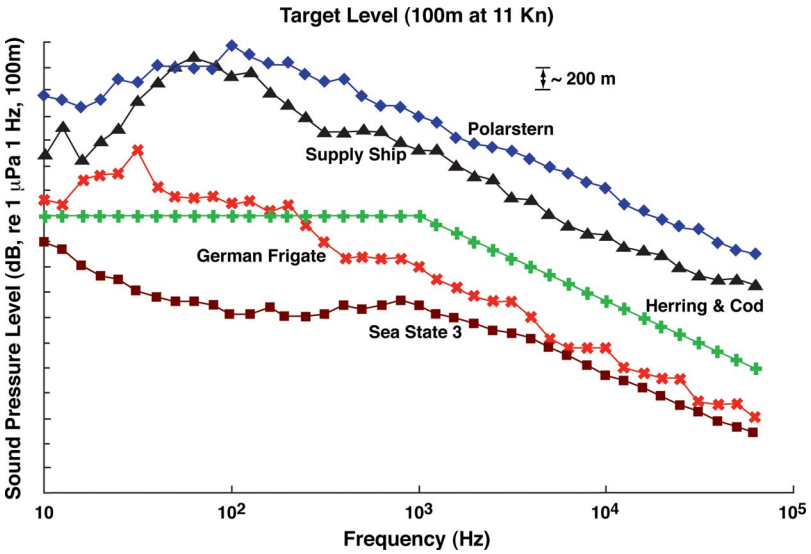

Fig. 2 International Council for the Exploration of the Sea (ICES) data on relative noise in ship and fish. The German frigate is quieter than fish. Fish are slightly noisier than the ambient at Sea State 3. Commercial ships are noisier than fish.

on geometrically scaled bristled and smooth wings show that the former produces lower levels of forces—not higher—during cruise or maneuver [3]. More research is needed on hairy appendages at low Reynolds numbers. Much of academic biorobotics is focusing on replicating the function and motion of animals. This effort is driven by curiosity and the hope for discoveries, inventions, and practical applications. One practical impetus is to keep man out of harm's way—for example, as in hazardous underwater salvage operations.

There are two distinct approaches to biorobotics. One seeks to understand the science principles first and then apply them, while the other merely mimics biology. Biology is not always superior to engineering. While turtles can navigate from the Florida coast to Africa and return to the same location within 100 m, undersea vehicles can roam around the globe and dock at their home pier within <1 m. While insect flight muscles have an efficiency of $<10\%$ [4], the efficiency of motors can be $\sim 30\%$. While evolution took millions of years, the laboratory or numerical "genetic" simulation of fin efficiency [5] and eel kinematics [6] can take minutes to hours, respectively. Thus, there is no guarantee that mimicry will fill a need. For these reasons, in this review, we identify the mechanisms and function in animals and their appendages first. Then, we discuss the successes in the practical renderings of the mechanisms. The focus is on leading-edge vortex formation by unsteady wings—a mechanism extensively used in swimming and flying animals and now being explored for engineering renditions.

2 Performance Gaps Between Nature and Engineering

How can the integration of unsteady hydrodynamics with different disciplines help close the gaps between the performance of animals and that of current similar man-made vehicles and devices? There is a need to conduct careful measurements in the natural environment because they best show how energy storage, sensory inputs, stability, and navigation are integrated in one system. Future animal flight research is proceeding toward controlled experiments in simulated natural environments where different disciplines are integrated [7]. Biorobotics also needs to do the same for rapid success in application. To make a case for animal-inspired fluids engineering, it is useful to quantify the gaps between the performance of current man-made vehicles and those of animals. The performance gaps in several variables in the underwater context have been determined in a series of investigations [5,8,9]. The variables considered are the turning radius of underwater vehicles, efficiency, radiated noise, sonar characteristics, and suction adhesion.

Figure 2 compares underwater noise for several ships and fish, with sea state 3 as a baseline. The vertical axis is in increments of 200 m and is not in dB. While ships are noisier than fish, the German frigate carried out noise abatement modifications to contain or absorb noise, leading to a remarkable improvement. The goal is to explore means of reducing noise and vibration at the source—i.e., at the propulsor and the power drives. Possible solutions include reducing propulsor rotational rates, which can be accomplished by implementing higher-lift hydrofoils, and improving the electromechanical efficiency of drives and power trains [10]. Profiles of new hydrofoils digitized from cadavers of swimming animals are discussed in a later section of this review. The hydrodynamic characteristics of these hydrofoils are worth exploring for improvement in propulsor performance.

One method of quantifying the performance gap between man-made vehicles and animals is to focus on underwater sound levels. The sound level under water is equivalent to the sound level in air plus 62 dB. A large airliner has a sound level of 120 dB (noise level at 1 m). This is equivalent to 182 dB in water. A cargo ship/tanker of sound level 190 dB is noisier than a large airliner. Even a tug and barge at 10 kn produces 170 dB. The onset of whale and dolphin avoidance response to industrial noise is at 120 dB, the ambient level in calm seas is 100 dB, and the coastal bay with snapping shrimp produces a noise level of 70 dB. Obviously, propulsion in man-made commercial vehicles is poorly designed compared with even large transcontinental swimming animals.

The variation in turning radius for constant normal acceleration between fish (such as bluefish and mackerel) and underwater vehicles of 1950s vintage and 1980s vintage shows gaps of several orders of magnitude [11,12]. Bluefish and mackerel are endowed with both speed and maneuverability. The fish data were generated from trajectories of fish navigating about obstacles in a laboratory environment. The vehicle data are from unmanned underwater vehicles traversing a figure-eight trajectory of scale on the order of kilometers in the ocean. The same trajectory curvature algorithm was used in both data sets. The comparison shows that for constant acceleration, fish make shorter radii turns. The gap in turning ability has been narrowed over time, although a factor-

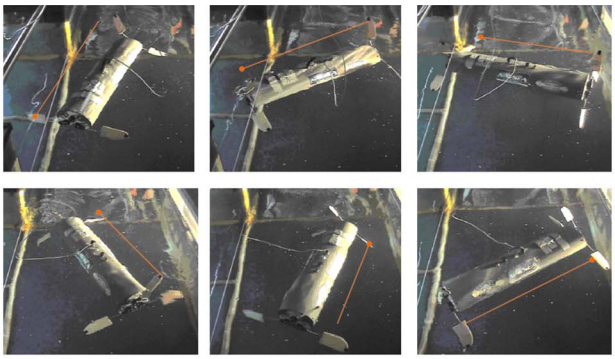

(*a*)

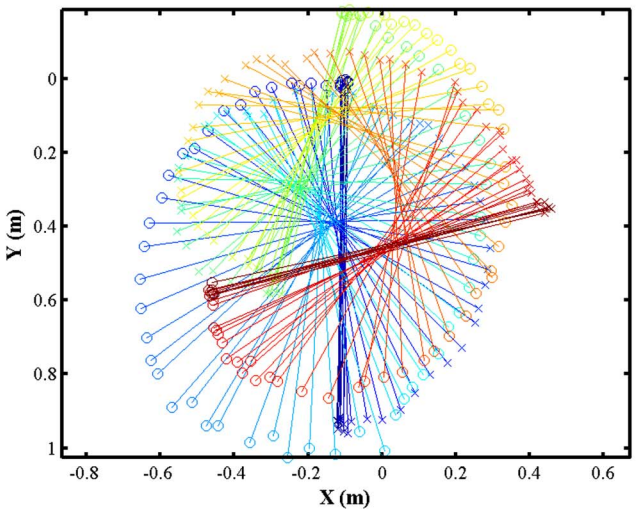

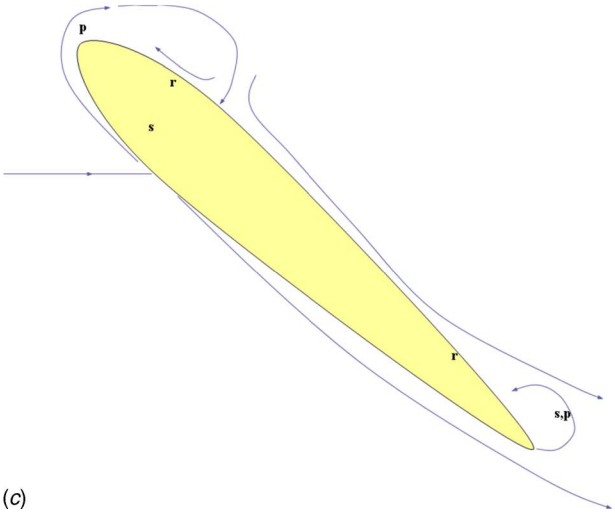

(*c*)

Fig. 3 (*a*) **Sequence of photographs from a video showing clockwise zero-radius turning achieved by the NUWC BAUV. Time increases in (*a*) from left to right by 2.17 s. (*b*) Digitization of vehicle yaw showing accuracy of zero-radius turning [13]; vehicle (160 cm long) axis positions with time are plotted; color changes from blue to green as the vehicle makes one turn and then to red as it makes a counter turn. (*c*) Schematic of dynamic stall on the flapping fins based on dye and surface hot-film sensors; s: stagnation point, r: reattachment point, and p: point of separation.**

of-10 gap remains. The narrowing is attributable to improvements in digital controllers and not to any hydrodynamics. Below, we discuss how the high-lift principles of swimming and flying animals have helped to close the gap completely.

A biorobotic autonomous underwater vehicle (BAUV) has been fabricated at the Naval Undersea Warfare Center implementing the dynamic stall high-lift principles of swimming and flying animals [5,8,13]. The cylindrical hull vehicle has six penguinlike fins that roll and pitch at the same frequency, with a 90 deg phase difference in between (Fig. 3). The kinematics of each fin is independently controlled. The fins undergo dynamic stall and produce higher-lift than is possible in steady flow. Figure 3(*a*) shows that it is now possible to take a cylinder and make it turn at zero radius. Figure 3(*b*) shows the digitized vehicle position at different times, with the vehicle undergoing clockwise and counterclockwise turns. The length of each line represents the vehicle axis. It is shown that the center of the vehicle moves little in comparison to the radius of turning or the length of the vehicle. This is a clear demonstration that the high-lift principles of swimming and flying animals have helped not only to match the turning abilities of fish but perhaps even to surpass them [11,12].

The distribution of propulsion power density of man-made underwater vehicles and that of swimming animals for which muscle energy density data are available have been compared [8]. The comparison shows propulsive power versus vehicle or fish volume. For cruise, there is a remarkable convergence between the two groups from nuclear submarines down to the tiny bonito—a stretch of eight decades of power and displacement. The animal-inspired BAUV vehicle (Fig. 3) is in excellent agreement with shark of similar size. Tactical-scale man-made maneuvering vehicles from the open literature are not generally speaking well designed, perhaps for lack of reference. Smaller and more maneuverable vehicles are likely to gain in performance from comparison with animals.

What is the gap in efficiency between swimming and flying animals and man-made fins and vehicles inspired by such animals? The answer to this question is shown in Fig. 4. Different kinds of efficiencies are shown. There is a dearth of reliable efficiency data on animals. These general trends may be tentatively discerned. Man-made unsteady fins can now be as highly efficient as those in animals as long as the leading-edge vortex high-lift sources are generated by appropriate rolling and pitching motions. However, in both animals and man-made vehicles comprising a multitude of single actuators, efficiency is much lower. In the two generations of man-made vehicles with animal-inspired high-lift actuators, efficiency has improved, although it is still lower than that in flying insects. The efficiency of insect flight muscle is quite low—less than 10% [4]. Good quality electric motors have an efficiency of ~20% or higher. So, what could explain the lower efficiency of man-made vehicles where the individual fins are just as efficient as those in swimming and flying animals? The answer may be frictional losses and the lack of a resonant design, and these possibilities are considered below.

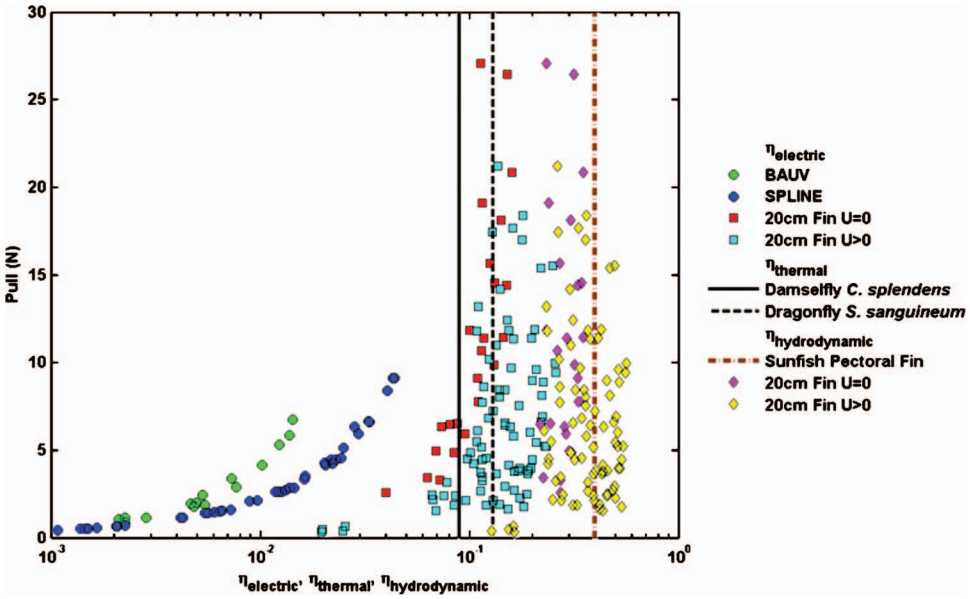

Fig. 4 Efficiencies due to flapping foils. Comparison of the efficiency of man-made vehicles and fins with those of swimming and flying animals [8]. The thrust of the biorobotic vehicles (BAUV and SPLINE) is measured as a pull (N) applied to a string and induced flow velocity is modeled. Single fin: 20 cm span, 10 cm chord. The limited animal data show efficiency only and are not versus pull. The sunfish data are from Lauder and Madden [93] and the insect data are from Wakeling and Ellington [46]. The sunfish pectoral fin hydrodynamic efficiency is taken as the ratio of added downstream kinetic energy to the total fluid kinetic energy when only the pectoral fins are active. The biorobotic fin hydrodynamic efficiency is taken as the ratio of the product of the cycle-averaged force in the forward direction and tow speed, and the input hydrodynamic power. The latter is equal to the sums of the products of torques and angular velocities for roll and pitch motions. The electric efficiency of vehicles and thermal efficiency of insects include power required to oscillate the fins. Thermal efficiency of insects is taken as the ratio of mechanical power output (=mechanical power for flight) to metabolic power input to muscles (=heat production immediately after flight).

In insects, wings operate in a narrow frequency band and a resonant oscillator design is employed. The quality Q of an oscillator in the neighborhood of resonance is defined as [14]

$$Q = 2\pi \frac{E_p}{E_d} \tag{1}$$

where E_p is peak kinetic energy of the oscillator and E_d is the energy dissipated per cycle. Sometimes, the numerator is taken to be the total kinetic energy stored in one cycle. The Q factor can be taken as the number of cycles it takes for the kinetic energy to dissipate to $1/e^{2\pi}=1/535$ of its original value. A resonant system can be considered critically damped ($Q=0.5$), overdamped ($Q<0.5$), or underdamped ($Q>0.5$). The Q factor is 6.5 for the fruit fly, 10 for the hawkmoth, and 19 for the bumblebee. For biological systems, these values are "impressive." In other words, the bumblebee wings resonate at higher amplitude at the resonant frequency than fruit fly wings do and their amplitude drops off more rapidly as well when the frequency moves away from resonant frequency. Flapping machines should also be designed as resonant systems. The controllers of underwater vehicles employing flapping fins do not have a resonant design, and the actuator drives have higher frictional losses.

Finally, a dolphin-inspired interaural time differencing sonar for underwater ranging at distances on the order of 100 m has been fabricated [15]. Emitter sound frequencies and the interaural spatial gaps are in the range of those in dolphins. It was found that the angular resolution can be about 1 deg—similar to that of dolphins, but higher than that of human beings. However, apparently much more energy needs to be input into the water for pinging than that used by dolphins, which employ short-duration, nonlinear chirps. The engineered sonar requires very little processing compared with conventional sonars; it is lightweight in air, neutrally buoyant in water, low powered in comparison, and fits biorobotic vehicles, which tend to be on the scale of 1 m. In these criteria, the biology inspiration did lead to some advantageous performance. However, a large gap in performance exists, and a better understanding of how dolphins process acoustic returns and create three-dimensional images of their surroundings could lead to greater benefits.

3 Understanding From Biology

3.1 Origin and Mechanism. The mechanisms of insect flight/fish swimming and the mechanics of animal-inspired control surfaces have been reviewed earlier [16–20]. The reader might also like to refer to the special journal issues on biology-inspired engineering [1,5,21]. Engineers can find a summary of the aspects of the fluid dynamics of swimming and flying animals that biologists think are of relevance in Ref. [22]. They may also see how gravity, jets, pumps, friction, and waves are being dealt with by swimming and flying animals and the diversity of boundary conditions and solutions for the same problem statement—after all, there are 1000 species of bats and 28,000 species of fish. While engineers may shudder to openly speculate, biologists consider speculation an extremely useful tool for research. Biologists, who in general are strong in observation and intuition, tend not to be adept in the mathematical tools of fluids engineers. A teaming of engineers and biologists could be very fruitful in bringing rigor to the evaluation of mechanisms and reigning controversies, such as follows: Are rotational effects or wake capture new phenomena? Are they present in flying animals? Is the leading-edge vortex spiraling and stable?

One can go farther by swimming and flying than by walking. So, swimming and flying have given a vast opportunity for diversity to animals. The biomechanics of swimming and flying are treated in Ref. [23]. A comprehensive account of what is known about insect flight and the directions of future research is also available [24]. The reader should also be on the lookout for a coming treatise on the biomechanics of flying by Ellington.

Our understanding of the mechanisms of high-lift in swimming and flying animals is based on scaling laws and models (such as physical and analytical models), but largely on physical models. Scaling laws have been mostly based on experimental observations of live animals. Physical modeling has been based primarily on experiments with model wings (in the case of flight) and on live animals (in the case of swimming). Computational fluid dynamics and quasisteady modeling have provided verification and clarification of the physical models to some extent. The quasisteady models provide design laws for scaling. The models have provided checks on internal consistencies in measurements and on our understanding. Controversies between physical models and differences between robotic models and live animals have helped to advance our understanding. In what follows, the understanding from these various approaches is first treated separately and then synthesized. Caution needs to be exercised in linking biorobotics to animal mechanics too sanguinely. For example, sometimes the leading-edge vortex (LEV) has been likened to the delta wing LEV. However, the delta wing has a detached vortex lift, whereas the flapping wing has an attached vortex lift. Of course, neither is shed and both are stable.

The high-lift mechanism of swimming and flying animals has been examined from several different perspectives. The emphasis has been on vorticity production on solid surfaces, the spatial distribution of vortices in the wakes, and measurement and modeling of the forces produced. The approaches may be likened to observers trying to decipher what an animal is like based on its footprints. One group of observers has managed to collect the information from under the foot while the animal was in the process of treading on the surface, while another group is examining the footprints after the animal has already left. Some researchers have looked for evidence of the mechanism on the control surface but on scaled models of dragonfly, fruit fly, and abstracted penguin wings. Others have extensively explored the behavior of vorticity in the near wake using the particle image velocimetry (PIV) technique with live fish in controlled laboratory flows. The notable results are summarized as follows. Ellington and Dickinson showed that dynamic stall is the primary high-lift mechanism in insect flying. Dynamic stall has been implicated for high hydrodynamic efficiency of propulsion [5,8]. Direct evidence that fish exploit vortex flow properties for minimization of the cost of locomotion comes from the PIV work, where it was found that trout slalom between Kármán vortices with lowered muscle activity [25]. It has been shown that fish caudal fins have a universal dominant Strouhal number of 0.25–0.35, and they produce a reverse Kármán vortex train of thrust jets [26].

In science, new diagnostics have led to new understanding, new data, and new product development. The use of digital particle image velocimetry (DPIV) for free-swimming animals in a controlled laboratory environment has allowed the development of new hydrodynamics models of fish swimming mechanisms for cruise and turning [27]. Forces and moments produced by free-swimming fish can be estimated from DPIV wake vortex traverse [28]. Fish with similar morphologies, such as superperch and sunfish, were found to use vortex dynamics differently. For this reason, one could argue that investigation of muscles and actuators is inherently linked to unsteady hydrodynamics and should be carried out in an integrated manner for comprehensive understanding. Some authors have focused on the near-wake vortex structures and not on the flow over the control surfaces. The following modern measurement techniques, if used for flow over the control surfaces, might fill this gap and lead to further developments. A projected comb fringe method of tracking the deformation of the transparent wings of a dragonfly in real time in free flight has been developed [29]. This method allows identification of a body-centered coordinate system using the natural landmarks on the dragonfly. The comb fringe pattern is projected onto the wing with high intensity and sharpness, and images of the distorted wing are then recorded using a high-speed camera. (The only assumption is that the leading edge is rigid.) The instantaneous attitude of the fly is also measured. This method needs to be explored in water. One method that might be useful in the list of contexts mentioned below is multi-exposure digital holographic cinematography. Such a portable instrument in fluids engineering context has been developed [30]. Over a depth of field on the order of 1 mm–1 cm, one can compare scanning planar systems with holograms, both with similar resolution. Measurement of velocities instantaneously over a larger depth of field is the advantage of the holographic method. The holographic method produces a large amount of data, and one tends to analyze only a small fraction of the data. Further development is expected to focus on the improvement of the quality of holograms and automation of analysis of holograms. Fluid velocity diagnostics based on digital imaging techniques have matured. They have been widely used by biologists and fluids engineers to examine wake vortex structures. However, this technique has not been used to examine the boundary layer flow on the lifting surfaces, which is the origin of the vorticity. This region is thin, particularly in animals, so measurement there is challenging. Movements of surfaces are further complications. But how to combine the above fringe method of measuring the movement of flexible, solid lifting surfaces with a diagnostic of the LEV roll-up in a live animal is perhaps the ultimate measurement challenge in biorobotics. Another area where high-resolution surface movement and flow velocity diagnostics would be useful is in exploring the mechanism and function of small surface roughnesses and irregularities that are widely found in the control surfaces of animals. Limited scaled-up experiments do not indicate what the value of these surface irregularities is and, in fact, suggest deterioration in performance. Swimming animals have mucus, so surface hot films cannot be used on such flexible surfaces. The holographic technique could be useful in such flow problems and could also be useful in investigating octopus suckers from behind roughened Plexiglas walls to understand if suckers are more active than they are credited with being [9]. For example, to determine if sucker adhesion to a porous surface is actively controlled, it would be useful to track the suckers' nerves, the motion of their microscopic surface irregularities, control of mucus surface tension, and flow rate with cup pressure, simultaneously. Such experiments would utilize advanced measurement techniques with animal-inspired active control to explore their fluids engineering value. The fringe method can give micrometer-level resolution in real time and, thus, could prove useful to fluids engineering investigations of intricate lifting surfaces of small swimming and flying animals. We have emphasized the importance of free-flight and free-swimming experiments in animals. These are difficult to conduct. High-speed photography of insects in free flight has been carried out [31]. A projection analysis technique that measures the orientation of the animal with respect to the camera-based coordinate system is used. The wing kinematics and body axes can be obtained from single frames.

3.2 Origin of High-Lift as Gleaned From Flight of Insects. In this section, we examine the wings of flying animals and pectoral fins of swimming animals as siblings, but treat the caudal fins of swimming animals differently. Also, with practical transition in mind, among vortex-based mechanisms we focus more on LEV, reverse Kármán vortex streets, and traveling waves, and leave others as tentative. For example, in flapping fins, there is general agreement regarding dynamic stall as a high-lift mechanism. However, there is some controversy regarding rotational effects and wake capture to be of general relevance.

3.2.1 Clap and Fling Mechanism of High-Lift. We first consider the rather uncommonly observed clap and fling mechanism in flying animals. In clap and fling, a pair of lift- and thrust-producing control surfaces is subjected to antiphase rotational oscillation and translation and the angle of attack constantly changes. With this mechanism, it is essential to have the surfaces in pairs. The earliest systematic investigation of insect high-lift and physical modeling [32] was followed by the analytical two-dimensional and inviscid modeling of the clap and fling mechanism [33]. A series of experiments and physical modeling [34–38] clarified the mechanism and set in motion a torrent of interest. LEV was implicated in high-lift and soon became the focus of investigations and applications that continue today. Flow visualization experiments with a pair of scale-model wings of wasps were carried out in an attempt to explain how they sustain their weight in flight in a low-density medium such as air—something that is difficult to account for by several factors with classical aerodynamics [32]. The clap and fling lift enhancement mechanism denoting the 0–180 deg and 180–360 deg phases of the wing motions was proposed. During clap, the leading edges of the two wings first come closer, producing two LEVs, which are the sources of high-lift. Then, the trailing edges rotate to close, ejecting the intervening fluid as a jet and augmenting the thrust. Subsequently, the leading edges rotate apart, again forming two LEVs. This is followed by the trailing edges rotating and translating apart, which again rushes in fluid as a jet and augments the vortex lift. During both the clap and fling phases, vortices do not form at the trailing edges. The LEVs form first during both clap and fling, which probably inhibits the formation of the trailing edge vortices. Other explanations for the absence of trailing edge vortices also appear in literature. The problem with this model of high-lift has been that many insects never clap, even though 25% higher-lift is produced compared with conventional wing beat [39]—probably because clapping damages the wings or because the wings have higher drag during forward flight. Because the clap and fling mechanism is not widely prevalent in nature, Ellington and co-workers resumed the search for the ubiquitous mechanism of high-lift. The stable attached LEV is the subsequent discovery implicated in high-lift, attributed to Ellington, which has withstood the pressure of time. It is presented below in various manifestations in flight and in swimming, also spurring novel applications. This review is built on this kernel. High-speed photography of many different insects in free flight shows that there are many variations of the clap and fling mechanism [31]. How much the two wings touch and how far they stay apart vary between species and during maneuvering. It may be that the separation distance provides a fine control of the lift forces produced [31]. The insect lift enhancement research shows two kinds of insect and bird wing beats—clap and fling (which is less prevalent) and conventional wing beat. LEV is produced in the latter. Maximum lift per unit flight muscle mass is $54-63\ \mathrm{N\,kg^{-1}}$ in those with conventional wing beats and $72-86\ \mathrm{N\,kg^{-1}}$ in those with clap and fling [39]. Insects using conventional wing beats and birds and bats had the same former limiting muscle-lift characteristic, implying evolutionary convergence in performance but not in morphology, which remains diverse. In other words, each animal has retained its specialized wings and kinematics while achieving a universal level of efficiency characteristic of the type of their wing beat. The present review implicates the near-universality of LEV for conventional wing beat.

3.2.2 Leading-Edge Vortex Mechanism of High-Lift. The LEV mechanism is the most commonly observed wing kinematics in flying and swimming animals. In contrast to the clap and fling mechanism, with LEV a single control surface simultaneously heaves and pitches at the same frequency with a preferred phase difference between the two, whereby the angle of attack constantly changes. In addition to heave and pitch, or roll and pitch, twist may also be present in the wing/fin. Insect and bird flights have been modeled on the lines of propellers and rotating disks [34–36,40]. The rate of change in momentum flux in the downward jet is equated to the weight. This analytical approach remains the foundation of experiments and of physical models. Experiments and numerical simulations have focused on circulation in the wake. For many insect wings, the spanwise variation in chord can be described by a beta function, implying universal wing loading behavior [41]. The presence of LEV on *Menduca sexta* has been shown [42]. Keeping these vortices attached for as long as possible is a strategy that insects probably use. Such studies on actual full insects are rare and difficult. The strategies that animals use to keep the stall vortices attached to their wings are open research topics. Research on the high-lift of animal control surfaces treats hovering and cruise separately. Biologists tend to conduct biomechanics experiments both on real animal wings and on models of animal control surfaces that are accurate to minute details. In hovering animals, in the Reynolds number range from 1100 to 26,000 and for aspect ratios of 4.53–15.84, aspect ratio has little effect on force coefficients [43,44]. The cause is attributed to the presence of clear LEVs. On the other hand, in conventional propellers (including wind turbines), delayed stall occurs only near the wing root. In the above, the fin aspect ratio is given by $AR=s/c$, where s is the span and c is the chord of the fin. The plate geometry ratio $R=c_{\mathrm{tip}}/x_{\mathrm{tip}}$ has been used to compare rectangular and triangular approximations of insect wings, such as butterfly wings, where c_{tip} is the chord at the tip and x_{tip} is the distance to the tip from the axis of rotation [45]. Dragonflies align their stroke plane normal to the thrust in contrast to what was previously thought [46]. Measurements of thermal changes after flight show that their mechanical efficiency is between 9% and 13%. The maximum muscle specific power is 156–166 W/kg.

Much controversy exists in our understanding of animal flight mechanisms or scaling laws. If dynamic stall is such a great boon from nature, then are there any system limitations in scaling up? The traditional view has been challenged [47]. It was thought that mass specific power from flight muscles varies as $m^{-1/3}$, where m is the body mass. In other words, less power is available with increasing mass, and different animals can fly in narrower and narrower speed ranges. Instead, it can be argued that lift production deteriorates with increasing size at lower speeds and mass specific power is not an intrinsic criterion [47]. Force and moment coefficients can be of instantaneous values of forces and moments or of averaged values over several cycles. Force (F) such as thrust or lift and drag is expressed as a coefficient, based on fin planform area or the swept area of the trailing edge, the former of the form as $C=F/\frac{1}{2}\rho U^2 cs$, where c is the fin chord and s is the fin span.

3.2.2.1 Wing interactions. The dragonfly uses fore and hind wings to fly. Wing sets can interact strongly. Even minor changes in wing kinematics can lead to dramatic changes in the forces produced. The effects of all four wings can be modeled as a single actuator disk [46]. The vortex interactions of a pair of two-dimensional upstream and downstream wings, cylinder and wings [48], and also the interactions of fish swimming with upstream Kármán vortices [25] are considered later. The flight muscle efficiency of insects is less than 10%, and their muscles have a good elastic storage of the inertial energy to oscillate their wings [4]. How insects manage wing rotation during turning has been examined [49]. Direct evidence of active control of timing between the left and right wings shows that this is done at the ends of strokes when the wing flips. The flip control in flying insects is then a method of executing maneuvers. Measurements of lift and drag and flow visualization on impulsively started two-dimensional flapping insect wings at an intermediate Reynolds number of 10–1000 have been carried out [50]. Studies on impulsively started wings are instructive for insect flight biomechanics. Several experiments have reported that, in impulsively started bluff bodies, the peak transient forces lag wing acceleration [51–56]. The aerodynamics during wing flip (i.e., rapid wing rotation during upstroke-to-downstroke transition), which is more prevalent in in-

sects, has been investigated [57] using two-dimensional wings. It has been observed that the generation of maximum lift is increased if the wing travels through the wake of previously generated vortices, and a lift coefficient as high as 4 has been reported. Force measurements and flow visualization have been carried out with tethered fruit flies [58]. Each cycle was found to produce one vortex loop. No shedding of wing tip vorticity has been observed. The circulation of the vortex loop has been estimated and an unsteady high-lift mechanism confirmed, and a small but observable phase lag in the force time history relative to the wing stroke has been reported—the measured forces are generated after some delay from what one would expect from a visualization of the vortex patterns. The reasons are not definitively known. This delay could be related to Wagner effects, which are treated later [5,17]. A large data set of time histories of forces produced for a large parameter range of fin oscillation is available [59]. The Reynolds number is 115. Stroke plane deviation between the left and right wings of insects is suggested as a control scheme for turning. The authors also present a quasisteady model. The inadequacies of their model, particularly for drag, have led them to question past estimates of mechanical power based on wing kinematics. From examining the forces on a hovering, flapping, mechanical wing starting from start, it can be concluded that force production is influenced by vortices produced in previous cycles [51]. This is known as wake capture and is thought to be an acceleration-reaction force caused by the downwash from vortices formed in the previous cycles acting on the fin [60].

Two-dimensional computations have been compared with measurements on three-dimensional robotic foils simulating fruit fly wings [61]. For hovering, pressure forces make a dominant contribution to fluid forces—something that would escape PIV diagnostics. Interestingly, the disagreements between computations and measurements become more obvious during the periods when the foil decelerates and accelerates at the ends of strokes. We note that circulation does not vary along the span in a two-dimensional foil, and tip losses of finite span are absent. It is unclear what lessons can be unambiguously learned by comparing two-dimensional computations with three-dimensional foil measurements where it is known that spanwise flow plays an important role in LEV stabilization.

The presence of the LEV due to flapping foils at low Reynolds numbers of 120 and 1400 has been confirmed [62]. In the past, LEVs were not seen clearly below a Reynolds number of 5000. Further, it has been shown that at the lowest Reynolds numbers the LEV is stable and spirals from the root to the tip of the foil. However, the severity of the tip-ward flow is Reynolds number dependent. There is a large unexplored area of theoretical research in flapping foils—namely, the Reynolds number dependent stability of leading-edge dynamic stall vortices.

The quasisteady model originally developed for hovering flight has been modified and extended for forward flight [63]. Measurements indicate that added mass effects make a small but measurable contribution to the forces produced. Detailed measurements of the velocity field around dynamically scaled flapping wings of insects have been carried out [64]. It was found that there is a stable pair of counter-rotating vortices at the leading edge, rather than a single vortex. Extensive smoke visualization of the flow around free and tethered flying dragonflies has been carried out [65]. The work largely confirms the attached stable LEV model of insect flight. Spanwise flow is found to be present in both directions but is not thought to be dominant. The LEV is formed when the angle of attack increases rapidly. Qualitative differences are found between model studies and those of live dragonflies. Both the formation and shedding of LEVs are controlled during extreme changes in angles of attack. The mean farfield around flying insects has been related with the nearfield wing kinematics, and semi-empirical theory has been developed [66,67]. The mean induced flow is approximately a function of flapping frequency and stroke amplitude, and the remaining effects are accounted for by a calibration factor that is wing shape dependent.

In addition to LEV, there can be other mechanisms in insect flight, such as wing-wing interactions and wing-wake interactions [17]. Traditional aerodynamic theories predict that performance improves with aspect ratio and stiffness. Swimming and flying animals have a vast diversity in aspect ratio and flexibility of their lifting surfaces. Unsteady potential flow analysis shows that aspect ratio and the proportion of wing area in the outer span determine the optimal wing form. Traditional notions apply only to low frequencies of wing motions and when the wings are stiff and tapered. Further work is needed to incorporate the nearfield unsteady wing kinematics into theoretical models of wing shape optimization.

Measurements of time histories of forces produced by a flapping wing of a fruit fly show that most of the lift force is attributable to two spikes produced near stroke reversal [68]. One of the spikes correlates with wing rotation, and the other occurs after the rapid wing rotation during stroke reversal. Combes and Daniel [68] attributed the rotation-dependent first peak in lift to a rotational mechanism similar to the well-known irrotational (inviscid) Magnus lift that is produced by the flow past a rotating cylinder. They attributed the rotation-independent second peak to wake capture, which is an interaction with the vortex formed during a previous cycle. These notions have been challenged [69]. An alternative explanation is that the first peak is due to vorticity produced because of wing rotation, and the second peak is because of reaction to accelerating an added mass of fluid [70]. Finite element computation of the forces produced by a fruit fly wing has been carried out [71]. The results are qualitatively similar to the measurements [68]. Some 50% of the forces are generated by the outer 25% of the wings. Advancing the phase of wing rotation with respect to stroke reversal was found to enhance force production, and the combination of translational and rotational mechanisms was thought to be important. A spiraling spanwise flow in the LEV was not found [72]. Also, the flow due to a maneuvering fruit fly has been simulated [73]. Both the wings and thorax, albeit in abstracted forms, were considered. There is a dearth of animal or biorobotic data on maneuvering to allow simulations to be compared accurately. Experimentally observed wing kinematics was used to show that turning (a sudden turning called *saccade*) involves a phase difference of 13 deg in the stroke angle between the left and the right wings, and the angle of attack in the inner wing is smaller by 6 deg. It was found that the leading edge and the tip vortex form a loop that is shed as a lambdalike vortex. It may be that the wake vortex loops for maneuvering animals, compared with the "simple" ring or elliptical vortices due to straight motion, have higher azimuthal modes of distortions. The role of vorticity structure harmonics in flight control is unknown. As synthesized in the section on LEV classification, each animal might have its own characteristic wake vortex topology produced during typical turning.

3.2.2.2 Effects of camber. Camber deformation in insect flight has minor effects [50,74]. But, some show otherwise [29]. Measurements on free-flying dragonflies have been carried out in the laboratory at a Reynolds number of 4×10^4. Positive camber deformation of the hind wing during the downstroke generates a vertical force for supporting weight, and negative camber deformation of the wing during the upstroke generates a thrust force. Some have speculated that the time-varying camber deformation is a strategy for delaying the formation and shedding of LEVs and enhancing the delay of dynamic stall [29].

3.2.2.3 How sinusoidal is the wing motion in insect flight?. Photographs of insects in free flight show that, as a first approximation, the wing motion may be considered sinusoidal [31]. However, there is an unmistakable presence of durations of higher accelerations and decelerations at either end of the wing beat, with constant velocities in the middle of half stroke. The second and

third moments of angular accelerations are, respectively, 4% and 9% lower than those in simple harmonic oscillations.

3.2.2.4 Generalized wake vortex model for bird flight. Experiments with bird flight in a very large wind tunnel have been carried out in an effort to develop a universal model of the wake vorticity pattern [75]. For one species (thrush nightingale), the entire speed range up to 11 m/s was covered. For birds, the mean flow speed can vary over 1–20 m/s and the mean chord over 1–10 cm. Thus, the Reynolds number can vary by a factor of 200. The work is a description of the Reynolds number effects on the wake vorticity. At low Reynolds numbers, the wake may appear to be dominated by elliptical vortices and, at high Reynolds numbers, the wing tip trailing vortices dominate the wake. However, the wake pattern is basically universal—it consists of a train of a pair of elliptical vortices followed by a rectangular vortex, the two being interconnected. The elliptical vortex is formed during the upstroke, while the rectangular vortex is formed during the downstroke. The vortex structures have sufficient momentum to support the weight of the bird. Note that dragonflies produce significant lift forces during the downstroke and thrust during the upstroke [29]. It may be that the elliptical vortex represents lift forces and the rectangular vortex represents thrust force; the former is more obvious at lower Reynolds numbers and the latter at higher Reynolds numbers.

3.2.2.5 Classification of leading-edge vortices. How many kinds of LEVs have been reported? The preliminary answer is two or three or four based on their topology. It is unclear if the variations are attributable to the differences in the sources, namely, the insect species [76]. The LEV descriptions and their variations are based on flapping mechanical models of a wasp [37] and of a tethered hawkmoth and dragonflies [77], and on tethered hawkmoths [72,76] and fruit fly models [7]. All descriptions of LEVs satisfy Kelvin's theorem that all vortices either form continuous loops or end on the surface. Based on Kelvin's theorem, there are two classes. The LEVs are differentiated largely based on whether the two LEVs from the two wings are connected at their roots over the thorax to form one continuous vortex, or whether the two LEVs attach to the solid surface at the root. If the two vortices connect at the thorax, then they inflect downstream to do so. Otherwise, there is no inflection and they attach to the surface at the root.

What about spanwise flow in the LEV? Maxworthy [37] pointed out that the spanwise core flow is necessary for stability, that is, for the LEV to remain on the near surface. In its absence, the LEV would continue to be fed with new vorticity generated at the leading-edge stagnation point and grow and, given enough time, would eventually be shed. Maxworthy [37] and Ellington et al. [72] clearly indicated spanwise core flow in their LEVs. Dickinson et al. [7] indicated spanwise flow but downstream of the LEV and not in the core. Dickinson et al. [7] reported a spiraling flow and a conical LEV with a root focus situated near the root. Therefore, a spanwise core flow can be expected. Dickinson et al. [7] observed that a boundary layer fence did not lead to the shedding of the LEV and suggested that the spanwise core flow is not essential for stability even in a conical LEV. Luttges [77] claimed two-dimensional flow and did not show any spanwise flow at any phase of wing motion. A synthesis of results shows that the Strouhal number, time period of flapping, and circulation can probably be tuned so that a vortex can grow in the absence of spanwise core flow, but not enough to be shed into the wake during the time period of flapping [76].

Insect LEVs are conical, blooming from the thorax outboard, but much less so in the case of the tethered hawkmoth and dragonfly LEV [77]. The tethered hawkmoth [72] and fruit fly model [7] LEVs are about 30% of the chord at midspan, and the tethered hawkmoth and dragonfly LEVs are higher. However, the tethered hawkmoth [76] LEV is in a class by itself, bearing some commonality with all of the above. This LEV is uniform from wing tip to wing tip through the thorax, with core thickness being about 10% of the chord and hardly any spanwise core flow. The LEV supports 10–65% of the bodyweight.

What about in water? Surface shear measurements in a penguin wing model flapping below 2 Hz in water have been carried out [78]. It was shown that the leading-edge stagnation point oscillates in space about the mean location sinusoidally in synchrony with the flapping waveform. This would mean that the LEV and the spanwise flow also oscillate in space with time. In other words, the LEV is quasistable and not steady. Surface sensor array and complementary dye flow visualization clearly identify two nodes—the forward stagnation point and the reattachment point. Including the rear stagnation point, there are three nodes. Arguing conversely, it can be asserted [79] that the LEV probably has a saddle at the wing base outside the wing. Future work should focus on stability analysis to determine if spanwise core flow in the LEV is essential for LEV stability. *The evidence so far seems to be that every swimming and flying animal has its own kind of LEV critical point topology.* Ideally, one needs to do experiments with live animals rather than robotic models if one seeks to understand the mechanism of animal flight or swimming. A close-scaled replica of the entire animal would be the second choice. However, for primary effects (such as whether the LEV is present or not and its contribution to forces and efficiency), the value of studies on robotic models of the control surfaces of animals has been vindicated.

3.2.2.6 Scaling law of flight. The variation in wing kinematics of birds with body size has been examined [80]. It was found that the common Strouhal number for direct fliers is 0.21, and intermittent fliers are at 0.25. Strouhal number is defined as fA/U, where f is the wing beat frequency, A is the stroke amplitude, $b\sin(\theta/2)$, where b is the wing span and θ is the stroke angle, and U is forward speed. The stroke angle follows the empirical power relationship $\theta=67b^{-0.24}$. Direct measurements of propulsive efficiency are lacking. It is believed that the propulsive efficiency reaches maximum values at these Strouhal numbers. Currently, animals are thought to oscillate their wings or tails in the Strouhal number range of 0.2–0.4. Future research should examine if the optimized Strouhal values vary with cruise and different kinds of maneuvering, such as hovering and constant-radius turning. Optimization experiments have been carried out on a two-dimensional translating and rotating flat plate to show that in the absence of rotation a stable LEV is not formed [81]. The ratio of the horizontal distance traveled by the plate to the projected chord is believed to be a key parameter for the formation of the LEV.

3.2.2.7 Bat flight: Effects of variable camber, droop, and membrane tension. Bat flight, which is dominated by large camber, droop, and the use of a thin membrane in tension, is being examined [82]. The downstroke consists of abduction, stretching of the wing, and large cambering and droop, while the return upstroke consists of adduction and retraction of the wing, resulting in loss of camber, droop, and membrane tension. During the downstroke, a wing tip vortex is shed. Stall occurs at higher angles of attack and is gentler compared with a similar wing with nondeforming membrane. A qualitative model of the compliant membrane is given, proposing that aerodynamic load is proportional to membrane tension. Direct evidence of the existence of any LEV and high-lift is yet to be available.

3.2.2.8 Vortex method. Simple models for analyzing the force production due to the wing beats of insects have been proposed [32,41]. Also, a vortex method of calculating the pressure distribution of insect wings has been developed. The forces and moments from these three methods have been compared with measurements [45]. The methods are in good agreement when the nondimensional plate geometry ratio R is less than 0.5. The simple models are not accurate when $R\sim 1$ (low-aspect-ratio wing). It is also not possible to take into account the interference between the

two wings in these methods. The vortex method is accurate when R is ~ 1 or is large (>2) and can take into account the interference of two wings. It is important to calculate the added mass effect accurately—particularly in the case of three-dimensional multiwing insects [45].

The vortex method has been used to analyze the takeoff flight of the butterfly [74]. To do that, the time histories of normal force and moment on a pair of finite triangular plates rotating symmetrically about an axis have been computed [45]. The potential flow method is used to compute the pressure field around the plates. The total velocity potential is divided into two components—noncirculatory and circulatory. The noncirculatory part of the velocity potential satisfies the wall boundary condition and Kutta condition at the edge. It does not shed vortices into the flow and is expressed by sources and sinks. The circulatory part does not affect the boundary condition on the plate and is generated by the vortices shed into the flow. The noncirculatory part of the velocity potential satisfies Laplace's equation, which is solved using the vortex lattice method. The total velocity potential is also obtained from Laplace's equation. Flow visualization is used to identify the outer edges where dominant vortices are formed that induce higher velocities and greater effect on pressure distribution on the plate. The wake is a sum of these vortices shed from the outer edge. These vortices reside on a surface extending to the triangular plate. The strength of this vortex sheet is calculated from the circulation at the four corners of elements of numerical calculation. In this manner, the velocity induced by the vortex sheet is calculated. Unsteady Bernoulli's equation is used to calculate the total normal force and moment from dynamic and impulsive pressures. The noncirculatory part of the normal force has two components—one is proportional to the angular acceleration, including the added mass and added moment of inertia effects; and the other is proportional to the square of the angular velocity. Expressions of shape factors are given that are proportional to the added mass and added moment of inertia, which are calculated by both numerical and experimental methods [74]. The added mass and added moment of inertia are functions of the opening angle between the two plates or wings and are constant in the case of one plate. The shape factors are also functions of the plate shape and separation distance of the plates. A similar method has been given where the flow is taken to be the summation of distributed singularities of sources and sinks on the solid surface and the shedding of discrete vortices. However, instead of using a panel method for numerical solution, Dickinson and Gotz [50] gave an unsteady analytical solution where the unsteady Laplace equation is solved to satisfy the Kutta condition at the leading and trailing edges. The method is used in a two-dimensional, rigid flat plate only. Comparison is made with measurements. It is concluded that the forces originate from added mass effects that act immediately and from the delayed effects of the shedding of leading and trailing vortices and body image vortices.

3.2.2.9 Potential flow theory of unsteady wings. An analytical method based on potential theory has been developed for the calculation of aerodynamic forces due to two-dimensional wings that are slightly cambered and are undergoing heaving, surging, and feathering motions [83]. The suction force at the leading edge of steady airfoils is obtained using Blasius's formula. Polhamus's leading-edge suction analogy of vortex lift is used to treat the flow separation at the leading edge. An analytical inviscid method has been given for calculating forces produced by two-dimensional models of fruit fly wings [84]. The wing is thin, rigid, and uncambered. A potential reference is developed in which the wing is at rest, whereby Blasius's theorem is applicable. The model includes bound circulation and also a LEV circulation that is stationary with respect to the plate. The Kutta–Joukowski condition is then applied at both edges. To allow comparison with measurements where the wings are three dimensional and the velocity changes along the span, a method simpler than the blade element method is used. The velocity used to evaluate forces is taken as the wing tip velocity times the square root of the nondimensional second moment of the wing area. Good agreement is obtained with the measurements [59]. It is proposed that because the stabilization of the LEV is attributable to flow three-dimensionality, wing camber might be an essential requirement.

3.3 Origin of High-Lift as Gleaned From Swimming Animals. Flying animals need to support their body mass against gravity, but swimming animals such as penguins do not very much need to. (Buoyancy devices are not considered here). Therefore, differences in the wings of swimming and flying animals can be expected. A golden eagle has nearly the same mass (4.7 kg) as a Humboldt penguin (4.2 kg). However, the planform area of the eagle wing is 38 times larger than that of the penguin [85].

Fish that use their body and caudal fins to move are fast swimmers. Those that use fins are good at maneuvering but are not fast swimmers. In this review, we concentrate on high-lift that comes primarily from the control surfaces (such as fins), and we focus, in particular, on the pectoral fins of sunfish, boxfish, bird wrasse, dolphins, and penguins, which include a range of decreasing flexibility (increasing rigidity) and increasing aspect ratio. In large-aspect-ratio wings, a substantial part of the lift force is produced in the outer part of the wing. Therefore, interesting questions can be raised. Are flexibility and aspect ratio two sides of the same coin? Is flexibility an extreme means for producing the results of large aspect ratio in low aspect ratio?

Many of the principles of fish swimming that are still with us date back to critical observations of long ago [86]. For motion, a fish generally uses its body to apply lateral forces in the water that cancel in the time mean but produce a net forward thrust. Body motion is in the form of a wave called a flexion. The form of this wave along the body is used to classify fish into three or four categories. Anguilliform swimming, named after eels, has been studied much less. In eels, the flexion amplitude remains unchanged, nose to tail. There is no discernable jet in the wake of an eel [87]. Sharks, which are also of the anguilliform, swim constantly and are suspected to be efficient. In carangiform and subcarangiform swimming, the flexion amplitude increases toward the tail, and more of the front part of the body is rigid. Lighthill used his elongated body theory to propose that this form of swimming is most efficient because there is the least amount of body motion and thrust is produced only in the tail. Carangiform swimming produces a jet in the wake. Most fish fall in this category and have been widely studied. In thunniform swimmers, only the caudal fin and a small part of the tail body move. The tuna fish, with an active crescent-shaped caudal fin, is an example.

Due to viscous friction, swimming is thought to require more power than is required by human-engineered land vehicles [88]. But aquatic animals are frugal in oxygen consumption as a result of breath holding. For example, the aerobic capacity of emperor penguins is lower than that of an emu or dog of the same mass [89]. This apparent paradox, which is akin to Gray's paradox [105], can be resolved by proposing that aquatic animals resort to drag reduction techniques and need to produce such minimal thrusts. However, aquatic animals may not only be lowering their drag but may also be lowering their abdominal temperature to lower metabolic rates for energy saving [90]. This possibility points out the importance of systems approach rather than a purely fluids engineering approach, when it comes to understanding the mechanisms of swimming and flying animals and their application.

3.3.1 Classification of Aquatic Propulsion. A survey of aquatic propulsion, followed by an analysis based on elongated body theory [91], has led to the classification of swimming in terms of Reynolds number (low and high), efficiency (greater than or less than 0.5), the variation in body undulation with length, and where in the body length the undulation starts. The theoretical hydrodynamic reasons for the distinctions between anguilliform and carangiform swimming can be deduced. In the former, the

mass of water energized by the anterior part is not in phase with the trailing edge motion, resulting in a lower efficiency. In the latter, the amplitude of the basic undulation grows toward the trailing edge and the energized water is in phase with the trailing edge, resulting in a higher efficiency. The explanation seems to be that the distribution of total inertia along the length, a combination of fish body mass and the virtual mass of water, is optimized to minimize "recoil," resulting in high thrust and efficiency. The evolution in several different lines to the common final result—namely, the lunate tail, which is a pair of highly-swept-back wings, for the enhancement of speed and efficiency—has been examined [92]. The need to reduce caudal fin area in relation to depth to reduce drag without significant loss of thrust leads to this planform. The hydromechanical advantages of lifting surfaces require leading or trailing edges to bow forward. This last remark may bear some relevance to the convoluted form that flexible pectoral fins (such as those of sunfish) undergo [93].

3.3.2 To Flap or to Row?. Many fish use their pectoral fins for propulsion, and this is known as labriform locomotion. Swimming with pectoral fins has been described by biologists in their two extremes—namely, drag-based (i.e., rowing) and lift-based (i.e., flapping) [22,94]. In rowing, which is used at low speeds, the fin moves forward and backward and there is little flow over the fin. In flapping, which is efficient at higher speeds, there is flow over the fin. Therefore, over a range of speeds, both types can be expected to be in use. The kinematics and related muscle activity of aquatic animals, focusing on the three-dimensional aspects of aquatic flight, have been examined [95]. Bird wrasse, for example, primarily use the lift-based mechanism—the fin twists, thereby changing the angle of attack along the span. In the abducted position, the bird wrasse pectoral fin planform is similar to that of insect wings. Six muscles actuate the fin motion in antagonistic groups. A simplified linkage model of the fin has been proposed. A blade element model has been used to compare the mechanical efficiency and thrust produced by an idealized fin undergoing elementary sinusoidal rowing or flapping motion [96]. In rowing, the fin rotates backward and forward about a vertical axis; in flapping, the fin moves up and down about a horizontal axis. Flapping fins are wing shaped and they taper away from the root, while paddle-shaped fins expand away from the root. Better performing pectoral fins of fish that rely on them for propulsion have a higher aspect ratio and a longer leading edge (compared with the trailing edge), and the center of the fin area is located closer to the root [97]. Efficiency is found to be higher in flapping, while thrust is higher in rowing, and it is suggested that rowing is useful in low-speed maneuvering, while flapping is useful in power-conserving cruising. These classifications receive some support from measurements [98,99].

Experiments show that as the frequency of flapping is increased, a foil no longer produces drag but starts to produce thrust attributable to a clear reverse Kármán vortex street [100]. Boundary layer thickness on the foil and Reynolds number do not play strong roles. It has been observed that fish and cetaceans flap their tails in a Strouhal number (fA/U) range of 0.25–0.35 [26]. A thrust-producing jet is convectively unstable, with a narrow range of frequencies of oscillation [101]. There is no modal competition between the natural mode (the absolutely unstable mode) and the forced mode, unlike that in bluff bodies. The flapping fin wake acts like a frequency-selective amplifier. Thrust reaches a maximum per unit of input energy at the frequency of maximum oscillation. The authors point out that saithe is an exception to the rule of preferred Strouhal number in nature and has a lower Strouhal number.

Flow visualization at a Reynolds number of 1100 and measurements of force and power at 40,000 on a two-dimensional heaving and pitching foil have been carried out [102]. Propulsive efficiency as high as 87% was reported, which is similar to the 85% claimed theoretically for whale flukes [103]. The following parameters were found to lead to optimum efficiency: a Strouhal number of 0.25–0.40, heave-to-chord (h/c) ratio of $\sim$1.0, angles of attack between 15 deg and 25 deg, and a phase angle of 75 deg between heave and pitch. For two-dimensional foils, the h/c ratio is important because maximum efficiency is achieved for $h/c = 0.75-1.0$.

Based on flow visualization, it is concluded that the vortex dynamics responsible for high efficiency involves the formation of a LEV in every half-cycle, which amalgamates with the trailing edge vortex to form a reverse Kármán vortex street. More careful later measurements [104] have tended to lower earlier efficiency measurements made in the same laboratory [102]. Efficiencies as high as 71.5% were reported, and the optimum phase angle between heave and pitch was found to be 90 deg for best thrust and efficiency. Therefore, the high efficiencies and the low angles of phase difference between heave and pitch for optimum efficiency and thrust in Ref. [102] are not supported. It has been shown [104] that a higher harmonic should be introduced to the heave motion to make the angle-of-attack time history sinusoidal. This produced a higher thrust coefficient at higher Strouhal numbers. Impulsively started foils are shown to produce mean force coefficients of up to 5.5 and instantaneous lift coefficients of up to 15.0, which could be useful for maneuvering.

3.3.3 Early History of Fish Biomechanics. The principles of swimming known to us are based on the early works of Gray [105], followed by Bainbridge [106,107], and Lighthill [91]. The historical milestones of modeling, scaling, measurement techniques, and debates on the 50th anniversary of Bainbridge's works on scaling laws of fish swimming have been recounted [108]. Gray's modeling work [105] on energetics and maximum speed focused attention on the relationship between fish speed and size. Bainbridge [106,107] carried out measurements in circular channels, which were replaced later with water tunnels, allowing more accurate measurements. He showed that tailbeat frequency controls speed, and he proposed a universal relationship of size, tailbeat frequency, and stride length (distance traveled per beat), $U/L = 0.25[L(3f-4)]$, where U, L, and f are speed, length, and frequency, respectively. This is reminiscent of the advance ratio in propeller theory, $J = V/2\phi nR = (V/(nR))/2\phi$, which is translational speed divided by the product of rotational rate and diameter, where V is the flight velocity, ϕ is the peak-to-peak wing beat amplitude in radians, n is the wing beat frequency, and R is the wing length [109]. In other words, advance ratio is forward speed in wing lengths per wing beat divided by 2ϕ. Note that this analogy leads to the representation of speed in terms of body length per second—a legacy from Bainbridge [106,107] that survives today. Gray's work [105] indicated paradoxes of unexplained differences between available and apparent power, and Bainbridge's [106,107] representation of speed showed that large fish swim faster, but that their relative speeds in terms of body length are lower. The works of Gray [105] and Bainbridge [106,107] influenced the slender body model of Lighthill [110,111] and gave a framework for estimating power and efficiency.

3.3.4 Interaction of Body and Pectoral Fin in Swimming. The steady swimming and rising or sinking of sturgeon and shark have been compared, which determine where large vertical forces are produced—in the main body or in the pectoral fins [112]. These are long, slender fish with pectoral fins. With their long body aspect ratio, these fish tilt their body in a manner similar to what is used in the underwater hydrodynamics of cylinders at lower speeds ($L/D \sim 10$, where L and D are length and diameter, respectively)—larger angles of attack at lower speeds to generate lift. This is one clue that pectoral fins are not needed to produce lift in such fish. The technique of near-wake traverse using DPIV was used to indirectly estimate the forces and moments produced. During steady swimming, the pectoral fins produce no lift; instead, the positive angle of the body produces lift and the two balance moments. However, sinking or rising is initiated by the pectoral fins to produce a starting vortex whose central jet thrust

helps alter the pitch of the body. The rear half of the pectoral fin is used as a flap to do this. The authors point out that two-dimensional simplification of pectoral fins can be grossly in error. The interaction of the body and the pectoral fin is strong in sturgeon. The leopard shark also uses its body and pectoral fin interaction in much the same manner to control moments for cruise and maneuvering, such as initiation of rising and sinking [113]. It further uses the dihedral angle between its body and its two pectoral fins to control roll motion. How does the bamboo shark control the morphology of its body and its slightly flexible pectoral fin for station-keeping near a floor, and how does it rise or sink [113]? The behavior is compared with that during steady horizontal swimming. This shark basically promotes maneuverability over stability. It uses a combination of body angle of attack (positive or negative angles and their amplitude) and the concavity of the pectoral fin (concavity upward or downward and the amplitude of the resulting dihedral angle) to produce the required vectored vortex jets.

3.3.5 Heterocercal Fish Tail: Why Is It Asymmetric?. High-speed photography and DPIV have been used to understand the role of heterocercal tails of free-swimming sturgeon [114]. Long, slender fish such as sturgeon and shark have such tails. Homocercal fins are symmetrical, but heterocercal fins are asymmetrical and have unequal lobes—the vertebral column turns upward into the larger lobe. This question is too complex and there is a need to know the force distributions along the body of free-swimming sturgeon and shark [114]. This topic is well suited to computational analysis and should consider maneuvering to reveal the mechanism.

3.3.6 Finlets and Caudal Fins: Are They Like Strakes and Delta Wings?. A synthesis of literature suggests that we should discuss finlets and caudal fins jointly because they might be working in a synergistic manner, although they do not seem to have been examined jointly in the emerging context of high-lift. Fish such as chub mackerel, bonito, and tuna have several small non-retractable triangular fins in the body margin between the main dorsal/anal fins and the caudal fins—that is, on both sides of the tail end of the body margin in the vertical plane. Some of them are rigid and flat, while others are flexible. It is unclear if the finlets are actively controlled. The total surface area of the finlets is only 15% of the caudal fin area. What is their role? It is hypothesized that these finlets direct the flow in the vicinity of the body toward the caudal fin to augment the vortex jet in the tail [115]. This hypothesis receives some support from visualization—the finlets produce a combination of longitudinal converging flow and a counter-rotating flow with axial vorticity [116]. The fish wake consists of a linked array of tilted, elliptical vortex rings with induced central jets [117]. The minor axis of the elliptical rings remains equal to the span of the caudal fin irrespective of speed, while the major axis in the axial direction scales with speed.

The finlets and the caudal fins are closely located and produce vortex-dominated flows. Are they related? Some have thought that the finlets control turbulence or drag or cancel vortices [118–121]). The suggestion [122] that the finlets produce longitudinal flow to augment caudal fin lift has been both partially supported and criticized [123] based on morphology. It is suggested that vortex enhancement is marginal [123]. While different biologists have focused on different species with variations in morphology, it would be useful to find any universal mechanism. None of the authors appear to have dwelled explicitly on vortex-based high-lift as the universal mechanism of finlets and caudal fins. We synthesize the available understanding to suggest the following vortex lift hypothesis to spur investigations. We draw analogy to the Swedish Viggen fighter jet's high-lift aerodynamics. The Viggen aircraft has two small strakes upstream of the main delta wing; these strakes both operate at high angles of attack, whereby they both produce LEV and high-lift. The strake vortex enhances the delta wing lift. In a similar manner, we speculate that the finlets and the caudal fin work in unison to produce vortex thrust for propulsion. The finlets enhance the main thrust jet by producing a pair of counter-rotating vortices with an intervening jet converging toward the tail, and they are formed alternately along the left and right vertical surfaces of the fish body. The finlet vortices rest on the low-pressure side of the caudal fin and enhance its lift force and augment the jet. It would be useful to conduct computational evaluation of this hypothesis.

3.3.7 Lateral Lagged Oscillation of Symmetric Fish Tail Fins. The caudal fins of homocercal species such as mackerel have extremely symmetrical caudal fins, and the symmetry extends to internal musculature. However, it has been shown that the posterior part of the caudal fin has fine motor control and the tail moves laterally as an acutely angled blade [124–126]. During the tail beat, tail height and area expand and contract. Lateral cyclic motion is lagged—the dorsal lobe (the upper part of the tail fin) leads the ventral lobe (the lower part of the tail fin)—and it undergoes a 15% greater lateral excursion. It has been suggested that such asymmetric motion produces upward lift during steady swimming [126]. The role of this fine control is not definitively known. This precision lateral tail fin actuation problem might benefit from computational investigation.

3.3.8 Multiple-Fin Propulsion in Fish. Some insects have a pair of wings for propulsion and lift. By and large, fish probably use multiple fins more commonly to cruise or maneuver. Wake traverse using PIV visualization has been done to determine the forces produced by various fins in bluegill sunfish [127]. For cruise, 50% of the thrust is produced by the pectoral fins, 40% of the thrust is produced by the caudal fin, and 10% is produced by the soft dorsal fins. For one example of turning, 65% of the force was produced by the pectoral fin and 35% was produced by the soft dorsal fin. The dorsal and caudal fin vortices interact to reinforce circulation, and they partition the force production among the fins. The control of moment may be an important determinant of multiple fin propulsion and their relative budgeting.

3.3.9 Production of Asymmetric Forces by Pectoral Fins for Turning. Fish spend a significant amount of time in turning compared with cruising. DPIV experiments on sunfish have been carried out to understand how asymmetric forces are produced by the pectoral fins that result in turning [127]. The fins modulate the pectoral fin stroke timing and wake momentum. The pectoral fin on the side from which the fish is turning away produces a lateral force that is four times the force it normally produces during cruising. The pectoral fin on the side of the fish toward which it is turning produces a thrust force that is nine times the force it normally produces for cruising. The result of the former is *rotation of the body*, while the result of the latter is *linear translation of the body* toward the center of turning. Fish obviously have a controller, yet to be discovered, that can partition or resolve the force and moment vectors instantaneously and assign monochromatic tasks (forces or moments) to independent fins. It may be that force production in fish for maneuverability and cruising is apportioned in such a manner that the net ability is conserved [128]. The hydrodynamics of bluegill sunfish and black superperch, which have similar fin morphology and are assumed to have similar reserves of energy, have been compared. Superperch have about twice the maximum speed, but sunfish are more maneuverable. They both use their pectoral fins to swim at low speeds and combine pectoral fins with the caudal fin at higher speeds. Pectoral fins are implicated in maneuvering. The superperch pectoral fin wake at all speeds consists of two vortex rings per fin cycle detached from the body. The sunfish pectoral fin wake consists of one detached vortex ring per fin cycle at low speeds and two vortex rings per fin cycle, with one attached to the body, at higher speeds. The orientation of the vortex rings is, however, characteristically different in the two—the sunfish pectoral fin rings always predominantly lie in the lateral plane, while the superperch rings predominantly lie in the horizontal plane. The orientation of the

central jet in the vortex rings explains why sunfish are marvels at maneuvering and superperch excel in speed.

3.3.10 Maneuverability and Flexible Pectoral Fins. Fish that swim in circles work harder than those that swim straight [129]. Power consumption density for propulsion based on red and white muscles, as well as that for underwater vehicles, is higher during maneuvering than during cruise [8]. Fish having flexible pectoral fins are highly maneuverable. The sunfish's pectoral fins are highly flexible, three dimensional, and have a low aspect ratio [130]. PIV studies show that attached vortices are formed at both edges of their fin [5]. A proper orthogonal decomposition of this fin's kinematics shows the fin modes with the proportion of forces that are produced [131]. The approximate three-dimensional vortex structure around an entire sunfish in steady swimming in the laboratory has been constructed from two-dimensional PIV measurements of velocity fields [132]. Longitudinal vortex structures found near the tips of all fins are reminiscent of wing tip vortices of three-dimensional bodies in a uniform flow—the signatures of induced drag. The maneuverability of rigid-bodied fish, such as box fish, propelled by multiple flexible fins, has been examined [133]. The results could help the design of autonomously stable underwater vehicles and automobiles. Most of the body of the box fish is made of inflexible bones, and its rigid body is restrictive of motion. Consequently, the fish has developed a set of fins to oscillate in a phase sequence to produce exquisite maneuvering ability in narrow confines. Flow visualization shows that large-scale tip vortex pairs are created at the sharp ventrolateral keels, and their trajectories relative to the body are manipulated to control stability autonomously. The body performs like a delta wing at a high angle of attack that has a detached LEV. One could conclude that the box fish is using its keel to produce the LEV, although largely to stabilize itself in a pre-existing stream. As a starting point to understanding fish motion, one could create a portfolio of the kinematics of pectoral fins, dorsal/anal fins, and caudal fins that fish (such as box fish, bird wrasse, etc.) use to produce braking, acceleration, spinning, cruising, hovering, and reversing [134]. Generally, for maneuvering, fish control the phase synchronization of several fins to produce a maneuvering motion. Sunfish are an exception; they use their pectoral fins only for station-keeping. Further research is needed on the controllers that manipulate the phase between a set of fins, or the dynamic flexibility of one set of fins to achieve the same result, and on how sensors such as lateral lines are integrated with controllers to close the loop.

3.3.11 Jets or Fins?. Primarily, fish use fins and squid use jets for propulsion. What is more efficient and what is worth considering for application? Squid typically have five to seven times higher oxygen consumption than fish [135], which suggests that jet propulsion is inefficient in comparison. There are squid, however, that use a mix of the two, apparently to compensate for the deficiency [136]. The limitation of jets comes from the fact that the rate of momentum transfer to water is greater with fins than with jets—the size of the bladder expelling fluid is limited and higher jet velocity costs more energy (=velocity squared). Jets due to ring vortices underpredict thrust, and entrained fluid also needs to be taken into account [137]. Environments, nozzle surface quality, active control, and appendages can all affect entrainment. In jet-dominated creatures, their effects on entrainment need closer scrutiny.

3.3.12 Conclusions on Pectoral Fin Mechanism. The hydrodynamic control surfaces on swimming animals have been categorized as passive and active [20]. Leading-edge tubercles of whale flippers and riblets on the skins of shark are passive devices that act as a boundary layer fence and viscous drag-reducing surface elements, respectively. Examples of active devices would include the flexible sunfish pectoral fins or penguin wings. Based on PIV measurements (made largely on station-keeping sunfish in a laboratory environment and not on maneuvering), the major conclusions for the biomechanics of the sunfish pectoral fin are as follows: The fin produces thrust throughout the movement cycle during steady swimming and does so by a combination of changes in the fin kinematics, which include (1) spanwise and chordwise flexibilities, which act to stabilize the upper edge vortex and orient the surface pressure force in the forward direction even during the outstroke; (2) active camber control of the fin surface; (3) an increase in surface area during the in-stroke to increase thrust; (4) surface deformation (cupping shape) to reduce within-stroke oscillation in lift (vertical forces) by producing dual simultaneous LEVs of opposite sign; and (5) a bending wave from root to tip to increase downstream (thrust) momentum. The penguin wing is much less flexible in comparison to the sunfish pectoral fin. The chordwise flexibility of the penguinlike wing increases its hydrodynamic efficiency from a maximum of 0.62 for rigid wings to 0.86 for an optimized wing, while the thrust coefficient remains unaffected [18].

3.4 Flexibility. The formation and evolution of vorticity from the wings and the body suggest that aquatic animals (such as sunfish) use their highly flexible fins to control the loading along the span, and the convolution is a dynamic optimization in synchrony with the unsteady high-lift mechanism. Recall that fish use lateral lines to sense the pressure field, and such a convoluted vortex sheet that might evolve into more than one vortex ring could offer a greater moment for stability control. But there is no evidence yet that the sunfish wake produces more than one vortex ring. Time-domain panel computation of flexible wings, whose planform is similar to that of whale flukes, has been carried out [138]. It was shown that passive operation of the wing degrades propulsive efficiency. However, if the phase of the spanwise flexibility is carefully controlled with respect to the wing motion kinematics, propulsive efficiency can be enhanced. The wing tip should be moved in the same direction of the overall wing. An attached flow is assumed, so future work needs to account for what we now know about LEVs, appropriately scaled for aquatic simulation. A pneumatically operated flexible microactuator made of silicon rubber, circumferentially reinforced with fibers, has been used to build a flexible fin for underwater use [139]. Shore stiffness is varied along the length by varying the density of the fiber reinforcement. Higher curvature is produced by increasing internal pneumatic pressure. A feathering motion has been produced.

3.5 Power. Because of the main role played by unsteady mechanisms, existing aerodynamic theories that use steady-state lift and drag coefficients cannot be used for estimating the induced power of swimming and flying [40]. Yet, fundamentals relating circulation and lift are applicable. Vorticity is produced only on the solid surface of the wings and body. One could track the trajectories of points on the surfaces during a wing stroke and arrive at the vorticity sheet. For a sunfish, this sheet is going to be highly convoluted. During hovering, the vortex sheet is simpler than during maneuvering. The presence of this sheet is a result of force generation—loading of the wings and the body. The sheet quickly rolls into ring vortices to arrive at a more stable configuration. The work done to create the rings can be used to estimate the induced power (the force produced is the reaction of the vortex ring momentum per stroke period). Thus, accurate measurement of the ring vortices in the near-wake and of circulation is an indirect but practical tool for determining the induced power of swimming and flying animals. Many researchers devoted much effort to using dye, smoke, and PIV visualization to document the formation and roll-up of vorticity on the wing surfaces and also of its roll-up into large ring vortices in the near-wake of swimming and flying animals.

3.6 Understanding of Mechanism From Computational Fluid Dynamics. Insect flight covers a Reynolds number range of $10-10^5$ [140]. Swimming animals tend to fall in the lower part of the range—the lower range of the limit drops to 10^{-2} for swimming sperm. The distribution of Reynolds numbers for swimming animals and man-made vehicles appears in Fig. 10 in Ref. [19]. A comprehensive theory of force production in swimming and flying animals is not available. Measurements, modeling, and numerical simulation are filling the void in bits and pieces. Numerical and analytical simulations of fruit flies of wing planforms that are slightly smaller than those in earlier works have been carried out [70]. The computed time histories are similar to those measured [49,59], but with a constant shift to higher values. The claim in Ref. [72] that there is an attached dynamic stall vortex formed at the leading edge is supported; the vortex does not get shed and there is no stall. In agreement with other works [72,141], wake capture [59,68] does not exist apparently because the LEV is not shed. The Magnus effect as the origin of one of the peaks in lift has also been questioned [68]. Note that lift produced by a surface at an angle of attack is Magnus-like, but it is unclear how a Magnus-like force can be attributed directly to the rotation of the wing about its span. In any case, a Magnus effect is irrotational, but a peak in drag accompanies the peak in lift attributed to a Magnus effect. Instead, added mass effects and vortex formations are the causes of the two lift peaks before and after the stroke reversal. It has been shown that the unsteady oscillation of the wings can indeed support the weight of hovering flies as measurements show [32]. Wing kinematics that is yet unexplored might produce higher lift forces. The drag of fruit flies is estimated to be 1.27 times the lift force required to sustain the fly's weight. The body mass specific power is 28.7 W/kg, the muscle-mass specific power is 95.7 W/kg, and the muscle efficiency is 17%. This drag-to-lift ratio is higher compared with those in large fast birds or in hovering helicopters. Computational methods [70,141] have been used to study dragonfly wing interactions, and very little of any interaction is found [142]. Both fore and aft wings produce lift peaks during their downward strokes. During those times, they produce vortex rings with downward momentum.

Navier–Stokes computation has been carried out on a full bird wrasse swimming underwater using an adaptive mesh grid [143]. The pectoral fins are flexible, although the dynamic geometry is not as detailed as that in later investigations of sunfish pectoral fins. Also, detailed time histories of forces produced on a bird wrasse are not available, and an accurate comparison of the computation is hindered. The authors in any case show that in the flexible fin swimming under water the LEV is large, is not of the spiraling type, there is no strong spanwise flow, and the LEV is shed during the upstroke. The flexible pectoral fin is dominated by a strong axial flow and not a spanwise flow. The forces produced by fish-inspired pectoral fins attached to a 30-cm-long and 10-cm-diameter rigid cylinder have been computed [144]. The unsteady Navier–Stokes solver with automatic adaptive remeshing had an unstructured grid. Station-keeping at 1.5 m/s could be possible with these parameters: 20 deg angle of attack at the root of the fin, 2 Hz flapping frequency, and a 114 deg flapping amplitude. The mean power required is 1.573 W, which is 0.79 J/cycle. Numerical simulation of flexible fins has been carried out [131]. Photographs of sunfish pectoral fins swimming in a constant-speed stream in a controlled laboratory environment were digitized to determine the variation in fin topology with time. The flow around the moving boundaries was simulated using Cartesian-grid-based, immersed boundary algorithm pioneered earlier [145] for flows in hearts and lungs [146]. The large-eddy simulation method was used to compute the forces produced by the fin. The method of proper orthogonal decomposition was used to determine the modes of the fin topology and determine their contributions to the thrust produced. Mode-1, which visually appears to capture most of the cupping shape of the fin, produces 45% of the total mean thrust, the glaring omission being the peak during the second half of the cycle. The addition of Mode-2 raises the contribution to 63%, and the second peak is partially generated. Although the further addition of Mode-3 generates 92% of the thrust, reproduction of the second peak remains elusive. Videography shows (simplistically, to this reviewer) that there may be at least two distinct kinds of deformations—those that are of the scale of the chord and span, resulting in cupping of the fin, and those that are distinctly smaller and extend over only a part of the fin. It would be worthwhile to examine the nonlinear interaction of these two scales of deformations, particularly in the augmentation of force peaks over a part of the cycle.

Numerical simulation of the flow due to flapping, rigid ellipsoids with varying aspect ratio has been carried out [147]. The relevance of freely flapping, rigid ellipsoids to the flapping fins of fish is unclear. The authors show that the gains in thrust and efficiency remain confined to aspect ratios of 2–3, and this is claimed to be the reason why such aspect ratios are commonly found in the pectoral fins among labriform swimmers. The fin wake is found to consist of vortex loops that convect downstream in two oblique directions to the flow, and their intervening angle is inversely proportional to the aspect ratio of the ellipsoid. Numerical simulation of a pair of rigid and finite flapping fins in tandem in the absence of a body has been carried out. As to be expected, certain spatial gaps between the fins can augment thrust and efficiency. However, the relevance of the two-dimensional rigid fin results to the hypothesis on the interaction between the dorsal and caudal fins of sunfish is tenuous [28]. The value of the vortex interaction and moment distribution due to fins around a body to the control of the whole animal/vehicle could be more important than thrust augmentation. The biomechanics works of biologists and biology-inspired hydrodynamics are yet to focus on the relationship of hydrodynamic properties and control.

3.6.1 Analysis. Vortex theory rests on the presence of concentrated regions of vorticity in the flow. The earliest vortex theory of insect and bird flights, developed to firmly supplant the momentum jet theory of continuous wake generation, is due to Rayner [40,148]. Both hovering and forward flights are considered. In hovering, the wake vortices are a stack of horizontal, coaxial, and circular rings. In forward flight, the rings are elliptical, but neither horizontal nor coaxial. Power reduction motivates the choice of flight style. This is illustrated by a comparison of the mallard and pheasant, which are large birds (>1 kg) that are not good in all conditions, such as hovering and fast flights. The mallard has large-aspect-ratio, thin, pointed wings, and the pheasant has low-aspect-ratio, broad, rounded wings. The mallard has lower power per unit mass and lower aerodynamic power at higher speeds. This explains why the mallard patters long before takeoff, while the pheasant can take off vertically if need be. Also, the mallard is one of the fastest flying birds, while the pheasant has a labored flight and rarely flies for long duration. The author gives a good discussion of the theoretical methods for estimating induced power. A theoretical model of how wing kinematics affects induced flow over insect bodies and the far-wake shows that wing beat frequency, stroke amplitude, and wing shape affect induced flow [66]. Navier–Stokes computations of a flapping wing at a low Reynolds number of 100 show the spanwise pressure gradient that prevents the LEV from being shed [149]. For the accurate determination of locomotive forces from wake traverse, both velocity and pressure field information are required [150].

3.6.2 Computation of Flow Due to Biorobotic Vehicles. Finite volume simulation of the inviscid forced-motion hydrodynamics of the MIT Robotuna vehicle has been carried out [151]. The Navier–Stokes equations are expressed in arbitrary Lagrangian–Eulerian form, and a mesh movement algorithm based on a modified form of the Laplace equation is developed to handle moving boundaries. The computed mean power compares with measurements within 10–15%, and the mean thrust compares with the

nonlinear potential method [152] within 12%. There is an intriguing phase difference in force and power time histories between the two computations.

3.7 Differences Between Rigid and Flexible Fins. Low-aspect-ratio, flexible fins produce LEVs that do not spiral, and the flow is dominated by axial flow and shedding of vortices. Large-aspect-ratio, rigid fins have strong LEVs that spiral spanward, creating vortex stability. We have preferred to demarcate, as above, in terms of flexibility rather than in terms of swimming and flying. Highly flexible, low-aspect-ratio wings do not seem to be used in flying where flapping frequencies need to be very high ($\times$10 to 100) and, apparently, it is difficult to flex simultaneously at such high frequencies. Avian flight analysis suggests that large-aspect-ratio wings are more suitable for high-speed sustained flight, while low-aspect-ratio wings are better suited for hovering.

3.8 Wagner Effects. The Wagner effect is one of the unsteady effects that need to be considered in the mechanism of force production in swimming and flying animals. It is known that there is a time delay in the production of forces in impulsively started lifting surfaces. This delay is called the Wagner effect, and it has been experimentally elucidated [153]. Due to viscous effects, there is a delay in the development of the asymptotic value of the circulation around the lifting surface, that is, a delay in the establishment of the Kutta condition. The proximity of the starting vortex near the trailing edge in the early stages also affects this delay. The reduction in lift and drag can be estimated using the simple Wagner function, accounting for the distance traveled during stroke reversal [154]. Some have suggested that this effect might not be strong in insect flight [50,68], although others think differently [69,96]. Force measurements have been carried out in an abstracted penguin wing at chord Reynolds numbers of up to 125,000 at tow speeds up to 1.25 m/s [5]. During hovering and at low speeds ($\rightarrow$0), a hysteretic effect reminiscent of the Wagner effect has been observed in the wing kinematics and forces measured. Because the accuracy of the estimation of the representative induced speed during hovering is somewhat doubtful, instead of relying only on lift coefficients, torque sensors were also used to determine if the observed hysteresis was genuine. The torque sensor measurements showed that some amount of hysteresis is definitely present, although it is not as large as given by the force coefficient plots. In addition, the hysteresis dropped as Reynolds number increased. A correlation of the motion of the stagnation point and lift forces also shows a phase difference reminiscent of the Wagner effect.

In the insectlike motion of wings, the wing mostly has steady kinematics except near the end, where the flip is rapid [59]. A time delay in forces has been observed during rapid wing flips at the end of wing travel, and it has not been examined if this happens when the flip is more gradual, as is the case in underwater experiments [8]. Models and numerical simulations do not compute lift and drag forces accurately during the rapid flips that are characteristic of insects, although they are otherwise accurate during the remaining phase of oscillation [59,61]. This is an area that needs further investigation. Also, future work is needed on the origin of the time delays found in the kinematics relevant to swimming and flying animals.

3.9 Added Mass Effects. When a lifting surface accelerates through a fluid, it experiences a reactive force due to the accelerated fluid. This is known as the added mass effect. It has also been termed "acceleration reaction" [60] and "virtual mass" [41,92], reflecting the authors' emphasis on the domination of acceleration or virtual mass for force generation. Due to the simultaneous presence of circulatory forces, it may be difficult to calculate forces due to added mass. Added mass components can be estimated using empirically derived coefficients measured for various bodies [155]. For fish, added mass coefficients for an entire fish are 0.405 and 0.9255 in the fore-aft and up-down directions, respectively, and 1.0 for the pectoral fin sections [134]. An expression for calculating the force due to the inertia of the added mass of the fluid has been given [156]. For a three-dimensional wing, it is calculated for each blade element and then is integrated along the span of the wing. In a pair of wings undergoing the "fling" motion, the interference of a pair of plates can increase the added mass of each plate, but only when the opening angle between the plates is small [45]. A method is available for estimating forces produced by swimming animals from the PIV measurements of velocity and added mass in the animal wake [157].

3.10 Effects of Twisting. High-speed photography of insects in free flight shows that the wing profile twists and flexes [31]. The wing is twisted along its span—the angle of attack being higher at the root. A theoretical model has been compared with measurements on a flapping foil that was passively twisting along its span [99]. The mechanical efficiency depended on advance ratio and wing twist, the maximum reaching a value of 0.83. This reviewer and co-workers have conducted measurements on twisting penguinlike fins, which show that twist affects efficiency ($\sim$5%) and thrust ($\sim$24%).

3.11 Flagellar Swimming: EEL Swimming. Here, we consider the swimming of eels and spermatozoa. Their kinematics and relationship to performance are summarized. Eels can swim thousands of kilometers and they have enough fat to undertake such a journey [158]. We consider eel swimming particularly because a robotic eel has been built and is an example of one of the earliest examples of robotic fish. The gait and low frequencies are amenable to shape memory alloys. Unlike fish, eels do not have a downstream pointing jet that is a reverse Kármán vortex [159]. However, they produce transverse jets. PIV measurements show that the drag and thrust vorticities in eels are not differentiated spatially as clearly as in carangiform fish, and the result is that the thrust jet is not discernable [87]. The cost of producing the wake increases with speed to the power of 1.48 and not 2.0. Eel propulsion efficiency is reported to be 0.43–0.97 [160]. Because of such wide disagreements, direct measurements of thrust forces produced are required and accurate measurements of efficiency are needed. Numerical simulation of eel swimming has been carried out where the kinematics for efficient swimming is obtained using a "genetic" algorithm to understand the relationship between body movement and forces produced [6]. It is unclear how comprehensively the technique has been validated, and claims of differences in flow physics with those observed experimentally are subjects of future studies. For example, an optimized Strouhal number in the range 0.6–0.7 has been reported, whereas it is known to be 0.2–0.4 for swimming and flying animals. However, while the condition of optimization of efficiency has been rigorously prescribed in the numerical simulations, most experiments have reported the Strouhal number of fin oscillation but have made no accurate measurements of efficiency. High efficiency is implicit in the popular Strouhal number—but this is not a rigorously established fact. Therefore, the questions are as follows: What is the efficiency of eel swimming? What is the optimized Strouhal number? Eels have two swim modes of kinematics; one is for efficient but slow swimming, and the other is for fast but inefficient swimming [161,162]. In the former, eels, nematoads, lamprey, or spermatozoa—whatever the flagellating animal may be—the animals undulate side to side down the length. In the latter, the front part of the body is kept straight and the thrust is generated in the rest of the body. In both kinds, ring vortices are shed and jets are produced. In any case, the reported work clarifies the vorticity composition of the wake. The lateral jets observed by experimenters [87,159] are shown to be due to ring vortices that are shed by the eel, two per cycle. One could then say that eels generate two lateral Kármán vortex streets and not one, and that they are vectored to the direction of motion. In this sense, their swimming is a variation in fish swimming. The experimenters also show that eel kinematics produces significant secondary flow, and the body undulation appears to interact with that. Producing too many vortices

per cycle and draining energy to the secondary flows might seem counterintuitive to efficient (or fast) swimming, as some indeed believe eel swimming to be. The interaction of the undulating body with the secondary flow might seem to be of higher order importance unless there is an exquisite nonlinear fluid and structure interaction. These are intriguing fluid-structure interactions in eel that require further investigation.

3.11.1 Flagellar Propulsion: Spermatozoa Swimming. Like eels, spermatozoa also use flagellar propulsion [6]. Swimming sperms have probably the lowest Reynolds number ($\sim 10^{-2}$) among swimming animals. A typical sperm is 1 μm in diameter and 25–55 μm in length—the head length is 5 μm, the remaining part being the flagellum (the tail). The helical flagellum is rotated at about 100 Hz by molecular motors embedded in the cell membrane. Its linear speed is reported to be between 0 and 160 μm/s [163]. It is estimated to consume 2×10^{-18} W of power, which can be obtained from the hydrolysis of a single adenosine triphosphate (ATP) molecule; this is considered to be efficient. ATP is like a "molecular currency" of intracellular energy transfer; it transports chemical energy within cells for metabolism. An exception to high-lift swimming and flying is the swimming of bacteria using the traveling wave of a rotating helical filament. The molecular drive is similar to that of a motor, with clearly identifiable stators and rotors. The stator has torque-generating units, and the rotor is made of ten rings of 45 nm diameter. The torque is generated in steps. The electrochemical gradient of sodium ion causes the stator to move or change shape, thereby imparting a torque to the rotor to which the filament is attached. The gradient could be used to slow down the filament rotational rate. The assembly of the molecular motor and the filament is called the flagellum. This is probably an example of the smallest rotary propulsor in nature.

3.11.2 Flagellar Motion. Typically, bacteria use four helical filaments to swim, rotating their body and the filaments. Depending on the direction of rotation (counterclockwise or clockwise), the filaments either bundle or disperse. Bundling allows propulsion. When the filaments disperse, the bacteria tumble and change direction. Experimental simulation has been carried out on a scale-model of bacterial flagellar bundling [164]. In the absence of the body, the bundling phenomenon was found to be purely mechanical—attributable to hydrodynamic interactions, bending and twisting elasticities, and geometry.

3.12 Propulsion of Microscopic Swimming Animals. The marine environment is teeming with microscopic animals swimming and feeding, while being constantly in motion. They swim in the transition range between Stokes ($\mathrm{Re} \ll 1$) and Oseen ($\mathrm{Re} \sim 1$) flows. An ocean-going, submersible, three-dimensional, digital, holographic system has been developed for tracking the motion of such small animals in their similarly scaled, naturally seeded surroundings [30]. The animals investigated are copepods of scale 1 mm, nauplii of scale 0.1 mm, and dinoflagellates of scale 10–30 μm. It is shown that the copepod has two kinds of motion—a periodic 0.5 mm upward jump to a point that is just short of the (lower) stagnation point of the previous recirculation zone, and a slower propulsion between jumps that partially counters the terminal sinking speed, thereby allowing the animal to see the same fluid as it slowly sinks. During the latter stage, the copepod develops a recirculation bubble spanning its extremities. When the recirculation bubble is fully explored or used for feeding, it initiates a jump to an as yet unexplored volume of fluid. The mechanism by which the feeding appendages produce the propulsive jet is not fully understood.

3.13 Limitations of Current Biomechanics Studies. The limitations of current biomechanics studies are discussed here from the point of view of engineering implementation. Fin kinematics is related to force production. Because application is system-based, the question is what kinematics can a fin produce under all circumstances from system point of view, and not what we observe it to have in a narrow, controlled environment. Although animal studies may seem to be closer to the biological world than the studies on their robotic appendages, tethered animal flight, for example, could still not be representative of untethered flight. For example, fruit flies clap their wings during tethered flight, but not in untethered flight [17]. Apparently, the tethered animal flies in desperation to escape trying to maximize wing roll and lift production. It may be that, counter to researchers' best intentions, stressed animals have more mechanisms in their portfolios and are, in fact, harder animals to conduct controlled experiments with than their untethered brethren. For example, it is known only from "genetic" algorithm-based numerical simulation that anguilliform animals have two modes of swimming—a leisurely but efficient swimming and a fast but inefficient swimming [6]. Most biological studies are limited in their range of flight or swim styles and, therefore, may not be representative of insect flight or aquatic swimming in general [46]. So, measurements of animal swimming or flying in a controlled laboratory stream cannot always be generalized.

If we want to truly understand the mechanisms of swimming and flying animals, it is important to study animals in free flight and those that are freely swimming. Free-flight experiments have been carried out in the laboratory [31,75]. Experiments on fish freely swimming around obstacles have been carried out, albeit in captivity [11]. There might be differences in the free swimming and free flight of animals in the wild and those in captivity. Engineers would find that the uncertainties in the measurements of forces, moments, and efficiency in biological studies can be higher than what they are accustomed to—that is, those in laboratory biorobotic model studies conducted in controlled environments. Direct measurement of variables such as forces or efficiency is difficult with animals. Biological databases can consequently be sparse, too. But, these data gaps have sometimes led biologists to come up with insightful hypotheses that have contributed greatly to our understanding.

3.13.1 Limitations of Biological Studies: Production of Cycle-Averaged Versus Instantaneous Forces. The current biological studies on hydrodynamics or aerodynamics are not closely related to studies on controllers. Why should this integration be important? Animals have evolved as a complete system. The force mechanism is intimately related to what kinematics the animal uses for control. Many studies—both with live animals and with their biorobotic renditions—have studied cycle-averaged, hydrodynamic characteristics. However, this averaging smears the phase information and the large instantaneous amplitudes that can be of value to maneuvering. Engineering controllers would normally utilize cycle-averaged values [13]. It is much more difficult to develop a controller that makes use of the instantaneous force vectors [165]. If a controller works on instantaneous force vectors, then what is the best phase in a cycle when the kinematics should be altered? Instantaneous force vectors produced by one flapping fin (an abstracted biorobotic penguin wing) are not in a spherical pattern [8]. The pattern is rather beautiful and has a preferential direction. This suggests that many fins on a hull are required to allow body motion fully in all quadrants. Vectorially, the fins are specialized, rather than generalized.

3.13.2 Limitations of Biological Studies: Anatomical and Hydrodynamic Mechanisms. How do swimming and flying animals operate their pectoral fins to produce the desired kinematics in an efficient manner? In flying insects, a resonant mechanism is used to produce the motion in a narrow range of frequency. In swimming animals, it is not known if the same is true, although anatomical studies of dead animals have been carried out. It would be useful to carry out spring-mass damping analysis of the linkage and muscle mechanism simultaneously with fluid dynamics simulation. Experimentally, it would be useful to make measurements of kinetic energy in the pectoral fin and of damping while the

forces are being produced. Such studies would help the implementation of the high-lift mechanism in an efficient manner.

3.14 Summary. In a simple statement of summary, research on flying has focused on the aerodynamics of the flow over the wing, while research on swimming has mostly focused on the hydrodynamics gleaned from wake studies, and not as much from the hydrodynamics of the flow over the control surfaces. Both flying and swimming involve the production of a leading-edge vortex in the pectoral appendages of various topological complexities. Fish swimming involves the shedding of ring vortices in the near-wake, and the orientation of these vortices and the vector of the central jet determine the mode of swimming—straight or turning, or sinking or rising. There is a close relationship between the kinematics of the body and appendages and performance. In the flagellar swimming of eels or spermatozoa, there are two modes—low speed but high efficiency and high speed but low efficiency. In the former, a wave travels down the body; in the latter, flagellar swimming resembles caudal fin oscillation, which involves simultaneous heaving and pitching motions. The latter is reminiscent of high-lift actuation. It might be possible to design new turbomachines by implementing the mechanisms with appropriate drive systems. For example, low-speed, quiet, and energy-efficient ventilation of mines, tunnels, or buildings [199], or long-endurance swimming could be target application areas.

4 Understanding From Fluids Engineering: Modeling, Experiments, and Optimization

4.1 Science Questions

4.1.1 Origin of Force Generation. In this section, we review the nature of high-lift force generation in flapping foils. Vortex dynamics (such as the formation of LEVs) and flow bifurcations (such as at the stagnation and reattachment points) have been revealed from dye and surface hot-film array studies. The results are synthesized in Refs. [5,8]. The formation of the LEV is shown both by dye and hot-film array diagnostics. Hot-film surface array and force measurements have shown a correlation between unsteady force generation and movement of the stagnation point. The flapping foil has unsteady kinematics. The first contact of the solid surface with the surrounding unsteady pressure field is at the stagnation points. How unsteady, therefore, is the point of stagnation? How is its motion related to the unsteady forces produced? The wall-shear sensor signals are interpreted from the surface hot-film time traces in the following manner. At the forward stagnation points and at the flow separation and reattachment points of the surface, streamline patterns diverge, causing a minimum in wall shear and heat transfer. A surface array of wall-shear sensors was used to mark the oscillating forward stagnation line in a rolling and pitching hydrofoil [8]. Note that lift and the angle of attack are nearly linear in both steady and unsteady flapping foils. The location of the stagnation point is a measure of the local angle of attack and this can be calibrated to lift forces. In this manner, it is confirmed that in steady flow—and, indeed, in unsteady flow as well—the angle of attack and the lift forces are linearly related. There is a slight phase difference (~30 deg) between the two, attributable to the delay between the kinematics and the forces produced due to Wagner effects.

4.1.2 Scaling Laws of Swimming. In bodies producing thrust jets, the frequency of wing oscillation can be expressed as a Strouhal number or as a reduced frequency [166]. In avian biology, the reduced frequency of a full animal is given as $\sigma=\omega c/U$, where ω is the radian frequency (2π Hz), c is mean chord (wing area/maximum length), and U is forward speed [167]. If σ is far below 0.50, then quasisteady flow can be assumed; otherwise, the lift enhancement due to unsteady flow needs to be accounted for. The lift coefficient typically is 0.2–1.3 [5,8] and, therefore, strong unsteady effects can be expected, which were indeed found to be the case. In avian biology of wings, the nondimensional angular velocity $\hat{\varpi}=\varpi\bar{c}/U_t$, where ϖ is the angular velocity, $\bar{c}$ is the mean chord, and U_t is the wing tip velocity [31]. Sometimes, wing tip velocity is expressed as a ratio of the chordwise components of forward velocity at the fin tip due to translation and revolution, $\mu=U\cos(\phi)/R\dot{\phi}$ [63]. In model fruit fly experiments, $\hat{\varpi}$ is in the range 0–0.374 [156]. Later investigations have shown that the Strouhal number is a more relevant parameter for unsteady kinematics of appendages because there is largely a convergence in its value among swimming and flying animals, albeit with some variation. In aquatic biology and aquatic biorobotics, in the case of a flapping caudal fin or pectoral wing, reduced frequency is also known popularly as the Strouhal number, although strictly speaking this is a misnomer [18], and is given by $\mathrm{St}=fA/U$, where f is the flapping frequency (unlike natural frequency in vortex shedding behind bluff bodies), A is the width of the jet downstream of the flapping foil or the excursion of the trailing edge of the fin, and U is the average jet speed or forward or flow speed. The difference between St and σ is in the choice of the length scale—it is flow aligned in the former and across the flow in the latter. These two length scales directly signify the difference between steady flow and unsteady flow. The former length scale is a legacy of classical steady aerodynamics as in a flow-aligned aircraft wing. The latter length scale denotes how much momentum is being put into the fluid at the same frequency. A feathering parameter is also used to express the wing oscillation. It is given as $\chi=(U\alpha_m)/(\varpi h)$, where α_m is the maximum angle of attack in the wing beat cycle, ϖ is radian frequency (2π Hz), and h is one-half of the wing beat amplitude. When α_m is large, $\chi=\alpha_m/\arctan(h_0\varpi/U)$. The feathering parameter is closer to St than σ is. In a two-dimensional heaving and pitching fin, the Strouhal number based on heave amplitude is $\mathrm{St}=4\pi h_0\varpi/U$, where h_0 is the heave amplitude in two-dimensional fin works, ϖ is the circular frequency in rad/s, and U is the forward or towing speed (or maximum heave velocity if hovering), $h(t)=h_0\sin(\varpi t)$, and $\theta(t)=\theta_0\sin(\omega t+\psi)+\theta_{\mathrm{bias}}$. Here, ψ is the phase angle between heave and pitch, usually set to 90 deg for best efficiency. In finite size fin rolling and pitching about a pivot point, the Strouhal number is given as $\mathrm{St}=2f\phi_0R_{\mathrm{av}}/U_\infty$, where $R_{\mathrm{av}}=\sqrt{r_o^2+r_i^2}/2$, and where r_o and r_i are the outer and inner radii in reference to the roll axis, respectively. Foil motion is determined by roll amplitude ϕ_0, frequency $\varpi=2\pi f$, pitch amplitude θ_0, pitch bias θ_{bias}, and the phase between roll and pitch (which, unless stated otherwise, is set to 90 deg). Also, $\phi(t)=\phi_0\sin(\omega t)$, $\dot{\phi}(t)=\omega\phi_0\cos(\omega t)$, and $\theta(t)=\theta_0\sin(\omega t+\psi)+\theta_{\mathrm{bias}}$.

Measurements of forces, moments, and torque have been carried out in a penguin-inspired flapping fin under water in hover and cruise [8]. The results were similar for 20-cm- and 30-cm-span fins. These relationships have been observed for hover. Thrust direction depends on pitch bias and the phase difference between pitch and roll, that is, +90 deg or −90 deg. The magnitude of the thrust is proportional to the squares of roll angle and frequency of oscillation. Power depends on pitch amplitude. The first harmonic of thrust and lift changes little with pitch bias, while the second harmonic depends on mean force. These trends can be used in the modeling of the laws of a controller. During cruise at 0.42–1.25 m/s, these relationships have been observed. In the mean sense, the advantage over steady fin diminishes as speed increases. For the same pitch bias of, say, 10 deg, increasing tow speed produced higher maneuvering forces. Sensitivity to foil profile was low—switching the leading and trailing edges produced no large discernable difference in the time traces of thrust, lift, pitch, or roll power.

4.1.2.1 Scaling laws of Strouhal number of tail fin oscillation and efficiency. Triantafyllou and co-workers [18,26] examined the scaling laws of fish swimming and of oscillating fins. Drag-producing flow past a rigidly held obstacle produces an alternating Kármán vortex train, with an intervening jet pointing upstream. A

Strouhal number defined as $St=fd/U$ of 0.21 describes the universal vortex shedding process in the Reynolds number Ud/ν range of 60 to 2×10^5 [168]. On the other hand, the thrust-producing flapping tail of a fish produces a reverse Kármán vortex train of alternating vortices, with an intervening jet pointing downstream at a universal Strouhal number fA/U of 0.25–0.35, probably in the length Reynolds number range of 10^2-10^7 [16,18,26]. Here, the Strouhal number is defined with f (the flapping frequency of the caudal fin), A (the peak-to-peak flapping amplitude at the tip of the caudal fin), and U (the stream velocity). The instability process leading to the two Kármán streets is different—in the rigidly held obstacle, drag-producing case, it is an absolute instability; in the thrust-producing flapping fin case, it is a convective instability [18]. For this reason, it has been argued that it is more appropriate not to call both universal frequencies Strouhal numbers, and "reduced frequency" might be a better name for the thrust-producing wake. But we saw earlier that Lighthill's reduced frequency has a different combination. So, a more appropriate name is "flapping number." As in the recent trends in medical sciences, it is useful to give informational names rather than eponyms.

4.1.2.2 Other scaling laws of fish swimming. Other scaling laws of fish and fishlike swimming include the wavelength/wave speed ratio of fish tail oscillation and fin stiffness [18]. Some authors have argued that thrust is produced not only by the various fins, but also by the fish body. In the flow over a wavy surface, one expects pockets of trapped, separated flow and high attendant drag. So, how do fish minimize drag and produce thrust to match that level? The ratio of the phase speed of the fish tail and the stream speed $c_p/U=f\lambda/U>1$ for thrust production ranges between 1.29 and 1.37 in cod, and for saithe it is 1.19. Here, λ is traveling wavelength. For two-dimensional surfaces, $C/U>1.0$ leads to drag reduction. In a robotic fish, turbulence in the boundary layer reaches a minimum at $C/U=1.2$. Thus, there is convergence in the various studies regarding the kinematics of the body. But, how much is known about the fluid-structure interaction of the body? Experiments show that, compared with a stiff foil, chordwise flexibility (measured by Shore toughness) can increase efficiency from 0.62% to 0.86%. Theoretical studies accounting for the unsteady effects are needed to understand why flexibility is more widely prevalent in the fins of swimming animals that have lower aspect ratio, the sunfish pectoral fin being one example.

Measurements of force and the motions of the wake vortices in an axisymmetric cylinder equipped with seal-inspired flapping caudal fins, using a phase-matched laser Doppler technique, have been carried out [169]. The authors examined the effects of interaction of the fins and the main body and between fins. The generation of the wake was classified as natural or forced. In the former, Reynolds numbers are low, a continuous sheet of vorticity is produced by the wake, and an instability process leads to wrapping into discrete vortices. Higher-order effects appear in the axial force coefficients when the Strouhal number is >0.15. The axial force coefficient is bounded between two asymptotes—the natural distribution given by inviscid theories at the lower end and an asymptote given by the characteristics of a forced and discrete shedding process at the higher end. In between, the nature is not universal, but transitional, where details such as the mode and frequency of flapping and the number of flaps are influential. Measurements of force and of vorticity-velocity vector maps in the axial and cross-stream planes show the region of the axial thrust jet. The efficiency of axial force production reached a peak below the Strouhal number range of 0.25–0.35. The Strouhal number of tail flapping does emerge as an important parameter governing the production of net axial force and efficiency, although it is by no means the only one; other parameters include flapping frequency and mode of flapping. The efficiency of thrust production, when the two caudal fins move in phase (waving), which is analogous to one caudal fin of fish, is higher than when they are in the opposite phase (clapping). The importance of induced drag has been traced to the flapping mode and the attendant interaction of the flap-tip axial vortices. The phase variation in simulated and minute head swaying can modulate axial thrust produced by the tail motion, within a range of $\pm10\%$, with no significant thrust improvement. This precision indicates that the phase relationship of vortex shedding from various discrete vorticity-generating surfaces is an effective tool of maneuvering in a fish. The general conclusion is that the mechanism of discrete deterministic and phased vortex shedding produces large, unsteady force vectors, which makes it inherently amenable to active control and suitable for precision maneuvering.

It is commonly thought that fish caudal fins have a Strouhal number of 0.25–0.35, because this is the predicted range for maximum efficiency, thereby uniquely relating Strouhal number to efficiency [12,26,169]. However, measurements of propulsion efficiency in animals are few and their accuracy is questionable, and efficiency may be dependent on other factors as well, whereby peak efficiency may occur at Strouhal numbers that are slightly different from the popular values of 0.25–0.35. Other factors may include the angle-of-attack range, amplitude-to-chord ratio, and the phase angle between roll and pitch motions [12,102,170]. Indeed, later measurements [171] show that these effects can cause a 20% reduction in the popular Strouhal number from that for the maximum efficiency. The Strouhal number of captive cetaceans—not their efficiency—has been measured. While the average Strouhal number of each species falls in the accepted range, the numbers vary over a large range within species and among individuals. 74% of Strouhal numbers fall in the range 0.20–0.30 and not in the range 0.25–0.35—the range predicted for maximum efficiency; only 54% of the values fall in the maximum efficiency range. Furthermore, in cetaceans, it is not just the Strouhal number that occurs in a narrow range, but the constituent variables f and A also do. Thus, it is not fully satisfying to claim that the Strouhal number captures the physics of thrust generation.

In the biorobotic work on a cylinder with attached caudal fins, efficiency depends on Strouhal number and another yet unidentified variable [169]. Measurements of efficiency have been carried out on a single abstracted penguin fin in water. The fin was undergoing rolling and pitching motions, and torque sensors were used on roll and pitch motors to measure efficiency. In the nonhovering case when pitch bias is set to zero, the data offered an opportunity to determine the effects of Strouhal number and fin kinematics on efficiency. It is shown that efficiency (η) can be as high as between 0.5 and 0.6 at Strouhal numbers of 0.25–0.70—a range higher than commonly given [26] for fish, which is 0.25–0.35. Here, the Strouhal number is defined with fin motion amplitude equal to the arc length traversed by the point on the fin that divides the swept area in two. Furthermore, for the single fin, efficiency has a peak distribution with Strouhal number and also with pitch amplitude. Pitch amplitude was varied in the range of ±15 deg to ±65 deg, and efficiency was found to peak ($\eta>0.55$) in the pitch amplitude range of ±25 deg to ±45 deg in the Strouhal number range of 0.28–0.55. Peak efficiency occurred at higher Strouhal numbers at higher pitch amplitudes and at lower Strouhal numbers at lower pitch amplitudes.

Because Strouhal number and efficiency have not been measured simultaneously in any species, it would be more accurate to conduct a direct numerical simulation of animal (fish/dolphin) swimming and calculate propulsive efficiency and Strouhal number to resolve this issue definitively. Perhaps the MIT Robotuna or other emerging biorobotic fish could also be used in a biorobotic experimental work to validate the simulations. In any case, the Strouhal number captures the bulk of the unsteady effects and is useful in the development of control laws. Pitch amplitude can offer more accurate tuning of the laws.

4.2 Modeling of Animal-Inspired Swimming. Penguin thrust has been modeled using experimental data on the drag of a

wingless carcass cast and the forces produced by flapping wings [85]. The flapping frequency was measured from swimming penguins. A blade element analysis was used to compute wing beat thrust. In blade element analysis, the wing along the span is divided into many segments, and quasisteady two-dimensional flow is assumed over each segment. The forces on the segments are summed to obtain the total force on the wing. The blade element analysis was found to be more reliable because it showed close agreement between the thrust and drag estimates, in the parameter range of penguin swimming studied. An unsteady modeling on the other hand did not give close agreement between thrust and drag, and future work is needed. The submerged and surface swimming powers (N m/s) are modeled, respectively, as $P_{T\text{-sub}}=3.71U_b^{3.0}$ and $P_{T\text{-sur}}=5.88U_b^{3.6}$, where U_b is the mean forward speed of the swimming or animal. LEV-based unsteady actuator flows do not have strong effects of Reynolds number, and inviscid effects dominate. A closed-form expression—a rarity—of forces and moments produced by a general two-dimensional Joukowski foil in arbitrary motion is available [172]. The theoretical hydrodynamic method of conformal transformation and point vortices is used in the inviscid analysis. Thrust-producing foil oscillation parameters reproduce a nonsinusoidal force time history that is beyond the scope of linear theory. The work shows that the effects of added mass and vortices are independent.

4.2.1 Modeling of Penguin Swimming as a Pendulum. The thrust jet wake vorticity patterns of fish swimming and fluttering objects bear similarity [12,19]. A simple plunging plate also produces the detailed features of flow seen in dragonflies [65]. This result can be used to model dolphin swimming as a pendulum. The fluid-structure interaction of a dolphinlike animal is used to produce the relationship between Strouhal number, speed, and the kinematics of the caudal fin (frequency and amplitude of oscillation). The natural frequency of oscillation is the inherent frequency in the Strouhal number because the body oscillates like a pendulum. The natural frequency is given by the body length, as in the law of the pendulum. The variation in frequency with body length and speed is described by this relationship.

4.2.2 Methods for Calculating Lift Over Wings Due to LEVs

4.2.2.1 Leading-edge suction analogy: Nonflapping wings. Before we consider biology-inspired, unsteady high-lift, it is instructive to recall what relevant matter is known from steady-state classical aerodynamics. A two-dimensional or large-aspect-ratio steady wing separates at high angles of attack and stalls when lift forces precipitously drop. On the other hand, delta-shaped main or canard wings that have a low aspect ratio and sharp leading edges are deliberately operated at high angles of attack and are partly separated near the leading edge in steady flow. The pressure distribution around the sharp leading edge produces suction, and a large detached LEV ensues. However, instead of approaching stall, the wing lift is nonlinearly augmented substantially above the potential lift. The steady flow vortex lift can be accurately calculated using computational methods, such as nonlinear panel methods or Euler or Navier–Stokes methods. The steady flow vortex lift component of the total lift has been modeled by assuming that the low pressure in the vortex core in the detached flow originates from the leading-edge suction effects in attached flow. The vortex produces a force that is normal to the chord, whereby it also has a small drag component. Another steady flow method, even simpler, is to add the component of drag due to a normal velocity to the delta wing to the lift direction.

4.2.2.2 Cross-flow drag vortex analogy: Flapping fins. The LEV due to three-dimensional rolling and pitching fins is analogous to the cross-flow drag vortices of the fin when normal to flow, as in a bluff body. The cross-flow drag vortices of a static fin placed normal to a steady flow are similar to the dynamic stall vortices of the unsteady fin [5,8]. It has been proposed that the rolling and pitching motions constantly change the angle of attack and keep the vortices attached to the fin. In this manner, stall is prevented and the steady behavior of lift and drag applies and one needs to know only the instantaneous angle of attack from the fin kinematics. Excellent agreement with instantaneous and time-averaged forces and power in flapping fins has been obtained. In delta wings, in the presence of a strong, adverse pressure gradient, the LEV bursts. When this happens, vortex lift is lost. No such vortex bursting and loss of lift have been reported in swimming and flying animals or in flapping wings.

4.2.3 Quasisteady Modeling. The difference between quasisteady modeling and unsteady modeling of forces produced by flapping wings has been examined [36]. The work reflects great physical insight. It was proposed that, if the mean lift coefficient required for hovering exceeds the maximum lift produced in steady state, then the assumption of quasisteady state is not valid. However, if the mean required lift coefficient is below the maximum measured steady lift coefficient, then the assumption might be valid. Literature survey indicated that the mean value of lift coefficient required for hovering is higher than the maximum measured steady-state values. This meant that unsteady models and not quasisteady models are required to compute insect flight. However, earlier works [36] did not benefit from accurate measurements of mean forces on isolated wings and of the time histories of forces [156]. Such measurements show that the maximum mean value of the lift coefficient of the wing is much higher than previously thought, and quasisteady modeling might be applicable. Sane and Dickinson [156] gave such a model with remarkably good general agreement with the measurements of time histories of forces. Total instantaneous force on the wing is considered to be the sum of inertia force due to added mass, instantaneous translational force, rotational force, and force due to wake capture. The first term is calculated using blade element analysis. The second term is obtained from the measurements of lift and drag. The rotational forces are determined at times when inertia and wake capture forces are small, by differencing the estimates of translational forces from the measurements of total forces. This type of quasisteady models is useful in understanding the mechanism budget. However, the model in Ref. [156] might benefit from further improvement. For example, during the short periods when upstrokes and downstrokes switch from one to the other, the spikes in the measured lift and drag values are not reproduced by their revised quasisteady model. But note that the wing kinematics used is not a simple harmonic—the translational and rotational velocities are constant during most of the stroke and abruptly change near the ends of the strokes. In previous sections on vortex methods and potential theories, the contributions based on conventional aerodynamic theories are given for modeling the forces produced by the wings of flying insects. The extension of the quasisteady model in Ref. [156] to flexible fins has not led to good agreement with the measurements of lift, thrust, or power for fish [134].

4.3 Efficiency. For aquatic propulsion, η, the hydrodynamic efficiency of propulsive flexural movements, has been defined as similar to Froude efficiency of a propeller as $\eta=U\bar{P}/\bar{E}$, where U is the mean forward velocity, $\bar{P}$ is the mean thrust required to overcome what viscous drag the fish would sustain for forward velocity U if it remained rigid and symmetrical, and $\bar{E}$ is the mean rate at which flexural movements work against the surrounding water [91]. For heaving and pitching fins, propulsion efficiency is defined as $\eta=C_T/C_P$, where C_T is the coefficient of thrust, C_P is the coefficient of power, and η_{thermal}, η_{electric}, and $\eta_{\text{hydrodynamic}}$ are electric, thermal, and hydrodynamic efficiencies, respectively (Fig. 4). The thermal efficiency refers to the mechanical efficiency of a flying insect based on the measurements of heat produced after flying [46,173,174]. The hydrodynamic efficiency is based on measurements of roll and pitch torques in the case of single fins [5]. In the case of the entire sunfish, the hydrodynamic effi-

ciency has been defined as the ratio of added downstream kinetic energy to the total fluid kinetic energy [131]. Efficiency in rolling and pitching fins of finite size is defined as $\eta = \bar{T}U_\infty / \bar{P}_{\text{hydro}}$. It can be shown that $\bar{P}_{\text{hydro}} = -\tau_\phi(t) \cdot \dot{\phi}(t) - \tau_\theta(t) \cdot \dot{\theta}(t)$, where τ is torque—roll (ϕ) or pitch (θ). In PIV wake traverse of the entire fish, the hydrodynamic efficiency has been defined as η = (added downstream kinetic energy)/(total fluid kinetic energy).

Measurements of propulsive efficiency of animals are extremely valuable but sparse. The output power of penguins has been measured from drag estimates [85,175]. The input power was measured from oxygen consumption. The ratio of these powers (called the energetic efficiency) varied with speed U as $\eta_0 = 0.103U\ (\text{m/s})^{2.8}$. The maximum efficiency η_0 measured at 1.26 m/s was 0.192. If the maintenance metabolism is subtracted from the input power, the propulsive efficiency is about 0.247. Literature has reports of considerably high estimates of propulsion hydrodynamic efficiency of penguins, dolphins, and other swimming animals that are indirectly obtained via hydrodynamic modeling, and they should be treated with caution. Measurements of forces and input power are not carried out with a tethered fish—a technique used with flying insects. Instead, an indirect method of estimation is from a balance model that measures the movement of the center of mass, which is body acceleration, of fish swimming in a flow tank [134]. The fish move back and forth over a cycle. It is estimated that the mechanical efficiency of the pectoral fins (i.e., the cycle-averaged thrust measured $\times U$/power measured) of three spine stickleback fish, a very small fish that has flexible fins, is between 0.13 and 0.29. The hydrodynamic efficiency of an abstracted penguin fin for hover and cruise has been measured [5]. These matrix (flow and fin kinematics) based conventional style measurements took nearly 18 months to carry out and were parametric in approach. Subsequently, a "simplex" and annealing based methodology was developed to search for the best efficiency at a given coefficient of thrust. The efficiency envelope was reproduced typically in a few minutes, starting from any randomly selected set of kinematic parameters. No explicit knowledge of hydrodynamics was used. However, selective input of hydrodynamic insight further accelerated the optimization process. In principle, this approach might allow vehicles to perform outside the design envelope. Fish swim in a way that all side forces are zero over time, drag is minimal, and thrust equals drag. Most studies have examined biomechanics from this point of view. For maneuvering, such budgeting for nonzero side forces has not yet been carried out. How animals match fluid-structure impedance to maneuver efficiently or increase thrust is an open question. The design laws that account for the fluid-structure interaction are not known.

4.4 Flapping Foils and Traveling Wave Propulsion. Flow visualization shows the wake structure of a low-aspect-ratio (span/chord=0.54) flapping plate at Strouhal numbers below and above 0.25 [176,177]. Below a Strouhal number of 0.25, the wake consists of single horseshoe vortices of alternating sign shed twice per cycle, which is termed "2S type" [178]. Above 0.25, a pair of vortices is shed in each half of the cycle, which is termed "2P type." Not all fish roll and pitch their pectoral fins for propulsion. For example, sting rays are thought to have enlarged pectoral fins, and undulatory waves pass down the fins to generate thrust—a form of propulsion called *rajiform*. The variation in the kinematics of the fin and the muscle motor pattern with speed has been examined [179]. Velocity increases with fin-beat frequency, wave speed, and the duty factors of the pectoral muscles. However, fin amplitude and the duration of muscle activity do not change with velocity. There is a clear delineation between muscle groups that do positive and negative work. Experiments on the oscillating fin model of a ray fish show that a wave travels downstream while the fin rolls [180]. The fin produces thrust during both the upward and downward strokes. The maximum efficiency is estimated to be 0.40, which occurs at a Strouhal number of 0.25, based on the spanwise average deflection of the trailing edge, and not on the wake width [101].

4.5 Real-Time Optimization of Leading-Edge Vortex. An optimization algorithm for moving bodies called the covariance matrix adaptation evolution strategy has been developed [162]. It relates the body kinematics with the cost function in an efficient manner. The property of the algorithm is that it identifies many minima rather than a single optimum point. In the numerical investigation of the optimization of the drag reduction in a cylinder, the algorithm converged after 260 iterations, and a Cray J90 computer took 4 h of CPU time. This can be compared with the experimental flapping foil optimization [5] of 4 min and 40 iterations for optimization of efficiency using a Pentium 2 personal computer, where the CPU time is less. The number of iterations required is probably a somewhat fairer basis for comparison than the CPU time because the flow is "free of time cost" in the experiments. The code is available as a patch that might facilitate future use in other simulations [162]. The value of the code appears to be in the optimization of computationally intensive problems. Real-time optimization and the control of the hydrodynamics of one or the assembly of many fins are exciting new areas of research where both cycle-averaged and instantaneous approaches are being pursued [13,165].

5 Applications of Understanding

There are lessons learned by comparing biological locomotion designs, their biorobotic implementations, and their conventional engineering implementations [19]. Gaps between biological designs and their biorobotic renditions remain. The differences are spread over many layers of underlying science principles/mechanisms, sensor characteristics, energy sources/handling, philosophy/architecture of controllers, and materials. Biological systems use analog processing and are adept at computing a vast number of events via nonlinear algorithms for actuator control, a process that is beyond the capability of digital technology today. Transitions from biology to engineering can be seen as a structure-function relationship where fabrication difficulties come across as the most important impediments to such transitions [181]. While we have focused on the hydrodynamics and aerodynamics of swimming and flying animals that lie external to the body (such as the formation of LEVs), less attention has been paid to how animals produce the observed wing kinematics. Engineers have been hesitant to apply unsteady fluid dynamics mechanisms of high-lift due to concerns regarding performance cost (penalty) and reliability. Therefore, it is instructive to understand how fish mechanically produce the intricate fin motions and hold them appropriately under load.

Generalized biomechanical models of the muscle, tendon, and bones of fish have been developed [182]. Physical models show the existence of strain energy storage under bending [183]—a system that can be used to store energy during deceleration of the control surface and that can be used during acceleration to enhance electromechanical efficiency. Fish that cruise over long distances have a fiber matrix that criss-crosses at 45 deg to the vertebral axis. This fiber architecture, along with twisted spines, is a candidate for such energy storage. The importance of energy storage systems in swimming and flying animals and their impact on unsteady fluid-structure interaction need further research. The oblique tandem arrangement of fish has been used to provide force transmission pathways to the backbone and gain mechanical advantage to bend the body. In nature, parts have broad application but poor performance in a narrow range, while it is just the opposite in man-made parts. For this reason, man-made assemblies of biorobots are unlikely to closely match animals. In other words, a hybrid system would require a judicious mix of architecture in nature and man-made components.

Theoretical analysis and experiments with two-dimensional flapping foils agree well in thrust in a wide range except for the case of zero forward speed [184]. A 7.5 m/s shallow-draft boat of 900 kg payload was designed. The conclusion was that oscillating foils can provide efficient propulsion with a high degree of maneuverability. For feasibility, hydrodynamics is not a limitation, and the mechanical drive system was considered a challenge in 1968, which may not be the case today.

5.1 Transitioning the Evolved Hydrofoils to Engineering. The tables of cross sections of National Advisory Committee on Aeronautics (NACA) profiles have played a seminal role in the development of aerodynamic and hydrodynamic turbomachinery blades, aircraft wings, and submarine sails. But they are meant to be used where dynamic stall is undesirable. So, the first question is as follows: How close are animal fin or wing cross sections to NACA profiles? Probably, a more useful question is the following: What can we learn from their flexible profiles and three-dimensional nature? The first question calls for a careful documentation of animal fins and dissemination of such fundamental data of nature's legacy to us. This was realized by this reviewer while heading the Biorobotics Program at the Cognitive and Neurosciences Division of the Office of Naval Research. Professor Frank Fish of Westchester University was commissioned to organize a team, in collaboration with the Smithsonian Institution and others, to collect CAT scans at 1 mm intervals. (The data set is contained in seven DVDs, which are in the public domain in the United States of America and may be obtained from Professor Fish of the University of Westchester, Westchester, PA.) Animals whose control surfaces were scanned are whales, seals, sea lions, manatee, penguins, sea turtles, rays, shark, and tuna. The data set remains largely unexplored. The highlights of the animal control surfaces are long, thin trailing edges particularly near the wing tips, wing-hull juncture cross sections, and thick leading edges. Because the scans also reveal the inner bone structure, the mass distribution can be gleaned as a clue to the elastic property of the dynamic wings. Measurements of the bodies and flukes of cetaceans have been reported, although they are not comprehensive. The cross sections and planforms of the flukes are thought to be related to performance. A systematic study of the relationship of these sections with those of the NACA profiles is worth undertaking. In particular, unlike the two-dimensional NACA profiles, the above data sets might give us benchmarks of what three-dimensionalities nature has optimized into. Measurements of humpback flippers show that the cross section resembles NACA 63_4-021 and NACA 0020 profiles [185,186]. The humpback flipper leading edge has been claimed to delay stall while increasing lift and decreasing drag. The experiments, however, were carried out in steady flow. Quasisteady modeling [5] suggests that the dynamic stall delay characteristics are an extension of the steady-state lift and drag characteristics. It is useful to know of steady behavior, but this should be considered to be only a precursor of more that needs to be known in unsteady flows. Furthermore, the six-series NACA profile was developed with an emphasis on laminar flow. At high angles of attack, such foils are less likely to reattach because the low kinetic energy fluid near the wall succumbs to the increasing pressure energy in the streamwise direction. So, how can the cross section of whale wings with their bulbous leading edge closely resemble the six-series in the mean? The answer might lie in the high Reynolds numbers of flippers. Even for steady flows, there is a need to focus on high Reynolds numbers where the flow might naturally become turbulent and allow reattachment of stall vortex while retaining the low-drag advantage of laminar flow in many regions of the flipper. What the close NACA cousins of the flipper cross sections are is an important question because the cross section presupposes similar characteristics.

5.2 Underwater Vehicles. Underwater vehicles implementing pectoral and caudal fins inspired by swimming and flying animals have been reviewed [19]. The research originating at the Office of Naval Research received focus and the need to integrate the high-lift mechanism with neuroscience-based control and artificial muscle was put forward to allow "instantaneous" phase synchronization of many actuators. The need to focus on science principles instead of biomimicry was also emphasized. The biorobotics progress made at the Naval Undersea Warfare Center in Newport, RI, up to the year 2000, has been reviewed [12]. The work pointed out the value of fish-inspired robotics to low-speed maneuvering, rather than to straight high-speed propulsion where propulsor efficiency has reached a high level of perfection. The value of artificial muscle in the context of active camber control of propulsor blades was explored.

5.3 Seal-Inspired Vehicle. Bull elephant seals have dual flapping caudal fins. Inspired by them, an experimental model was built with a pair of flapping foils at the tapered tail end [169]. The foils could clap (out of phase) or wave (in phase). A divider plate was placed between the foils to enhance the clap and fling effects. Efficiencies as high as 0.60 of the flapping foils and as high as 0.40 of the combined cylinder and foils were measured. For the waving foil motion (which mimics a fish's caudal fin motion), the dominant Strouhal number was close to that found in fish but only in a narrow frequency range [26]. A sliding protrusion was also incorporated near the nose to simulate the formation of any vortices due to the head swaying of animals. It was found that this modulated the thrust within $\pm 10\%$.

5.4 Biorobotic High-Lift Vehicles. A flapping wing producing a LEV of high-lift is an intelligent structure—not in the cognitive sense, but in the sense of efficient and flexible use of structures. "Challenge is not simply to replicate an insect wing, but to create a mechanism that flaps it just as effectively" [181]. Figure 3(*a*) shows a six-finned BAUV built at NUWC by the author's team, whose hull is cylindrical and rigid [8,13]. The fins are abstracted penguin wings. Two generations of vehicles, the BAUV and SPLINE (Fig. 4), have been built, the latter with motors of higher torque and efficiency but fewer degrees of freedom. The fins are simplified rigid versions of penguin wings [5]. Both open-loop and closed-loop controllers have been developed [13]. An olivocerebellar nonlinear controller has also been developed to produce instantaneous phase synchronization of the fins or give them any desired phase shifts [165]. Each fin is capable of operating at its own kinematic settings—such as frequency, roll, pitch angle, and phase difference between roll and pitch. The result is a vehicle with multiple degrees of freedom. The following examples of precision maneuvering have been accomplished: practically zero-radius turning (Fig. 3), alternate pitching, crabbing, entering, parking in and leaving a small side chamber in a channel, precision depth and thrust control, and sideways motion between two narrow parallel walls. The vehicle's displacement is similar to that of shark, and its propulsive power is similar as well. The vehicle produces very low levels of radiated noise, which is a global measure of the absence of conventional sources of propulsor noise such as ingested turbulence, blade tonals, and trailing edge vibration. At MIT, several versions of a Lycra and foam sheathed robotic vehicle (the Robotuna) have been built that are very similar to a bluefin tuna. The goal was to build a propulsor that is better than the conventional propulsors, remaining faithful to fish form but to only the zeroth order. The drive system resided outside the fish. The Robotuna is a useful exercise in the synthetic integration of our understanding of caudal fin-based fish swimming, kinematics, scaling, control architecture, design, fabrication, and practicality. The Robotuna has allowed the direct confirmation of Gray's paradox [105]. It is indeed true that the drag of the swimming fish, constituted of an undulating body and an oscillating caudal fin, is lower than that of the rigid body, where the body is not undulating and the caudal fin is not oscillating. However, while Gray's paradox [105] implies a sevenfold reduction in drag, the reduction in the Robotuna is about half. The Robotuna work has succeeded in

creating a great deal of popular and professional interest in biorobotics and has been an invaluable training ground. Modern underwater propulsors are highly efficient (>80%), and it is unlikely that any fish-based mechanism would have significant impact on the design. Realizing this, it has been more fruitful to focus attention on the high-lift mechanism of pectoral fins and on maneuvering rather than on cruising [19,169]. However, at low speeds (<5 kn), propulsors could be supplanted by biology-inspired propulsion systems. The pectoral fin kinematics of the black bass on a rigid cylinder has been implemented [98]. Three motor and gear drives are used to roll the rigid fins forward and backward, upward and downward, and for rotation about the span. It is unclear if any high-lift LEV is being utilized or what the efficiency is. A rule-based fuzzy controller has been developed. A ± 90 deg phase difference between pitch and roll between the left and right fins is used for turning [13]. Maneuvering in a quiescent tank has been demonstrated.

5.5 Biorobotic Rendition of Propellers. Inspired by the fanned wing tips of soaring birds, winglets have been successfully incorporated into modern aircraft. The fanned wing mechanism of breaking up induced drag vortices for drag reduction has been used to design a novel propeller that has no wing tip [187]. A three-bladed propeller, for example, has the wing tips joined in a convoluted ring. Quiet and efficient performance is claimed.

5.6 Vortex Energy Extraction and "Free-Ride". Behavioral observations indicate that flocks of birds and schools of fish (or fish behind obstacles) orient in a way that suggests they are utilizing the energy in the incoming vortex to enhance propulsion efficiency. These hypotheses receive support from synthetic laboratory experiments [48] and the controlled experiments with fish swimming in a laboratory stream behind an obstacle [25]. Flow visualization at a low Reynolds number of 550 and complementary force and torque measurements have been carried out at a high Reynolds number of 20×10^3 on a two-dimensional foil heaving and pitching behind an obstacle in a stream. The effects of the phase relationship between the incoming Kármán vortex stream and the foil oscillation on the resulting vortex street in the wake of the two interacting bodies and on the efficiency of the foil's propulsion have been examined. The foil in this synthetic arrangement may be likened to a fish keeping station behind an obstacle shedding Kármán vortices in a stream. Three types of vortex streets may form. In the noninteracting case, the counterrotating Kármán vortices from the two bodies remain distinct in the resulting wake. In the other two types, the vortices from the body and the foil interact destructively and constructively and, although measurements are not available, it is believed that circulation of the vortices in the resulting wake is diminished and enhanced, respectively. The peaks in efficiency and, therefore, in vortex-energy extraction are associated with destructive interaction, and the troughs in efficiency are associated with constructive interaction. Echoing these results, the PIV technique has been used to show that a trout alters its body undulation to match the Kármán gait [25]. Electromyogram time traces show that muscle activity is reduced during such favorable interaction. It was not investigated if the Kármán vortices are also weakened behind the trout when their energy is apparently extracted. A budgeting of the vortex circulation in the resulting wake would provide a quantitative validation of the hypothesis of energy extraction and destructive interaction. A foil rigidly held to a boat experiences thrust due to surface waves [188]. The wave changes the foil's angle of attack, which effectively undergoes heaving and pitching motions. The streamwise turbulent intensity in the wake of a pitching foil can be canceled by another pitching foil downstream by proper control of the relative phase and amplitude of the pitching [189]. It has been shown that a passively mounted high-aspect-ratio foil located behind a vortex shedding bluff body resonates in the natural mode with the incoming Kármán street [25,190]. In the process, the foil can extract energy from the vortices and propel itself upstream. The energy extracted is sufficient to overcome the foil's drag. Energy extraction by the large-aspect-ratio foil is apparently higher than that in fish, whose aspect ratio is lower. It appears that the foil in this experiment may have been extracting a very small amount of the available vortex energy. It would be useful to explore the parameter space further in this experiment to increase energy extraction. It would also help if we could separate what the foil accrues from energy extraction and the thrust that it self-generates because the vortex imposes heaving and pitching motions. In other words, the dynamic and kinematic contributions of the incoming vortex street are worth separating. Practical devices for energy extraction from Kármán streets in water have been attempted where a polyvinylidene difluoride (PVDF) "eel" is freely excited by a Kármán vortex street behind a bluff body [191]. PVDF is a polymer that has a ten times larger piezoelectric property than other polymers and may be suitable for capacitive buildup and trickle charging of power storage devices. This work focused on Reynolds number effects of the membrane. A resonance between the imposed Kármán perturbation and, ideally, a damping-free membrane is most desirable to maximize strain energy and mechanical power. It was possible for a membrane to oscillate at the same frequency as that of the Kármán vortex, with identical amplitude and wavelength—a desirable "lock-in" condition. Modeling of the membrane as an Euler–Bernoulli beam gives the condition for lock-in. Work is needed to demonstrate energy harvesting over a range of Reynolds numbers. Extraction of energy from shed vortices is enticing to fluids engineers. However, the dynamics of drag varies richly with Reynolds number and the nature of the bluff body and how rigidly it is held. Matching electroactive materials over such a wide dynamic range is a challenge. Demonstration of a meaningful reliable net benefit remains elusive.

5.7 Flagellar Motion-Inspired Mixer. Pumping fluid in small systems efficiently is a challenge because the flow has a low Reynolds number that is viscosity dominated, and it has small scale. Chaos-based systems have not been successful. Low concentrations (<0.5% by volume) of bacteria and their flagellar motion have been used to enhance mixing in microchannels [192]. In a Y-shaped microchannel, using a fluorescing technique, the authors show that the diffusion coefficient rises markedly when motile *E. coli* bacteria are inserted into a stream of Dextran, which has high molecular weight. Direct visualization of bacterial motion and pressure drop, together with wall-shear measurements, would throw more light on the nature of flagellar mixing, efficiency, and their practical value.

5.8 Flagellar Swimming Robot. A single, helical, rigid flagellum has been built and its thrust has been compared with the measurements given by resistance force theory [193]. The experiments were carried out in silicone oil (350 cS viscosity) and the Reynolds number was comparable to that of microorganisms. The head of the swimmer was a 14.5-mm-diameter, 16.5-mm-long, two-phase stepper motor. The flagellum consisted of 1.23-mm-diameter steel wires, and it had a helical diameter and pitch of 14.8 mm. The frequency range was 5–15 Hz. The measurements of thrust are in near agreement with those calculated using resistive force theory. Thrust force varies linearly with frequency. A small swimming robot with a single helical rigid flagellum has also been built [193]. It weighs 1.85 g and is 16 mm in diameter and 46 mm long. It swims in silicone oil of viscosity 100 cS. The body of the robot is a brushless dc motor covered with Styrofoam for buoyancy control. The flagellum is made of a 0.42-mm-diameter steel wire. The wavelength is 13 mm, the wave amplitude is 23.5 mm, and the length of the flagellum is 20 mm. Linear swimming at predicted velocities was achieved.

5.9 Lateral Line-Inspired Sensors. Seal whiskers, the hairs on spider legs, the lateral lines of fish, and the tiny hairy cells in the human inner ear are a clustering of sensors that are used to

detect predators or preys. These sensors detect, amplify, and convert sound waves or vibration/pressure fluctuations or distributions. The clustering, filtering process, motion, and stereoscopic differencing give these sensors directional ability and three-dimensional ranging. They act as a substitute for vision. "Hair sensors" have been shown to detect flow speeds of 1 mm/s, although sensor noise is an issue. Rapid signal processing to allow the cognition of the spatial patterns of the surroundings is also a challenge. Controllers that make use of the sensory feedback also need to be developed. Micromachining of polymer has been used to build cantilever arrays that act as strain gauges or hot-film arrays. "Lateral line sensor arrays" have been shown to be effective in detecting dipole sources [194].

5.10 LEV-Based Flapping Machines. Insects stay aloft and propel themselves by pushing air downward and tilting the plane of their wing beat. During hovering, most insects move their wings back and forth in a horizontal plane, and this plane is tilted more and more as the insect moves forward at higher speeds [34]. Observing the similarity with rotor craft, the insect flow field has been modeled using the theoretical foundation of propeller aerodynamics [148,195]. Insect-inspired flapping machines have also been designed [14]. However, rotor craft blades are dominated by rotation, while insect flight wings are dominated by oscillatory motion. Differences in the mechanism and inaccuracies in modeling can be expected, although they both have the ability to hover if they are modeled in a similar manner. Animals use an elastic storage system to oscillate wings [4]. Biorobotic designs of such systems are yet to be carried out and could be attempted with artificial muscles. It has been proposed that the LEV dynamic stall mechanism be used for the micro-air vehicle design, rather than the fling and clap mechanism [14]. Design laws are given, and it is suggested that the preliminary design be based on hovering not only for simplicity but also because if the vehicle hovers well it is likely to support its mass and have adequate power at all practical speeds.

5.11 Micro-Air Vehicles. The micro-air vehicle (MAV) is an application where the old and new approaches to practical flight compete. In modern flying vehicles that are large, lift generation and propulsion are treated separately. However, in insect flying, no such separation is made. The MAV design, based on traditional fixed-wing aerodynamics, is more mature than that of flapping wings. MAVs are roughly the size of the palm of our hand. The current state-of-the-art is given in Ref. [196]. The link between the aerodynamic design and the insect high-lift mechanism of LEV and the appropriate wing kinematics that produce and sustain the LEV with MAVs have been discussed [197]. The microflying insect (MFI) is an example of the implementation of the high-lift principle of insect flight [198]. The MFI is remarkable in its closeness to fruit flies. Laboratory tethered flight has been demonstrated to show that adequate lift forces are produced. Further progress has been limited by the availability of energy sources.

5.12 Performance Enhancement of Existing Devices. In one of the most innovative applications of the high-lift principle, a novel delayed-stall propulsor has been patented [199]. Normally, propulsor designers strive to achieve azimuthal uniformity of flow. However, in the delayed-stall propulsor, there is a variable pitch in the upstream stator blades, whereby the downstream, rotating, conventional rotor blades experience a variable gust that simulates the heaving and pitching motions of flying insects. In other words, instead of oscillating the blades, Usab et al. [199] produced an oscillating flow and subject the rotor blades to that flow, which constantly changes the angle of attack as the blade moves circumferentially. The rotor blades are set at higher angles of attack than normal for effective delayed-stall vortices to form. Furthermore, the diametrically opposite blades are given an opposite but equal pitch about a mean value to cancel the noise sources. The design leads to an increase in total pressure rise across the fan stage compared with the baseline case, the maximum increase being 50%. Alternatively, in a propulsor at the same forward speed, a reduction in rotational rate is possible, potentially leading to a reduction in noise of 4 dB, which is measurable.

5.13 Fishlike Tail Articulation of Propulsor Blades for Wake Momentum Filling. In a propulsor where a rotor is located behind a stator, the wake velocity defect of the stator causes a lift gradient on the rotor blades, which is a source of noise. Because of the well-defined periodicity of rotation and blades, the noise produced appears as a spike in the noise spectrum and is called a blade tonal. Observing that fish tail articulation produces a jet, this reviewer had proposed that the tails of the stator blades in an underwater propulsor be articulated appropriately to exactly fill the wake deficit. Preliminary theoretical and experimental investigations indicated that some reduction in noise might be possible [10]. More extensive experimental investigations were subsequently carried out at realistic Reynolds numbers and in the Strouhal number range found commonly in fish, although not in a full-scale propulsor [200]. A net noise reduction of 3–5 dB is indicated although difficulties in scaling remain. Future work should focus on accurate simulation of flow and noise and the use of artificial muscles for active tail actuation.

5.14 Octopus-Inspired Suction Cups. Aquatic animals such as octopus, limpets, and echeneid fish are reported to have the ability to adhere to other animals with rough skins for feeding and riding. These animals notably utilize suction cups and hooks. Do animals produce higher levels of suction (that is, lower differential pressures) in their suction cups and how do they attach to rough host surfaces under water without any seeming continuous suction cost to overcome leakage [9]? In laboratory measurements of the differential pressure inside the suction cup and in the ambient until the cup was released, the release force—expressed as tenacity (release force per unit area of adhesion)—was found to be similar to that in animals. However, it was found that when the host surface was rough and/or porous, the suction pump had to be left on for the man-made cups to remain attached. Is this a disadvantage in terms of energy consumption and complication over what animals do? Animals do not have any central pump or plumbing connecting their suction cups. They have a radial and circumferential muscle architecture that expands to create lower internal pressure. However, they have a microfine beaded cup-lip construction with radial grooves. Observing the matching of host surface (sharkskin riblet) topology in echeneid fish suckers, it was found that biorobotic sealed contact over rough surfaces is also feasible when the suction cup makes a negative copy of the rough host surface. However, for protracted, persistent contact, the negative topology would have to be maintained by active means. Energy has to be spent to maintain the negative host roughness topology to minute detail, and protracted hitch-riding on a shark for feeding may not be free for echeneid fish. Further work is needed on the mechanism and efficiency of the densely populated tiny actuators in fish suckers that maintain leak-proof contact with minimal energy cost and the feasibility of their biorobotic replication.

6 Research Recommendations

Biology-inspired unsteady fluids engineering has untapped payoffs in efficiency, noise reduction, and performance—such as lower pressure drop/increased mass flow and lightweight, low-power passive sensor technologies. To succeed in the transition of the sciences and the design principles gleaned from biology, it is recommended that some benchmarks be identified—the benchmarks could be from existing performers. It is best to apply the principles to gain in function rather than mimic any animal in morphology or function because human needs are optimized for different functions than those in animals. The end product is likely to have a greater practical impact if the unsteady hydrodynamics or aerodynamics is integrated with appropriate control methodologies right from the beginning. Although electroactive polymers

are not yet developed as actuator materials, integration of the hydrodynamics with such polymers would usher in many successful transitions. The laws of probability tell us that integration of disparate disciplines is problematic, but such integration also offers the opportunity for significant payoffs. Caution needs to be exercised in slavishly mimicking nature. For example, it is known that the porpoising behavior of the penguin, where it builds up speed and then spreads bubbles around its body, reduces drag and helps it leap in the air. Recent embedded data loggers indicate that penguins traverse only 3.8% of the total distance traveled during the porpoising cycle [201]. They "porpoise" only at the beginning and end of their trip, presumably to avoid predators. It may be that this method of drag reduction is on the whole costly and should be used only in spurts. There are important differences between the performance characteristics of wild animals and those in captivity. The following are specific recommendations for future research, categorized in terms of mechanism (general, two-dimensional versus three-dimensional effects, interaction of hydrodynamics and control, and jets), computation and modeling, experimental methods, and application.

6.1 Mechanism: General. Any given high-lift mechanism should be investigated over a broad range of Reynolds numbers to determine generalities and scaling potential. The wake vortices need to be dissected in terms of lift and thrust vortices and their typical topology. The importance of energy storage systems in swimming and flying animals and their impact on unsteady fluid-structure interaction need further research. A budgeting of the vortex circulation in the resulting wake behind a trout in a Kármán stream would provide a quantitative validation of the hypothesis of energy extraction and destructive interaction. It will be useful to examine the nonlinear interaction, if any, between the different modes of flexible fins and determine if such interaction augments the force peaks over a part of the cycle. In particular, the modes that sprawl over the entire fin and those that are confined over a much smaller part may have some root in what animals seem to resort to. What are the distinguishing aspects of the mechanisms of eel swimming for speed and efficiency?

6.2 Mechanism: Two-Dimensional and Three-Dimensional Effects and Rigid Versus Flexible Fins. NACA profiles are two dimensional. On the other hand, we now have the profiles of the entire three-dimensional lifting surface and even of the entire animal. It would be worth exploring if nature is implementing any new principle of three-dimensional body and system optimization. Rigid, large-aspect-ratio, three-dimensional, and two-dimensional fins both have a maximum efficiency of about 0.60. Therefore, the question is the following: Do flexible fins have higher efficiency than rigid flapping fins? Related questions are as follows: Do jumbo squid, sunfish pectoral fins, and lamprey wings—all of which have visually similar fin cupping—have similar modes of folding/cupping? Do they all produce LEVs? Is a flexible fin the ultimate in efficient propulsion? Unsteady control surfaces produce redundant forces instantaneously which average to zero over the time period of oscillation of the surface. How can the production of such forces be minimized?

6.3 Mechanism: Interaction of Hydrodynamics and Control. It will be useful to determine the relationship between the unsteady hydrodynamics of the pectoral fins of fish with their neuromotor characteristics and spring-mass damper models. This could give us a clue as to how strain energy storage is controlled by the muscles and how the mechanism can be applied to engineering. The works of biologists and biology-inspired hydrodynamics have yet to focus on the relationship of hydrodynamic properties of the lifting surfaces and the control of the entire animal or hull. In this sense, the price of abstraction of the lifting surfaces in animals needs to be explored. During flapping, what is the best phase during which fin kinematics should be changed?

6.4 Mechanism: Jets. In jet-dominated creatures, the effects of environment, nozzle surface quality, active control, and appendages on entrainment need closer scrutiny. If any fluids engineer is attracted to complication, then one needs to go no further than the squid. After all, what other animal has a critical velocity above which it swims tail first? What other animal combines both jet and fin propulsion? It will be very interesting if we discover the interaction between the unsteady flow around a squid and its body that automatically causes the switch from head-first to tail-first at the critical speed. Is jet propulsion and maneuvering less efficient compared with LEV-based flapping fins?

6.5 Modeling and Computation. The quasisteady models need to be successfully extended to flexible flapping foils, such as the pectoral fins of fish. An accurate modeling of the induced velocity during hovering would be useful. The modeling of Wagner effects and added mass effects during fin flip would be useful. An accurate computational investigation of fish swimming freely would help resolve questions regarding (1) the role of tail fins in homocercal and heterocercal species, (2) interactions of body and pectoral fins, (3) the role of fine lateral and lagged motor control of the posterior part of the tail fins, and (4) the role of the interactions between finlets and caudal fins.

6.6 Experimental Methods. The fringe pattern method needs to be extended to water; for example, it needs to be used on the pectoral fins of fish. The combination of a fringe method for tracking the movement of the flexible control surfaces of animals and a holographic method of velocity measurement would open a new avenue of research of the mechanisms that animals are utilizing. Due to advances in sensors and computers, biomechanics measurements of swimming and flying in natural environments are more feasible today and might lead to new discoveries.

6.7 Application. Improving the efficiency of devices where pressure drop, mixing, and noise production are involved would have practical impact. Devices that can produce suction by deforming the cup (without any pumping or plumbing, as in the octopus) would be useful. Success in application would be influenced by our ability to integrate the disparate disciplines. Because this review is multidisciplinary in nature, cultures in biology and engineering could have an impact on how this research is carried out. For biorobotics to succeed, it is implied that engineers and biologists know of each others' professional cultures. This is a thorny issue, and one can only give a personal opinion. Biologists tend to diversify and account for multiple variables, and many disciplines are integrated in their work. Engineers tend to simplify, minimize the number of variables, and preferably integrate disciplines that are well developed. Biologists in the United States tend to name their laboratories after themselves, but engineers do not. Biologists, while they deal with multidisciplinary products, such as life, still use the science principle of stripping the problem to a bare minimum and developing a hypothesis. A narrow focus plays an important role in the advancement of both science and engineering. We have chosen to review primarily the emerging science and technology of the animal-inspired high-lift mechanism and its application. The more familiar animal-inspired research in fluids engineering, such as riblets, compliant coating, bubble injection, mucus secretion, and surface curvature, have not been considered.

7 Remarks

Consider these questions. Why is it that we can now build frigates that can cruise more quietly than schools of fish (Fig. 2), but we cannot yet build quiet hair dryers or lawn mowers? Why is it that massive cruising vehicles (such as nuclear or diesel submarines) follow the same energy scaling law as the red muscles of fish, which are used for cruising, and yet smaller maneuvering vehicles consume proportionately more energy than the scaling law given by white muscles of fish, which are used for maneuver-

ing [8]? Why is it that engineering is proficient in cruising as stated above over eight decades of scales in both length and shaft horsepower, but is incompetent in maneuvering compared with animals over a scale of less than four decades? Why is it that there exists such a wide gap in turning ability between fish and underwater vehicles and how can this gap be closed?

It is possible to understand the above observations if we realize that, in certain situations, there is convergence in the evolution of the biological world and engineering because we have understood the underlying physics principles and have optimally implemented them in design. It is useful that we can quantify several situations where convergence exists and those where a gap exists. But where convergence or progress is eluding us, we need to look for new science principles and seek new inspirations for design. The latter conscious departure from conventional teachings of hydrodynamics has led to engineering gains, and two demonstrated results are worth citing. In one, substantial power saving is possible due to heaving and pitching actuators compared with conventional propulsors. In the other, by departing from the age-old hydrodynamic gospel that we should strive for axisymmetry in inflows to propulsors, it has now been possible to enhance pressure recovery in fan ducts. In other words, the rotational rates of axisymmetric pumps or propulsors can be lowered for the same discharge or forward speed, leading to quieting. Implementation of such principles can reduce the number of blades required in fan jets, while producing the same amount of thrust. These tangible benefits are the result of a biology-inspired, multidisciplinary fluids engineering approach. When one strives to understand the physics principles first, and biomimicry is not resorted to, the Reynolds number variation between the world of swimming/flying animals and engineering is not necessarily a barrier to implementation.

In closing, the unsteady high-lift mechanism is widely prevalent in nature. It may be that all flying animals (such as birds and insects) and all swimming animals (such as fish and penguins) that have flapping pectoral wings or fins in one form or another implement the mechanism in its most universal form, which is the production of a LEV. The flapping of the pectoral fin produces and sustains a LEV, which is a major source of force. Other mechanisms, such as rotational effects and wake capture, have largely been discounted, although further work is necessary to comprehensively do that in many species. While in man-made flying vehicles, propulsion and lift are separately produced, in nature, they are produced together. In nature, flying animals need a large control surface to stay aloft and propel themselves, while swimming animals have relatively smaller control surfaces (relative to their bodyweight in air) that are used primarily for propulsion and maneuvering. The topology of the LEV in swimming and flying animals varies widely, depending on aspect ratio, flexibility, and the thorax or main body. LEVs can be straight or curved, two or three dimensional, and conical or cylindrical; they can originate from the thorax or the wing root; they can have large or negligible spanwise spiraling flow; and they can even be highly convoluted. It may be that all swimming and flying animals that have flapping (simultaneously rolling and pitching) appendages have their own unique form of LEV, if we are willing to account for the differences in critical points in their flow topologies. It is perhaps more important to investigate, model, measure, visualize, and accurately compute the LEVs, which are the source of force production, than it is to dwell on the wakes, although the latter is easier. The LEV is a sink of vorticity and its dynamics is key to the force production and stability of the animal or the vehicle. It is most desirable to investigate the LEV on an actual swimming and flying animal, rather than on any robotic scaled model. While that is the task of biologists, engineers are in a more enviable position of "getting away" with investigations on models, bearing in mind the implied departure from the biological inspiration that might entail. One of the most fascinating topics that is ripe for fluids engineering investigation is flexible wings. The spectrum of flexible wings or pectoral fins waiting to be examined is enormous. At one end is the three-dimensional, highly convoluted, and beautiful thin pectoral fins of sunfish, and the other is the spanwise twisting, thick penguin wing or bending bird wing. Their hydrodynamic mechanism—namely, the nature of their LEVs—and their active optimization of oscillation parameters both need attention.

If in the ultimate analysis energy consumption is the Achilles heel, then efficiency is the most important variable that we need to pay attention to. However, most reports of efficiency of animal propulsion are unreliable to different extents, and even many engineering reports of efficiency are in error. This is remarkable because several mechanisms and preferred scaling laws are justified in terms of efficiency. More direct measurements of efficiency are needed. The modeling of unsteady thrust and drag needs to be improved. Accurate measurement and modeling of efficiency are important opportunities for fluids engineers. The effects of active cambering of wings on unsteady fluid dynamics are unclear. Wing kinematics and control strategies for turning need to be explored and compared with those for forward motion. Two-dimensional modeling is useful if it is analytical and complements experimentally derived physical models as in Refs. [32,33]. On the other hand, numerical simulation of two-dimensional wings is of little value for extension to measurements with robotic models or live animals. Numerical fluid dynamics simulation and theoretical modeling of flapping foils receive lower priority among biologists. With their mathematical skills, fluids engineers should be able to fill in a timely need. But works should preferably deal with three-dimensional foils, and extension of results from two-dimensional heaving and pitching foils is fraught with questions than it is helpful. Eel swimming might be ripe for investigations of the fluid-structure interaction. Why should eels resort to such seemingly inefficient swimming that produces significant secondary flows and two widely separated lateral streams of ring vortices for propulsion? Is there any subtle nonlinear mechanism that allows eels to swim to far-off places? One area where there is very little fluid dynamics information either from biologists or from engineers is the nature of the interaction of the unsteady appendage with the hull or thorax or main body. The main body may or may not be deforming with time as well. The effects on drag or stability are not known. Another area in which we have little information is the nature of vorticity roll-up at the oscillating wing tip. At extremely low Reynolds number flights, the limited measurements on the effects of surface furs on wings are counterintuitive and need closer inspection. An intriguing aspect is the rarity of cavitation in underwater LEVs or at the fin tip even in shallow water, although one would think that the fins/wings are more loaded than in steady swimming. Noise measurements or noise modeling of flapping foils are also rare. Unsteady fluids engineering is inherently amenable to emerging artificial muscle technologies and requires the development of new control theories. Much less work has been done on the integration of unsteady fluid dynamics inspired by swimming and flying animals with either artificial muscle technology or the development of control theories, although there are indications that such work is going to be rewarding. In fact, the very success in the implementation of high-lift mechanisms such as LEVs might depend on such integration. Because much work remains to be done in such ideal integration, accelerated progress might seem to happen if conventional technologies are used instead in the implementation of LEV, although lower performance than the full potential might thwart continued interest. Supplanting conventional motor drives with artificial muscle technologies that have higher electromechanical efficiency would favorably impact the overall system efficiency—the key to success. The development of controllers that first use cycle-averaged hydrodynamic force and moment characteristics and then produce unsteady main body behaviors throws away the key strengths in unsteadiness of swimming and flying animals [13]. Neuroscience-based nonlinear control would allow instantaneous control of fluid forces, thereby allowing the full potential of LEV-based unsteady fluid dynamics to be truly realized [165].

Acknowledgment

The author is grateful to the Cognitive and Neurosciences Program of the Office of Naval Research for the support of his biorobotics research over many years. Work with the following coworkers from the Naval Undersea Warfare Center in Newport, RI is acknowledged: Dr. David N Beal, Dr. Alberico Menozzi, Dr. John Castano, Mr. William Nedderman, Mr. Henry Leinhos, Mr. Stephen Forsythe, Mr. J. Dana Hrubes, Mr. Dan Thivierge, Mr. Albert Fredette, Mr. Thomas Fulton, Mr. William Krol, and Mr. James Rice. The author also acknowledges collaboration with the Visiting American Society of Engineering Education (ASEE) Distinguished Summer Faculty—Professor Anuradha Annaswamy of the Mechanical Engineering Department of the Massachusetts Institute of Technology and Professor Sahjendra Singh of the Computer Sciences and Electrical Engineering Department of the University of Nevada at Las Vegas. He also wishes to acknowledge collaboration with Dr. William Macy of the University of Rhode Island Graduate School of Oceanography and with Naval Research Enterprise Internship Program (NREIP) visiting summer graduate students Michael Boller and Sarah Warren of the University of Rhode Island Biology and Ocean Engineering Departments, respectively. Finally, S. Schael of Wehretechnische Dienstelle 71, BWB, Koblenz, Germany is thanked for providing Fig. 2. Professor George Lauder and Dr. Peter Madden of the Harvard University Biology Department are thanked for the sunfish data in Fig. 4.

References

[1] Bandyopadhyay, P. R., 2004, "Guest Editorial: Biology-Inspired Science and Technology for Autonomous Underwater Vehicles," special issue of IEEE J. Ocean. Eng., **29**(3), pp. 542–546.
[2] Editorial, 2005, "Fly Guys," IEEE Spectrum, **42**(11), p. 10.
[3] Sunada, S., Takashima, H., Hattori, T., Yasuda, K., and Kawachi, K., 2002, "Fluid-Dynamic Characteristics of a Bristled Wing," J. Exp. Biol., **205**, pp. 2737–2744.
[4] Ellington, C. P., 1985, "Power and Efficiency of Insect Flight Muscle," J. Exp. Biol., **115**, pp. 293–304.
[5] Bandyopadhyay, P. R., Beal, D. N., and Menozzi, A., 2008, "Biorobotic Insights Into How Animals Swim," J. Exp. Biol., **211**, pp. 206–214.
[6] Kern, S., and Koumoutsakos, P., 2006, "Simulations of Optimized Anguilliform Swimming," J. Exp. Biol., **209**, pp. 4841–4857.
[7] Dickinson, M. H., Farley, C. T., Full, R. J., Koehhl, M. A. R., Kram, R., and Lehman, S., 2000, "How Animals Move: An Integrative View," Science, **288**, pp. 100–106.
[8] Bandyopadhyay, P. R., Beal, D. N., Leinhos, H. A., Thivierge, D. P., and Mangalam, A., 2009, "Biomechanics of High Lift to Swim Better," J. Fluid Mech., under review.
[9] Bandyopadhyay, P. R., Hrubes, J. D., and Leinhos, H. A., 2008, "Biorobotic Adhesion in Water Using Suction Cups," Bioinsp. Biomim., **3**, p. 016003.
[10] Krol, W. P., Annaswamy, A., and Bandyopadhyay, P. R., 2002, "A Biomimetic Propulsor for Active Noise Control," Technical Report No. 11,350, Naval Undersea Warfare Center, Newport, RI.
[11] Bandyopadhyay, P. R., Castano, J. M., Rice, J. Q., Philips, R. B., Nedderman, W. H., and Macy, W. K., 1997, "Low-Speed Maneuvering Hydrodynamics of Fish and Small Underwater Vehicles," ASME J. Fluids Eng., **119**, pp. 136–144.
[12] Bandyopadhyay, P. R., 2002, "Maneuvering Hydrodynamics of Fish and Small Underwater Vehicles," Integr. Comp. Biol., **42**, pp. 102–117.
[13] Menozzi, A., Leinhos, H., Beal, D.N. and Bandyopadhyay, P.R., 2008, "Open-Loop Control of a Multi-Fin Biorobotic Underwater Vehicle," IEEE J. Ocean. Eng., **33**, pp. 59–68.
[14] Ellington, C. P., 1999, "The Aerodynamics of Insect-Based Flapping Machines," 14th Bristol International UAV Conference, pp. 37.1–37.12.
[15] Forsythe, S., Leinhos, H. A., and Bandyopadhyay, P. R., 2008, "Dolphin-Inspired Maneuvering and Pinging for Short Distance Echolocation," J. Acoust. Soc. Am., **124**, pp. EL255–EL261.
[16] Triantafyllou, M., Triantafyllou, G. S., and Yue, D. P. K., 2000, "Hydrodynamics of Fish-Like Swimming," Annu. Rev. Fluid Mech., **32**, pp. 33–53.
[17] Sane, S., 2003, "The Aerodynamics of Insect Flight," J. Exp. Biol., **206**, pp. 4191–4208.
[18] Triantafyllou, M. S., Hover, F. S., Techet, A. H., and Yue, D. K. P., 2005, "Review of Hydrodynamic Scaling Laws in Aquatic Locomotion and Fish-like Swimming," Appl. Mech. Rev., **58**, pp. 226–237.
[19] Bandyopadhyay, P. R., 2005, "Trends in Biorobotic Autonomous Undersea Vehicles," IEEE J. Ocean. Eng., **30**, pp. 109–139.
[20] Fish, F. E., and Lauder, G. V., 2006, "Passive and Active Flow Control by Swimming Fishes and Mammals," Annu. Rev. Fluid Mech., **38**, pp. 193–224.
[21] Beal, D. N., and Bandyopadhyay, P. R., 2007, "A Harmonic Model of Hydrodynamic Forces Produced by a Flapping Fin," Exp. Fluids, **43**, pp. 675–682.
[22] Vogel, S., 1996, *Life in Moving Fluids*, 2nd ed., Princeton University Press, Princeton, NJ.
[23] Azuma, A., 1992, *The Biokinetics of Flying and Swimming*, Springer-Verlag, New York.
[24] Dudley, R., 2003, *The Biomechanics of Insect Flight: Form, Function, and Evolution*, Princeton University Press, Princeton, NJ.
[25] Liao, J. C., Beal, D. N., Lauder, G. V., and Triantafyllou, M. S., 2003, "Fish Exploiting Vortices Decrease Muscle Activity," Science, **302**, pp. 1566–1569.
[26] Triantafyllou, G. S., and Triantafyllou, M. S., 1995, "An Efficient Swimming Machine," Sci. Am., **272**(3), pp. 64–71.
[27] Lauder, G. V., 2000, "Function of the Caudal Fin During Locomotion in Fishes: Kinematics, Flow Visualization, and Evolutionary Pattern," Am. Zool., **40**, pp. 101–122.
[28] Drucker, E. G., and Lauder, G. V., 1999, "Locomotor Forces on a Swimming Fish: Three-Dimensional Vortex Wake Dynamics Quantified Using Digital Particle Image Velocimetry," J. Exp. Biol., **202**, pp. 2393–2412.
[29] Wang, H., Zeng, L., Liu, H., and Yin, C., 2003, "Measuring Wing Kinematics, Flight Trajectory and Body Attitude During Forward Flight and Turning Maneuvers in Dragonflies," J. Exp. Biol., **206**, pp. 745–757.
[30] Malkiel, E., Alquaddoomi, O., and Katz, J., 1999, "Measurements of Plankton Distribution in the Ocean Using Submersible Holography," Meas. Sci. Technol., **10**, pp. 1142–1152.
[31] Ellington, C. P., 1984, "The Aerodynamics of Hovering Insect Flight. III. Kinematics," Philos. Trans. R. Soc. London, Ser. B, **305**, pp. 41–78.
[32] Weis-Fogh, T., 1973, "Quick Estimates of Flight Fitness in Hovering Animals, Including Novel Mechanisms for Lift Production," J. Exp. Biol., **59**, pp. 169–230.
[33] Lighthill, M. J., 1973, "On Weis-Fogh Mechanism of Lift Generation," J. Fluid Mech., **60**, pp. 1–17.
[34] Ellington, C. P., 1978, "The Aerodynamics of Normal Hovering Flight: Three Approaches," *Comparative Physiology: Water, Ions and Fluid mechanics*, K. Schmidt-Nielsen, L. Bolis, and S. Maddrell, eds., Cambridge University Press, Cambridge, pp. 327–345.
[35] Ellington, C. P., 1980, "Vortices and Hovering Flight," *Instationare Effekte An Schwingended Fluegeln*, W. Nachtigall, ed., F. Steiner, Wiesbaden, pp. 64–101.
[36] Ellington, C. P., 1984, "The Aerodynamics of Hovering Insect Flight, IV—Aerodynamic Mechanisms," Philos. Trans. R. Soc. London, Ser. B, **305**, pp. 79–113.
[37] Maxworthy, T., 1979, "Experiments on the Weis-Fogh Mechanism of Lift Generation by Insects in Hovering Flight. Part 1. Dynamics of the 'Fling,'" J. Fluid Mech., **93**, pp. 47–63.
[38] Spedding, G. R., and Maxworthy, T., 1986, "The Generation of Circulation and Lift in a Rigid Two-Dimensional Fling," J. Fluid Mech., **165**, pp. 247–272.
[39] Marden, J. H., 1987, "Maximum Lift Production During Takeoff in Flying Animals," J. Exp. Biol., **130**, pp. 235–258.
[40] Rayner, J. M. V., 1979, "A Vortex Theory of Animal Flight. Part 2. The Forward Flight of Birds," J. Fluid Mech., **91**, pp. 731–763.
[41] Ellington, C. P., 1984, "The Aerodynamics of Hovering Insect Flight. II. Morphological Parameters," Philos. Trans. R. Soc. London, Ser. B, **305**, pp. 17–40.
[42] Ellington, C. P., 1995, "Unsteady Aerodynamics of Insect Flight," Symp. Soc. Exp. Biol., **49**, pp. 109–129.
[43] Usherwood, J. R., and Ellington, C. P., 2002, "The Aerodynamics of Revolving Wings—I. Model Hawkmoth Wings," J. Exp. Biol., **205**(11), pp. 1547–1564.
[44] Usherwood, J. R., and Ellington, C. P., 2002, "The Aerodynamics of Revolving Wings—II. Propeller Force Coefficients from Mayfly to Quail," J. Exp. Biol., **205**(11), pp. 1565–1576.
[45] Sunada, S., Kawachi, K., Watanabe, I., and Azuma, A., 1993, "Fundamental Analysis of Three Dimensional 'Near Fling'," J. Exp. Biol., **183**, pp. 217–248.
[46] Wakeling, J. M., and Ellington, C. P., 1997, "Dragonfly Flight I—Gliding Flight and Steady-State Aerodynamic Forces," J. Exp. Biol., **200**, pp. 543–556.
[47] Ellington, C. P., 1991, "Limitations on Animal Flight Performance," J. Exp. Biol., **160**, pp. 71–91.
[48] Gopalkrishnan, R., Triantafyllou, M. S., Triantafyllou, G. S., and Barrett, D., 1994, "Active Vorticity Control in a Shear Flow Using a Flapping Foil," J. Fluid Mech., **274**, pp. 1–21.
[49] Dickinson, M. H., and Lehmann, F. O., 1993, "The Active Control of Wing Rotation by Drosophila," J. Exp. Biol., **182**, pp. 173–189.
[50] Dickinson, M. H., and Gotz, K. G., 1993, "Unsteady Aerodynamic Performance of Model Wings at Low Reynolds Numbers," J. Exp. Biol., **174**, pp. 45–64.
[51] Birch, J. M., and Dickinson, M., 2003, "The Influence of Wingwake Interactions on the Production of Aerodynamic Forces in Flapping Flight," J. Exp. Biol., **206**, pp. 2257–2272.
[52] Hamdani, H., and Sun, M., 2000, "Aerodynamic Forces and Flow Structures of an Airfoil in Some Unsteady Motions at Small Reynolds Number," Acta Mech., **145**, pp. 173–187.
[53] Odar, F., and Hamilton, W. S., 1964, "Forces on a Sphere Accelerating in a

Viscous Fluid," J. Fluid Mech., **18**, pp. 302–314.
[54] Sarpkaya, T., 1982, "Impulsively-Started Flow About Four Types of Bluff Body," ASME J. Fluids Eng., **104**, pp. 207–213.
[55] Sarpkaya, T., 1991, "Non-Impulsively Started Steady Flow About a Circular Cylinder," AIAA J., **29**(8), pp. 1283–1289.
[56] Sarpkaya, T., 1992, "Brief Reviews of Some Time-Dependent Flows," ASME J. Fluids Eng., **114**(3), pp. 283–298.
[57] Dickinson, M. H., 1994, "The Effects of Wing Rotation on Unsteady Aerodynamic Performance at Low Reynolds Numbers," J. Exp. Biol., **192**, pp. 179–206.
[58] Dickinson, M. H., and Gotz, K. G., 1996, "The Wake Dynamics and Flight Forces of the Fruit Fly Drosophila Melanogaster," J. Exp. Biol., **199**(9), pp. 2085–2104.
[59] Sane, S. P., and Dickinson, M. H., 2001, "The Control of Flight Force by a Flapping Wing: Lift and Drag Production," J. Exp. Biol., **204**(15), pp. 2607–2626.
[60] Daniel, T. L., 1984, "Unsteady Aspects of Aquatic Locomotion," Am. Zool., **24**, pp. 121–134.
[61] Wang, Z. J., Birch, J. M., and Dickinson, M. H., 2004, "Unsteady Forces and Flows in Low Reynolds Number Hovering Flight: Two-Dimensional Computations Versus Robotic Wing Experiments," J. Exp. Biol., **207**, pp. 449–460.
[62] Birch, J. M., Dickson, W. B., and Dickinson, M. H., 2004, "Force Production and Flow Structure of the Leading Edge Vortex on Flapping Wings at High and Low Reynolds Numbers," J. Exp. Biol., **207**, pp. 1063–1072.
[63] Dickson, W. B., and Dickinson, M. H., 2004, "The Effect of Advance Ratio on the Aerodynamics of Revolving Wings," J. Exp. Biol., **207**, pp. 4269–4281.
[64] Poelma, C., Dickson, W. B., and Dickinson, M. H., 2006, "Time-Resolved Reconstruction of the Full Flow Field Around a Dynamically-Scaled Flapping Wing," Exp. Fluids, **41**, pp. 213–225.
[65] Thomas, A. L. R., Taylor, G. K., Srygley, R. B., Nudds, R. L., and Bomphrey, R. J., 2004, "Dragonfly Flight: Free-Flight and Tethered Flow Visualizations Reveal a Diverse Array of Unsteady Lift Generating Mechanisms, Controlled Primarily Via Angle of Attack," J. Exp. Biol., **207**, pp. 4299–4323.
[66] Sane, S. P., 2006, "Induced Airflow in Flying Insects, I: A Theoretical Model of This Induced Flow," J. Exp. Biol., **209**, pp. 32–42.
[67] Sane, S. P., and Jacobsen, N., 2006, "Induced Airflow in Flying Insects, II: Measurement of Induced Flow," J. Exp. Biol., **209**, pp. 43–56.
[68] Combes, S. A., and Daniel, T. L., 2001, "Shape, Flapping, and Flexion: Wing and Fin Design for Forward Flight," J. Exp. Biol., **204**(12), pp. 2073–2085.
[69] Walker, J. A., 2002, "Rotational Lift: Something Different or More of the Same?," J. Exp. Biol., **205**, pp. 3783–3792.
[70] Sun, M., and Tang, J., 2002, "Unsteady Aerodynamic Force Generation by a Model Fruit Fly Wing in Flapping Motion," J. Exp. Biol., **205**, pp. 55–70.
[71] Ramamurti, R., and Sandberg, W. C., 2005, "A Three-Dimensional Computational Study of the Aerodynamic Mechanisms of Insect Flight," J. Exp. Biol., **205**, pp. 1507–1518.
[72] Ellington, C. P., van den Berg, C., Willmott, A. P., and Thomas, A. L. R., 1996, "Leading-Edge Vortices in Insect Flight," Nature (London), **384**, pp. 626–630.
[73] Ramamurti, R., and Sandberg, W. C., 2007, "A Computational Investigation of the Three-Dimensional Unsteady Aerodynamics of Drosophila Hovering and Maneuvering," J. Exp. Biol., **210**, pp. 881–896.
[74] Sunada, S., Kawachi, K., Watanabe, I., and Azuma, A., 1993, "Performance of a Butterfly in Take-Off Flight," J. Exp. Biol., **183**, pp. 249–277.
[75] Spedding, G. R., Rosen, M., and Hedenstrom, A., 2003, "A Family of Vortex Wakes Generated by a Thrush Nightingale in Free Flight in a Wind Tunnel Over Its Entire Range of Flight Speeds," J. Exp. Biol., **206**, pp. 2313–2344.
[76] Bomphrey, R. J., Lawson, N. J., Harding, N. J., Taylor, G. K., and Thomas, A. L. R., 2005, "The Aerodynamics of Manduca Sexta: Digital Particle Image Velocimetry Analysis of the Leading-Edge Vortex," J. Exp. Biol., **208**, pp. 1079–1094.
[77] Luttges, M. W., 1989, "Accomplished Insect Fliers," *Frontiers in Experimental Fluid Mechanics*, Springer, Berlin, pp. 429–456.
[78] Bandyopadhyay, P. R., Beal, D. N., and Mangalam, A., 2008, "Experiments on the Mechanism of Force Production in Rolling and Pitching Foils," J. Fluid Mech., to be submitted.
[79] Lighthill, M. J., 1963, "Introduction to Boundary Layer Theory," *Laminar Boundary Layers, Part II*, L. Rosenhead, ed., Oxford University Press, Oxford, pp. 46–113.
[80] Nudds, R. L., Taylor, G. K., and Thomas, A. L. R., 2004, "Tuning of Strouhal Number for High Propulsive Efficiency Accurately Predicts How Wingbeat Frequency and Stroke Amplitude Relate and Scale With Size and Flight Speed in Birds," Proc. R. Soc. London, Ser. B, **271**, pp. 2071–2076.
[81] Milano, M., and Gharib, M., 2005, "Uncovering the Physics of Flapping Flat Plates With Artificial Evolution," J. Fluid Mech., **534**, pp. 403–409.
[82] Tian, X., Iriarte-Diaz, J., Middleton, K., Galvao, R., Israeli, E., Roemer, A., Sullivan, A., Song, A., Swartz, S., and Breuer, K., 2006, "Direct Measurements of the Kinematics and Dynamics of Bat Flight," Bioinspir. Biomim., **1**, pp. S10–S18.
[83] Azuma, A., and Okamoto, M., 2005, "Theoretical Study on Two-Dimensional Aerodynamic Characteristics of Unsteady Wings," J. Theor. Biol., **234**, pp. 67–78.
[84] Minotti, F. O., 2002, "Unsteady Two-Dimensional Theory of a Flapping Wing," Phys. Rev. E, **66**, p. 051907.
[85] Hui, C., 1988, "Penguin Swimming. I. Hydrodynamics," Physiol. Zool., **61**, pp. 333–343.
[86] Breder, C. A., 1926, "The Locomotion of Fishes," Zoologica (N.Y.), **4**, pp. 159–297.
[87] Tytell, E. D., and Lauder, G. V., 2004, "The Hydrodynamics of Eel Swimming. I. Wake Structure," J. Exp. Biol., **207**, pp. 1825–1841.
[88] Schmidt-Nielsen, K., 1972, "Locomotion: Energy Cost of Swimming, Flying, and Running," Science, **177**, pp. 222–228.
[89] Kooyman, G. L., and Ponganis, P. J., 1994, "Emperor Penguin Oxygen Consumption, Heart Rate and Plasma Lactate Levels During Graded Swimming Exercise," J. Exp. Biol., **195**, pp. 199–209.
[90] Green, J. A., Butler, P. J., Woakes, A. J., and Boyd, I. L., 2003, "Energetics of Diving in Macaroni Penguins," J. Exp. Biol., **206**, pp. 43–57.
[91] Lighthill, M. J., 1969, "Hydromechanics of Aquatic Animal Propulsion," Annu. Rev. Fluid Mech., **1**, pp. 413–446.
[92] Lighthill, M. J., 1970, "Aquatic Animal Propulsion of High Hydromechanical Efficiency," J. Fluid Mech., **44**, pp. 265–301.
[93] Lauder, G. V., and Madden, P. G. A., 2006, "Learning From Fish: Kinematics and Experimental Hydrodynamics for Roboticists," Int. J. Autom. Comput., **3**, pp. 325–335.
[94] Blake, R. W., 1983, *Fish Locomotion*, Cambridge University Press, Cambridge.
[95] Westneat, M. W., 1996, "Functional Morphology of Aquatic Flight in Fishes: Kinematics, Electromyography, and Mechanical Modeling of Labriform Locomotion," Am. Zool., **36**, pp. 582–598.
[96] Walker, J. A., and Westneat, M. W., 2000, "Mechanical Performance of Aquatic Rowing and Flying," Proc. R. Soc. London, Ser. B, **267**, pp. 1875–1881.
[97] Walker, J. A., and Westneat, M. W., 2002, "Performance Limits of Labriform Propulsion and Correlates With Fin Shape and Motion," J. Exp. Biol., **205**, pp. 177–187.
[98] Kato, N., 1999, "Hydrodynamic Characteristics of Mechanical Pectoral Fin," ASME J. Fluids Eng., **121**(3), pp. 605–613.
[99] Archer, R. D., Sapuppo, J., and Betteridge, D. S., 1979, "Propulsion Characteristics of Flapping Wings," Aeronaut. J., **83**, pp. 355–371.
[100] Kadlec, R. A., and Davis, S. S., 1979, "Visualization of Quasiperidodic Flows," AIAA J., **17**, pp. 1164–1169.
[101] Triantafyllou, G. S., Triantafyllou, M. S., and Grosenbaugh, M. A., 1993, "Optimal Thrust Development in Oscillating Foils With Applications to Fish Propulsion," J. Fluids Struct., **7**, pp. 205–234.
[102] Anderson, J. M., Streitlien, K., Barrett, D. S., and Triantafyllou, M. S., 1998, "Oscillating Foils of High Propulsive Efficiency," J. Fluid Mech., **360**, pp. 41–72.
[103] Bose, N., and Lien, J., 1989, "Propulsion of a Fin Whale (*Balaenoptera Physalus*): Why the Fin Whale is a Fast Swimmer," Proc. R. Soc. London, Ser. B, **237**, pp. 175–200.
[104] Read, D. A., Hover, F. S., and Triantafyllou, M. S., 2003, "Forces on Oscillating Foils for Propulsion and Maneuvering," J. Fluids Struct., **17**, pp. 163–183.
[105] Gray, J., 1933, "Studies in Animal Locomotion. III. The Propulsive Mechanism of the Whiting (*Gadus Merlangus*)," J. Exp. Biol., **10**, pp. 391–400.
[106] Bainbridge, R., 1961, "Problems of Fish Locomotion," Symp. Zool. Soc. Lond., **5**, pp. 13–32.
[107] Bainbridge, R., 1962, "Training, Speed and Stamina in Trout," J. Exp. Biol., **39**, pp. 537–555.
[108] Webb, P., 2006, "Bainbridge Sets the Stage on Scaling in Fish Swimming," J. Exp. Biol., **209**, pp. 1789–1790.
[109] Ellington, C. P., 1999, "The Novel Aerodynamics of Insect Flight: Applications to Micro-Air Vehicles," J. Exp. Biol., **202**, pp. 3439–3448.
[110] Crocker, M. J., 1999, "Sir James Lighthill and His Contributions to Science," *Keynote Lecture, Sixth International Congress on Sound and Vibration*, Technical University of Denmark, Lyngby, Denmark.
[111] http://www.iiav.org/sirjameslighthill.pdf.
[112] Wilga, C. D., and Lauder, G. V., 2000, "Three-Dimensional Kinematics and Wake Structure of the Pectoral Fins During Locomotion in Leopard Sharks *Triakis Semifasciata*," J. Exp. Biol., **203**, pp. 2261–2278.
[113] Wilga, C. D., and Lauder, G. V., 2001, "Functional Morphology of the Pectoral Fins in Bamboo Sharks, *Chiloscyllium Plagiosum*: Benthic vs. Pelagic Station-Holding," J. Morphol., **249**, pp. 195–209.
[114] Liao, J., and Lauder, G. V., 2000, "Function of the Heterocercal Tail Fin in White Sturgeon: Flow Visualization During Steady Swimming and Vertical Maneuvering," J. Exp. Biol., **203**, pp. 3585–3594.
[115] Nauen, J. C., and Lauder, G. V., 2001, "Three-Dimensional Analysis of Finlet Kinematics in the Chub Mackerel (*Scomber Japonicus*)," Biol. Bull., **200**, pp. 9–19.
[116] Nauen, J. C., and Lauder, G. V., 2001, "Locomotion in Scombird Fishes: Visualization of Flow Around the Caudal Peduncle and Finlets of the Club Mackerel *Scomber Japonicus*," J. Exp. Biol., **204**, pp. 2251–2263.
[117] Nauen, J. C., and Lauder, G. V., 2002, "Hydrodynamics of Caudal Fin Locomotion by Chub Mackerel, *Scomber Japonicus* (*Scombridae*)," J. Exp. Biol., **205**, pp. 1709–1724.
[118] Wardle, C. S., 1977, "Effects of Size on the Swimming Speeds of Fish," *Scale Effects in Animal Locomotion*, T. J. Pedley, ed., Academic, New York, pp. 299–313.
[119] Aleev, Y. G., 1969, *Function and Gross Morphology in Fish*, Keter, Jerusalem.

[120] Helfman, G. S., Collette, B. B., and Facey, D. E., 1997, *The Diversity of Fishes*, Blackwell Scientific, Malden, MA.
[121] Lindsey, C. C., 1978, "Form, Function, and Locomotory Habits in Fish," *Fish Physiology*, Vol. VII, W. S. Hoar and D. J. Randall, eds., Academic, New York, pp. 1–100.
[122] Magnuson, J. J., 1970, "Hydrostatic Equilibrium of *Euthynnus Affinis*, A Pelagic Teleost Without a Gas Bladder," Copeia, **1**, pp. 56–85.
[123] Nauen, J. C., and Lauder, G. V., 2000, "Locomotion in Scombrid Fishes: Morphology and Kinematics of the Finlets of the Chub Mackerel *Scomber Japonicus*," J. Exp. Biol., **203**, pp. 2247–2259.
[124] Bainbridge, R., 1963, "Caudal Fin and Body Movements in the Propulsion of Some Fish," J. Exp. Biol., **40**, pp. 23–56.
[125] Webb, P. W., 1975, "Hydrodynamics and Energetics of Fish Propulsion," Bull. - Fish. Res. Board Can., **190**, pp. 1–159.
[126] Gibb, C., Dickson, K. A., and Lauder, G. V., 1999, "Tail Kinematics of the Chub Mackerel *Scomber Japonicus*: Testing the Homocercal Tail Model of Fish Propulsion," J. Exp. Biol., **202**, pp. 2433–2447.
[127] Drucker, E. G., and Lauder, G. V., 2001, "Wake Dynamics and Fluid Forces of Turning Maneuvers in Sunfish," J. Exp. Biol., **204**, pp. 431–442.
[128] Drucker, E. G., and Lauder, G. V., 2000, "A Hydrodynamic Analysis of Fish Swimming Speed: Wake Structure and Locomotor Force in Slow and Fast Labriform Swimmers," J. Exp. Biol., **203**, pp. 2379–2393.
[129] Weihs, D., 1981, "Effects of Swimming Path Curvature on the Energetics of Fish," Fishery Bulletin, **79**, pp. 171–176.
[130] Lauder, G. V., Anderson, E. J., Tangorra, J., and Madden, P. G. A., 2007, "Fish Biorobotics: Kinematics and Hydrodynamics of Self-Propulsion," J. Exp. Biol., **210**, pp. 2767–2780.
[131] Mittal, R., Dong, H., Bozkurttas, M., Lauder, G. V., and Madden, P., 2006, "Locomotion With Flexible Propulsors: II. Computational Modeling of Pectoral Fin Swimming in Sunfish," Bioinspir. Biomim., **1**, pp. S35–S41.
[132] Tytell, E. D., 2006, "Median Fin Function in Bluegill Sunfish Loomis Marchers: Streamwise Vortex Structure During Steady Swimming," J. Exp. Biol., **209**, pp. 1516–1534.
[133] Bartol, I. K., Gharib, M., Webb, P. W., Weihs, D., and Gordon, M. S., 2005, "Body-Induced Vertical Flows: A Common Mechanism for Self-Corrective Trimming Control in Boxfish," J. Exp. Biol., **208**, pp. 327–344.
[134] Walker, J. A., 2004, "Kinematics and Performance of Maneuvering Control Surfaces in Teleost Fishes," IEEE J. Ocean. Eng., **29**, pp. 572–584.
[135] O'Dor, R. K., and Weber, D. M., 1986, "The Constraints on Cephalopods: Why Squid Aren't Fish," Can. J. Zool., **64**, pp. 1591–1605.
[136] Bartol, I. K., Mann, R., and Patterson, M. R., 2001, "Aerobic Respiratory Costs of Swimming in the Negatively Buoyant Brief Squid Lolliguncula Brevis," J. Exp. Biol., **204**, pp. 3639–3653.
[137] Krueger, P., 2001, "The Significance of Vortex Ring Formation and Nozzle Exit Overpressure in Pulsatile Jet Propulsion," Ph.D. thesis, California Institute of Technology, Pasadena, CA.
[138] Liu, P., and Bose, N., 1997, "Propulsive Performance From Oscillating Propulsors With Spanwise Flexibility," Proc. R. Soc. London, Ser. A, **453**, pp. 1763–1770.
[139] Ando, Y., Kato, N., Suzuki, H., Suzimori, K., Kanda, T., and Endo, S., 2006, "Elastic Pectoral Fin Actuators for Biomimetic Underwater Vehicles," Proceedings of the 3rd International Symposium on Aero. Aqua Biol.-Mechanisms, ISABMEC, Ginowan, Okinawa, Japan, Jul. 3–7, pp. 1–8.
[140] Dudley, R., 2000, *The Biomechanics of Insect Flight*, Princeton University Press, Princeton, NJ.
[141] Mao, S., and Hamdani, H., 2001, "High-Lift Generation by an Airfoil Performing Unsteady Motion at Low Reynolds Number," Acta Mech. Sin., **17**, pp. 97–144.
[142] Sun, M., and Lan, S. L., 2004, "A Computational Study of the Aerodynamic Forces and Power Requirements of Dragonfly (Aeschna Juncea) Hovering," J. Exp. Biol., **207**, pp. 1887–1901.
[143] Ramamurti, R., Sandberg, W. C., Löhner, R., Walker, J. A., and Westneat, M. W., 2002, "Fluid Dynamics of Flapping Aquatic Flight in the Bird Wrasse: Three-Dimensional Unsteady Computations With Fin Deformation," J. Exp. Biol., **205**, pp. 2997–3008.
[144] Ramamurti, R., and Sandberg, W. C., 2006, "Computational Fluid Dynamics Study for Optimization of a Fin Design," AIAA Paper No. 2006–3658.
[145] Peskin, C., 1972, "Flow Patterns Around Heart Valves: A Numerical Study," J. Comput. Phys., **10**, pp. 252–271.
[146] Mittal, R., and Iaccarino, G., 2005, "Immersed Boundary Methods," Annu. Rev. Fluid Mech., **37**, pp. 239–261.
[147] Dong, H., Mittal, R., and Najjar, F. M., 2006, "Wake Topology and Hydrodynamic Performance of Low-Aspect-Ratio Flapping Airfoil," J. Fluid Mech., **566**, pp. 309–343.
[148] Rayner, J. M. V., 1979, "Vortex Theory of Animal Flight, I—Vortex Wake of a Hovering Animal," J. Fluid Mech., **91**, pp. 697–730.
[149] Lan, S. L., and Sun, M., 2001, "Aerodynamic Properties of a Wing Performing Unsteady Rotational Motions at Low Reynolds Number," Acta Mech., **149**, pp. 135–147.
[150] Dabiri, J. O., 2005, "On the Estimation of Swimming and Flying Forces From Wake Measurements," J. Exp. Biol., **208**, pp. 3519–3532.
[151] Smith, R.W., and Wright, J.A., 2004, "Simulation of RoboTuna Fluid Dynamics Using a New Incompressible ALE Method," AIAA Paper No. 2004–23–2347.
[152] Zhu, Q., Wolfgang, M. J., Yue, D. K. P., and Triantafyllou, M. S., 2002, "Three-Dimensional Flow Structures and Vorticity Control in Fish-Like Swimming," J. Fluid Mech., **392**, pp. 183–212.
[153] Walker, P. B., 1931, "Experiments on the Growth of Circulation About a Wing and an Apparatus for Measuring Fluid Motion," Rep. Memo. Aeronaut. Res. (Great Britain) 1402.
[154] Fung, Y. C., 1993, *An Introduction to Aeroelasticity*, Dover, New York.
[155] Brennen, C.E., 1982, "A Review of Added Mass and Fluid Inertial Forces," Report No. CR82,010, Naval Civil Engineering Laboratory, Port Hueneme, CA.
[156] Sane, S. P., and Dickinson, M. H., 2002, "The Aerodynamic Effects of Wing Rotation and a Revised Quasi-Steady Model of Flapping Flight," J. Exp. Biol., **205**, pp. 1087–1096.
[157] Peng, J., Dabiri, J. O., Madden, P. G., and Lauder, G. V., 2007, "Non-Invasive Measurement of Instantaneous Forces During Aquatic Locomotion: A Case Study of the Bluegill Sunfish Pectoral Fin," J. Exp. Biol., **210**, pp. 685–698.
[158] van Ginneken, V. J. T., and van den Thillart, G. E. E. J. M., 2000, "Eel Fat Stores Are Enough to Reach the Sargasso," Nature (London), **403**, pp. 156–157.
[159] Müller, U. K., Smit, J., Stamhuis, E. J., and Videler, J. J., 2001, "How the Body Contributes to the Wake in Undulatory Fish Swimming: Flow Fields of a Swimming Eel (*Anguilla Anguilla*)," J. Exp. Biol., **204**, pp. 2751–2762.
[160] Tytell, E. D., 2004, "The Hydrodynamics of Eel Swimming, II. Effect of Swimming Speed," J. Exp. Biol., **207**, pp. 3265–3279.
[161] Blackburn, L., 2006, "Swimming Secrets," J. Exp. Biol., **209**, pp. i–ii.
[162] Milano, M., and Koumoutsakos, P., 2002, "A Clustering Genetic Algorithm for Cylinder Drag Optimization," J. Comput. Phys., **175**, pp. 79–107.
[163] Katz, D. F., and Dott, H. M., 1975, "Methods of Measuring Swimming Speed of Spermatozoa," J. Reprod. Fertil., **45**(2), pp. 263–272.
[164] Kim, M., Bird, J. C., Avan Parys, J., Breuer, K. S., and Powers, T. R., 2003, "A Macroscopic Scale Model of Bacterial Flagellar Bundling," Proc. Natl. Acad. Sci. U.S.A., **100**, pp. 15481–15485.
[165] Bandyopadhyay, P. R., Singh, S. N., Thivierge, D. P., Annaswamy, A. M., Leinhos, H. A., Fredette, A. R., and Beal, D. N., 2008, "Synchronization of Animal-Inspired Multiple High-Lift Fins in an Underwater Vehicle Using Olivo-Cerebellar Dynamics," IEEE J. Ocean. Eng., **33**(4), pp 563–578.
[166] Lighthill, J., 1975, *Mathematical Biofluiddynamics*, Society for Industrial and Applied Mathematics, Philadelphia, PA.
[167] Lighthill, M. J., 1975, "Aerodynamic Aspects of Animal Flight," *Swimming and Flying in Nature 2*, T. Y. Wu, C. J. Brokaw, and C. Brennen, eds., Plenum, New York, pp. 423–492.
[168] Schlichting, H., 1979, *Boundary-Layer Theory*, 7th ed., McGraw-Hill, New York, pp. 31–32.
[169] Bandyopadhyay, P. R., Castano, J. M., Nedderman, W. H., and Donnelly, M. J., 2000, "Experimental Simulation of Fish-Inspired Unsteady Vortex Dynamics on a Rigid Cylinder," ASME J. Fluids Eng., **122**, pp. 219–238.
[170] Wang, Z. J., 2000, "Vortex Shedding and Frequency Selection in Flapping Flight," J. Fluid Mech., **410**, pp. 323–341.
[171] Rohr, J. J., and Fish, F. E., 2004, "Strouhal Numbers and Optimization of Swimming by Odontocete Cetaceans," J. Exp. Biol., **207**, pp. 1633–1642.
[172] Streitlien, K., and Triantafyllou, M. S., 1995, "Force and Moment on Joukowski Profile in the Presence of Point Vortices," AIAA J., **33**, pp. 603–610.
[173] Wakeling, J. M., and Ellington, C. P., 1997, "Dragonfly Flight II—Velocities, Accelerations, and Kinematics of Flapping Flight," J. Exp. Biol., **200**, pp. 557–582.
[174] Wakeling, J. M., and Ellington, C. P., 1997, "Dragonfly Flight III—Lift and Power Requirements, J. Exp. Biol., **200**, pp. 583–600.
[175] Hui, C., 1988, "Penguin Swimming, II. Energetics and Behavior," Physiol. Zool., **61**, pp. 344–350.
[176] Buchholz, J., and Smits, A. J., 2005, "Vortex Structures in the Wake of a Flapping Plate," Phys. Fluids, **17**, p. 091102.
[177] Buchholz, J. H. J., and Smits, A. J., 2006, "On the Evolution of the Wake Structure Produced by a Low Aspect-Ratio Pitching Panel," J. Fluid Mech., **546**, pp. 433–443.
[178] Williamson, C. H. K., and Roshko, A., 1988, "The Hydrodynamics and Eel Swimming, II: Effects of Swimming Speed Vortex Formation in the Wake of an Oscillating Cylinder," J. Fluids Struct., **2**, pp. 355–381.
[179] Rosenberger, L. J., and Westneat, M. W., 1999, "Functional Morphology of Undulatory Pectoral Fin Locomotion in the Stingray Taeniura Lymma (Chondrichthyes: Dasyatidae)," J. Exp. Biol., **202**, pp. 523–3539.
[180] Clark, R. P., and Smits, A. J., 2006, "Thrust Production and Wake Structure of a Batoid-Inspired Oscillating Fin," J. Fluid Mech., **562**, pp. 415–429.
[181] Dickinson, M. H., 1999, "Bionics: Biological Insight Into Mechanical Design," Proc. Natl. Acad. Sci. U.S.A., **96**(25), pp. 14208–14209.
[182] Westneat, M. W., 2001, "Mechanical Design for Swimming: Muscle, Tendon, and Bone," Fish Physiol., **19**, pp. 271–311.
[183] Wainwright, S. A., 1983, "To Bend A Fish," *Fish Biomechanics*, P. W. Webb and D. Weihs, eds., Praeger, NY, pp. 68–91.
[184] Scherer, J. O., 1968, "Experimental and Theoretical Investigation of Large Amplitude Oscillating Foil Propulsion System," Technical Report No. 662–1, Hydronautics Inc., Laurel, MD.
[185] Fish, F. E., and Battle, J. M., 1995, "Hydrodynamic Design of the Humpback Whale Flipper," J. Morphol., **225**, pp. 51–60.
[186] Miklosovic, D. S., Murray, M. M., Howle, L. E., and Fish, F. E., 2004, "Leading Edge Tubercles Delay Stall on Humpback Whale (Megaptera Novaeangliae) Flippers," Phys. Fluids, **16**, pp. L39–L42.
[187] Bannasch, R., 2001, "From Soaring and Flapping Bird Flight to Innovative Wing and Propeller Constructions," *Fixed and Flapping Wing Aerodynamics*

for Micro Air Vehicle Applications, T. J. Mueller, ed., Prog. Astro. Aero., Vol. 195, AIAA Publishers, Reston, VA, pp. 453–472.
[188] Isshiki, H., and Murakami, M., 1984, "A Theory of Wave Devouring Propulsion," J. Soc. Nav. Archit. Jpn., **156**, pp. 102–114.
[189] Koochesfahani, M. M., and Dimotakis, P. E., 1988, "A Cancellation Experiment in a Forced Turbulent Shear Layer," AIAA Paper No. AIAA-88-3713.
[190] Beal, D. N., Hover, F. S., Triantafyllou, M. S., Liao, J. C., and Lauder, G. V., 2006, "Passive Propulsion in Vortex Wakes," J. Fluid Mech., **549**, pp. 385–402.
[191] Allen, J. J., and Smits, A. J., 2001, "Energy Harvesting Eel," J. Fluids Struct., **15**, pp. 629–640.
[192] Kim, M. J., and Breuer, K. S., 2007, "The Use of Bacterial Carpets to Enhance Mixing in Microfluidic Systems," ASME J. Fluids Eng., **121**, pp. 319–324.
[193] Behkam, B., and Sitti, M., 2005 "Modeling and Testing of a Biomimetic Flagellar Propulsion Method for Microscale Biomedical Swimming Robots," IEEE Advanced Intelligent Mechanotronics Conference, Monterey, CA, Jul. 24–28.
[194] Chen, J., Fan, Z., Zou, J., Engel, J., and Liu, C., 2003, "Two-Dimensional Micromachined Flow Sensor Array for Fluid Mechanics Studies," J. Aerosp. Eng., **16**(2), pp. 85–97.
[195] Ellington, C. P., 1984, "The Aerodynamics of Hovering Insect Flight, V—A Vortex Theory," Philos. Trans. R. Soc. London, Ser. B, **305**, pp. 115–144.
[196] Wootton, R., 2000, "From Insects to Microvehicles," Nature (London), **403**, pp. 144–145.
[197] Zbikowski, R., 2002, "On Aerodynamic Modeling of an Insect-Like Flapping Wing in Hover for Micro-Air Vehicles," Philos. Trans. R. Soc. London, Ser. A, **360**, pp. 273–290.
[198] Yan, J., Avadhanula, S. A., Birch, J., Dickinson, M. H., Sitti, M., Su, T., and Fearing, R. S., 2001, "Wing Transmission for a Micromechanical Flying Insect," J. Micromechatronics, **1**(3), pp. 221–238.
[199] Usab, W. J., Hardin, J., and Bilanin, A. J., 2004, "Biology-Inspired Delayed Stall Propulsor," IEEE J. Ocean. Eng., **29**, pp. 756–765.
[200] Opila, D. F., Annaswamy, A. M., Krol, W. P., and Raghu, S., 2004, "Biomimetic Reduction of Wake Deficit Using Tail Articulation at Low Reynolds Number," IEEE J. Ocean. Eng., **29**, pp. 766–776.
[201] Yoda, K., Sato, K., Niizuma, Y., Kurita, M., Bost, C.-A., Le Maho, Y., and Naito, Y., 1999, "Precise Monitoring of Porpoising Behaviour of Adélie Penguins Determined Using Acceleration Data Loggers," J. Exp. Biol., **202**, pp. 3121–3126.